Numerical simulation of turbidity currents: a new perspective for small- and large-scale sedimentological experiments

Snorre Heimsund

Thesis for Candidatus Scientiarum degree
in Sedimentology/Petroleum Geology

Department of Earth Science
University of Bergen
2007

ABSTRACT

Turbidity currents are a variety of subaqueous sediment-gravity flows, in which the suspension of sediment by water turbulence produces a water-sediment mixture that is denser than the ambient water and hence flows due to gravity along a topographic gradient. This type of sediment gravity flow is the most important mechanism for the dispersal and deposition of sand on deep-sea floors, as well as on the underwater slopes of many deltas and lakes.

The hydrodynamics of turbidity currents are difficult to study in the natural environments, whereas laboratory experiments are limited to small-scale flows, time-consuming and not necessarily easier when it comes to the measuring of flow properties and establishing of the relationships between the turbulent flow structure and the transport and deposition of sediment. Mathematical models of turbidity current, integrated by computational fluid dynamics (CFD) and realized as numerical simulations, can be used to obviate these difficulties, and also to upscale laboratory datasets and to integrate the data from nature and experiments. The concept CFD refers to the numerical solution, by computational methods, of the governing equations describing fluid flow: the set of Navier-Stokes equations and the multi-phase fluid dynamics. CFD is widely used in the engineering branches of fluid mechanics, but is a relatively new numerical approach in the field of sedimentological research.

In the present study, a three-dimensional model has been constructed by using the CFD software Flow-3D™ to simulate the flow of turbidity currents, including their internal hydraulic characteristics as well as sediment erosion and deposition. The Flow-3D™ model employs finite difference and finite volume methods and the turbidity current is being simulated by a range of physical models: 1) the turbulent flow structure is simulated by a turbulence model based on renormalization group theory that employs statistical methods to calculate turbulence quantities; 2) the water-sediment mixture is calculated by a drift-flux technique that describes the relative flow of two miscible fluids with different densities; 3) interactions between the continuous fluid and the dispersed mass particles are calculated by the particle model; and 4) the erosion and deposition of sediment are calculated by the sediment scour model.

Simulations of small-scale turbidity currents imitating particular laboratory flows have shown that the results of Flow-3D™ are realistic and reliable. Similar series of flow simulations have been used further: 1) to display in a flow-parallel axial section the main hydraulic characteristics (bulk density, shear-strain rate, dynamic viscosity, velocity magnitude and its x-y-z components) of a channel-confined current; 2) to display of the shear stress, sediment concentration and velocity magnitude for several ‘probing stations’ in a channel-confined current expanding abruptly on an open-space flat floor; 3) to study the responses of the confined and unconfined parts of a current (in terms of its velocity magnitude, shear stress and sediment concentration) to changes in such principal controlling parameters as the channel slope angle, sediment grain size, floor roughness and initial sediment concentration; 4) to display sediment grain-size segregation in a current (using a flow run with poly-sized sediment suspension); 5) to display the velocity time series for a surge-type and a sustained turbidity current; and 6) to show the responses of turbidity current to various obstacles and to a hydraulic jump at the channel outlet.

Two large-scale simulations of ‘real-life’ turbidity currents have been performed, one imitating modern flow events in the Soquel and Monterey canyons, offshore California, and another pertaining to the deposition of the Egga reservoir unit in the Ormen Lange field, Mid-Norway Continental Shelf.

The present study has evaluated Flow-3D™ as a possible means of simulating hydrodynamic behaviour of turbidity currents. The comparison of numerical and flume data indicates that the CFD-based Flow-3D™ models can give realistic results and serve as an attractive alternative to laboratory flume experiments. The use of a CFD software, such as the Flow-3D™, has several great advantages: 1) it allows a much wider range of flow parameters to be determined and continuously monitored with a relatively high accuracy; 2) it permits the response and relative importance of the individual flow parameters to be assessed with respect to changes in the initial conditions; 3) it allows turbidity currents to be up-scaled to natural conditions; and 4) it provides an unprecedented insight in the detailed hydrodynamic aspects of turbidity current. The study indicates that our understanding of turbidites and their variability can be significantly improved by this type of experimental research.

The thesis is dedicated to the loving memory of my father

Odd-Eirik Heimsund

February 21, 1938 - September 8, 2006

ACKNOWLEDGEMENTS

The present thesis is a part of the fulfilment of my study programme for a *Candidatus Scientiarum* degree in Sedimentology/Petroleum Geology at the Department of Earth Science, University of Bergen. This research project was supervised by Prof. Dr. Wojciech Nemec (University of Bergen), whom I wish to thank for his vital guidance, for stimulating and insightful discussions and for a critical reading of an earlier version of the manuscript. The project was sponsored by the Hydro Research Centre in Bergen, with scientific support and encouragement from Prof. Dr. Gunnar Furnes and Dr. Ole J. Martinsen.

I am also grateful to my external advisors, Dr. Jaco H. Baas (The University of Wales, Bangor) and Ernst W. M. Hansen (Complex Flow Design AS, Trondheim), for their valuable discussions and collaboration. Jaco Baas kindly provided datasets from some of his laboratory work for the purpose of my numerical experiments, whereas Ernst Hansen offered constructive critique of my simulation ideas and numerical procedures. The late Dr. Tor H. Nilsen (Menlo Park, California) is thanked for his comments of some parts of the manuscript.

I also wish to express gratitude to my fellow geology students and the department's staff for their support and plenty of good will. A special thanks to my dear friend and brother, Bjørn-Ove Heimsund, for all the help and encouragement when I needed it the most. Last, but not least, I am very grateful to my friends and family for their patience and unlimited support throughout the entire period of my extended studentship.

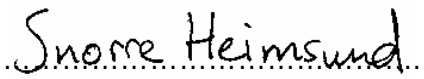

Snorre Heimsund Bergen, May 2007

CONTENTS

1. INTRODUCTION

The general aim of the present study was to use the methods of computational fluid dynamics (CFD) offered by the commercial software Flow-3D™ to simulate the dynamics of turbidity currents, and to adjust further the software to account for the corresponding modes of transport and deposition of 'natural' (poly-sized) sediments. The study was meant to evaluate the usefulness of numerical simulations as a possible alternative to the costly and time-consuming laboratory tank experiments, with the highly attractive perspective of up-scaling laboratory data and performing simulations at a scale of natural sedimentary basins.

The original plan was thus to assess the reliability of the Flow-3D™ numerical models by simulating particular laboratory experiments and comparing the results. The preliminary simulations came out to be not only very promising, but opening some unprecedented insights in the turbidity current dynamics (Heimsund et al., 2002, 2003a, b, 2004, 2005a, b, 2006). Encouraged by the positive response of peer sedimentologists, including the Best Poster Award from the 16th International Sedimentological Congress in 2002, the author has decided to extend the project's scope. A wider range of specific aims have been selected, including some large-scale simulations of 'real-life' modern and ancient turbiditic systems. This broader and more ambitious plan obviously required more time to be realized, and also brought the author into a full-time cooperation with the Complex Flow Design AS in Trondheim.

The specific aims of the study have been defined as follows: 1) to cross-check the Flow-3D™'s numerical options against some reliable sets of laboratory data on turbidity currents in order to select an optimal version of the numerical model on a best-fit basis; 2) to use the Flow-3D™ for the up-scaling of laboratory currents (measured datasets) to natural conditions; 3) to evaluate the influence of particular controlling variables on the dynamics of a turbidity current; 4) to study the relationship between the turbidity current's dynamics and its mode of sediment deposition; 5) to study the dynamics of surge-type vs. sustained (quasi-steady) turbidity currents and their responses to a hydraulic jump, or slope-break conditions; and 6) to assess the reliability of large-scale simulations by designing numerical models imitating particular natural settings and by comparing the results with field observations.

Two sets of such natural-scale simulations have been performed: one based on the modern seafloor topography and flow measurements reported from the Monterey Submarine Canyon, offshore California (Xu et al., 2004), and another based on the basal-surface palaeotopography and turbidite stratigraphy of the Egga Reservoir Unit in the Ormen Lange field, Mid-Norway Continental Shelf (Blystad et al., 1995). This latter set of pilot simulations

was done as a small consultancy project for the Hydro Research Centre and A/S Norske Shell, and the corresponding report (Heimsund, 2005b) is attached to the thesis as **Appendix**.

The thesis begins with a short historical overview of the concept of subaqueous sediment-gravity flows, particularly turbidity currents, followed by a summary of the modern physical notions of mass-flow behaviour (**Chapter 2**). In this review, the author puts emphasis on the concept evolution and related controversies, and also takes the opportunity to point out and clarify some of the main misconceptions. The methodology of the present study is then outlined (**Chapter 3**), with a brief introduction of the Flow-3D™ software, its purposes and design. In the next and main part of the thesis, the results of the numerical study are presented and discussed (**Chapter 4**), and are followed by concluding remarks (**Chapter 5**). The thesis closes with a list of literature **References.**

2. SEDIMENT-GRAVITY FLOWS

2.1. The physical concept of subaqueous sediment-gravity flows

As pointed out in the recent reviews by Friedman and Sanders (1997) and Shanmugam (2000), geologists prior to the 1950s were sceptical about the role of sediment-gravity flows in eroding submarine canyons and depositing graded sand beds in the deep sea. The general belief was that the deep sea was a tranquil realm free of current activity, where only pelagic (sea-born) or hemipelagic (land-derived) mud accumulated by slow settling from the water column, even though signs of deep-water currents had already been inferred from the local breaks of submarine telegraph cables so early as the late 19th century (Milne, 1897). Shallow coring of continental margin and abyssal-plain sediments at the beginning of the 1940s confirmed the existence of currents and related gravity-controlled deposition in the deep sea, but the real turnaround came with the paper by Kuenen and Migliorini (1950) invoking ”turbidity currents as a cause of graded bedding”. From then onwards, many researchers focused on the deep-marine deposits and their origin.

During the 1950s and 1960s, evidence of a gravity-driven sediment transport from shelf edge to base-of-slope and beyond came from the observations of currents in modern submarine canyons (e.g., the seafloor cable breaks caused by the Grand Banks event; Heezen and Ewing, 1952), from deep-sea sediment cores and outcrop studies (e.g., the classical study of the Annot Sandstone outcrops in southeastern France by Bouma, 1962) and – most importantly – from laboratory experiments (Kuenen, 1950, 1957; Bagnold, 1962; Middleton, 1966a, b, 1967). Kuenen (1957) coined the term *turbidite* to denote the deposit of a turbidity current. Bouma (1962) was the first to define a vertical facies model for turbidites on the basis of his pioneering study of the Annot Sandstone, although – as pointed out by Shanmugam (2000) – the vertical sequence of sedimentary structures that would later become known as the Bouma sequence was earlier recognized by Sheldon (1928).

The characteristics of many deep-marine deposits appeared to not match the definition of turbidite as ‘a graded deposit originating through suspension fall-out from a turbid underflow’. Therefore, other gravity-driven mechanisms were proposed for the transport of sediment in deep water, such as sliding and slumping (Doreen, 1951), debris flow (Doreen, 1951; Crowell, 1957) and high-concentration cohesionless granular flow referred to as grain flow (Bagnold, 1954; Hsü, 1959). The importance of these other processes (cohesive debris flows, grain flows, liquefied flows, slumps and slides) for the origin of the Annot Sandstone was discussed by Stanley (1963). Other researchers noted that not all sediment transport on the continental slope and in the deep ocean was gravity-driven, and introduced the terms

”contour current” and ”contourite” for parallel-to-slope thermohaline bottom currents and their deposits.

Gradually, the Earth-science community came to realize that a whole range of processes, not all of them gravity-driven, were responsible for the transport of large amounts of sediment to the deep sea over periods long enough to be potentially influenced by changes in the sea-level, climate and tectonic activity. This notion initiated the development of submarine-fan models based on cores and outcrop studies, first for modern passive-margin fans (Normark, 1970) and ancient active-margin turbiditic systems (Mutti and Ricchi Lucchi, 1972). Based on these studied, Walker (1978) proposed a generalized submarine-fan model (Fig. 1) with the classical division of a submarine fan into an upper, middle and lower segment, encompassing deposits from the slope break to the abyssal basin plain. The hydrocarbon reservoir potential of turbidites was first discussed by Sullwold (1961), whereas Walker (1978) focused on the stratigraphic traps for hydrocarbon exploration in ancient fan deposits.

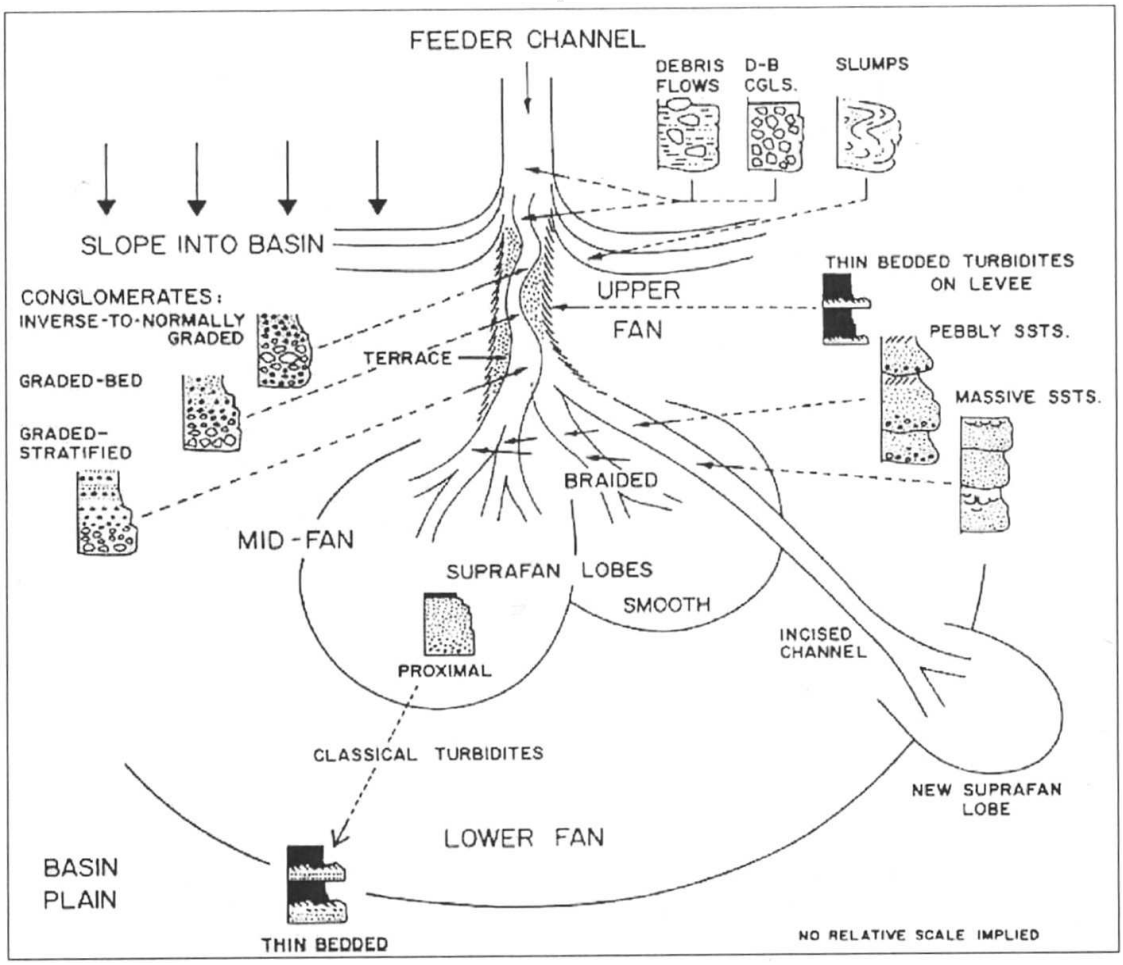

Fig. 1. Schematic illustration of a (passive) continental-margin setting, showing the transition path of sediment from a hinterland to a deep-marine basin beyond the continental shelf and slope cut by a feeder canyon/channel. The diagram portrays the classical model for a submarine turbiditic fan postulated by Mutti and Ricci-Lucchi (1972), modified by Walker (1978) to account for Normark’s (1970) observations from the modern Navy Fan.

In the 1970s, the wide availability of seismic sections added a new dimension to the development of fan models based on cores and outcrops. This new type of subsurface data initiated the development of seismo-stratigraphic fan models and deep-marine facies classifications (Payton, 1977).

Experimental laboratory work on gravity-driven sediment transport in the 1960s, building upon Kuenen's pioneering work, focused on the hydrodynamics of turbidity currents and their modes of sediment transport. Bagnold (1962) elaborated the concept of auto-suspension, originally proposed by Knapp (1938), which postulates that, depending on the ratio of particle settling velocity to the product of mean flow velocity and bed slope, the sediment suspends itself in a sense, such that no net expenditure of energy by the flow is needed to keep the grains suspended. In brief, the entrainment of any additional sediment into suspension adds to the flow's mass and energy, which in turn increases turbulent shear stresses and helps to keep the sediment in suspension. Using flume experiments, Middleton (1966a, b) studied the anatomy of turbidity currents and recognized the existence of a head, a body and a tail, with the first and the second element linked by a relatively thin neck in some cases. He concluded that the velocity of the head depends on the flow mass, but is independent of the seafloor slope. Komar (1971) was probably the first to discuss the origin and significance of hydraulic jumps in turbidity currents. In a later pioneering publication, Komar (1977) applied a simple, one-dimensional hydrodynamic model to investigate the behaviour of turbidity current with the use of a computer.

Dott (1963) was the first who introduced a classification of submarine sediment-gravity flows based on the flow rheology (i.e., based on the physical characteristics of the process, rather than the deposit). He recognized that the hydrodynamic behaviour of sediment-gravity flows is controlled largely by the volumetric concentration of sediment and its cohesiveness. A related classification of submarine sediment-gravity flows, based on the sediment-support mechanism, was proposed by Middleton and Hampton (1973), who invoked the following mechanisms of sediment-particle support: buoyancy (a universal factor in non-dry flows), matrix strength, grain interactions (hindered settling or collisions and dispersive pressure), escaping pore fluid (liquefaction or fluidization) and fluid turbulence (specific to turbidity currents). Hampton (1972) was also the first to conduct experiments on subaqueous debris flows. A classification scheme combining flow rheology and sediment-support mechanism was proposed by Lowe (1979, 1982) (Fig. 2).

Lowe (1982) defined debris flows as rheological Bingham-type plastic flows and distinguished their two categories: mudflows (or cohesive debris flows) and grain flows (Fig. 2). However, Nemec and Steel (1984) pointed out that not every debris flow must necessarily behave like a Bingham plastic (e.g., grain flows are characterized by a dilational, non-Bingham plastic behaviour; Bagnold, 1954) and, likewise, not every non-cohesive debris

flow must necessarily be a grain flow (i.e., characterized by a pervasive shear, high shear-strain rate, intense particle collisions, dispersive pressure and pronounced dilation). The momentum transfer in a granular flow may occur by the particles persistently rubbing against one another without significant collisions (see the 'frictional regime' of Drake, 1990), or be limited to a thin basal layer of colliding particles (Campbell, 1989b). Therefore, Nemec and Steel (1984) have modified Lowe's categories by classifying debris flows into cohesive and cohesionless, with mudflow and grainflow as the end-members of a possible flow spectrum. The former debris-flow type involves chiefly cohesive shear strength and the latter type is governed by frictional shear strength, which are the two yield-strength components specified by the classic Coulomb criterion for rheological plastics (Nemec and Steel, 1984) and widely used in the engineering classification of 'soils', or natural clastic materials, into cohesive and cohesionless (Keedwell, 1984; Craig, 1987).

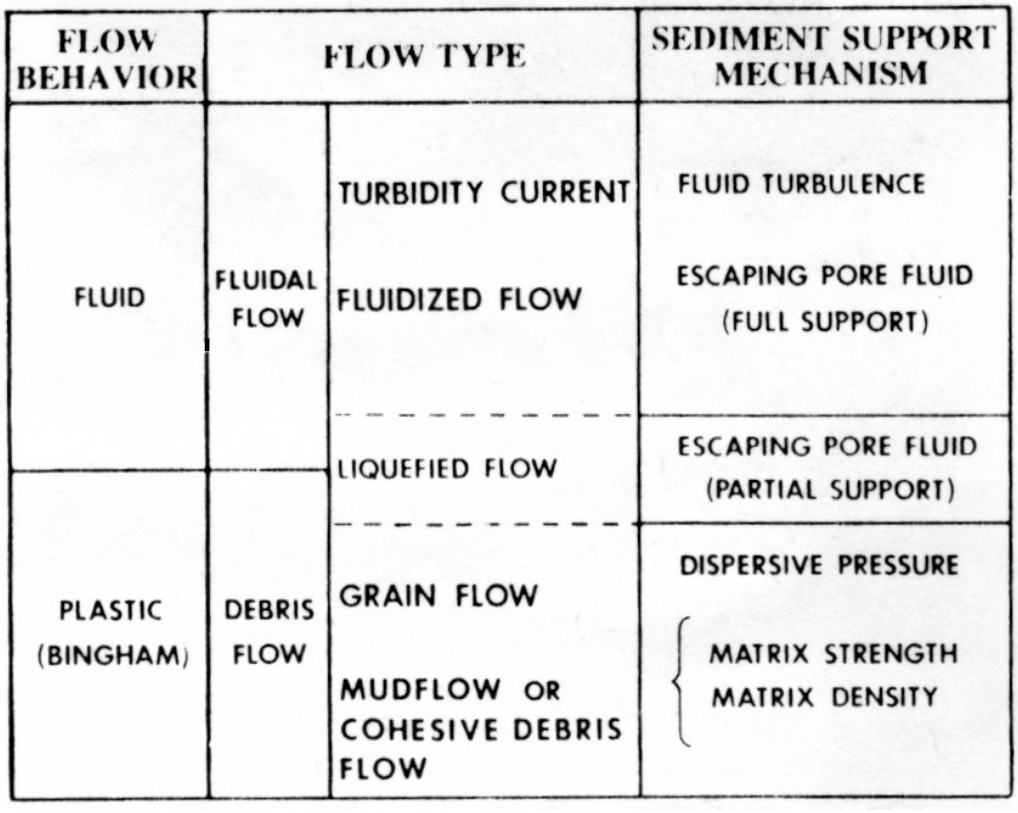

Fig. 2. Classification of sediment-gravity flows by Lowe (1982).

In his classification, Lowe (1979) made an important distinction between 'liquefied flow' and 'fluidized flow', the two terms that were earlier used mainly as synonymous. In either flow, it is the upward-escaping pore fluid that reduced grain friction and renders the sediment mobile, or 'liquidized'. In the former case, however, it is the collapsing or settling grain framework that displaces the pore fluid upwards, as in a common quicksand, with the grains

subject to only partial support (fluid drag). In the latter case, in contrast, the pore fluid is escaping by itself, as does gas in a pyroclastic flow or external water injected from the bottom in a debris flow; and the grains are thus subject to full support by the fluid.

Lowe (1979, 1982) also introduced the concept of "high-density turbidity currents (HDTCs)" – which has subsequently been subject to a considerable debate (Shanmugam et al., 1995, 1997; Shanmugam and Moiola, 1995, 1997; Shanmugam, 1996, 2000, 2002; Bouma et al., 1997; Coleman, 1997; D'Agostino and Jordan, 1997; Hiscott et al., 1997; Lowe, 1997; Slatt et al., 1997). Much of this controversy derives from two sources: a) a misunderstanding of Lowe's very definition of a HDTC; and b) the common mistaken notion that turbidity current must necessarily behave like a Newtonian fluid, or otherwise be a debris flow. These two points are worth explaining here.

In Lowe's definition, if the concentration of sediment settling from suspension in turbidity current becomes sufficiently high, relative to the current's competence (turbulence intensity level), the turbulence in the lower part of the current becomes suppressed and the deposition occurs *en masse*, rather than grain-by-grain from traction. A portion of massive, normally-graded sediment, the Bouma division A (see later Fig. 6), will be dumped directly from suspension, possibly as an upward-freezing 'moving bed' (Vrolijk and Southard, 1997); or a massive, inversely-graded traction carpet may form and abruptly freezes beneath the turbulent, tractive current (Nemec, 1997). According to Lowe, such a turbidity current is a 'high-density' current. The Lowe definition is such behaviouristic, so to speak: if the current behaves in such-and-such way (i.e., suffers temporary sediment overcharge), it is a HDTC; and its deposit is recognizable by such-and-such sedimentary features. Instead of appreciating this simple and practical notion, some researchers – such as Shanmugam (op. cit.) – discard this definition as 'poor and confusing', because it 'fails to specify the exact threshold value (vol. %) of sediment concentration'. These critics fail to realize that the threshold concentration necessarily depends upon the flow energy and sediment grain size, and hence may vary from current to current. Furthermore, the exact threshold value for a particular current is virtually irrelevant, because sediment concentration is the last thing that can possibly be recognized in a deposit. Some other researcher, in turn, confuse Lowe's notion of a HDTC with the terms 'high-density' or 'high-concentration' current adopted quite arbitrarily in various laboratory experiments for the sake of distinguishing between flow runs with higher and lower sediment concentrations. Some researchers, yet, draw a false, superficial notion from Lowe's own selected examples of the deposits of HDTCs and assume that a HDTC is the one carrying gravel. Paradoxically, many silty or fine-sandy turbidites may be products of HDTCs, whereas a thick gravelly turbidite, if fully stratified (i.e., tractionally deposited) (e.g., see Winn and Dott, 1979; Janbu et al., 2007), will obviously represent a low-density turbidity current (LDTC) in Lowe's classification.

The second source of misunderstanding is the widespread mistaken notion that a turbidity current, just like any water current, has the rheological behaviour of a Newtonian liquid (i.e., has a constant viscosity, determined by the suspended sediment load and independent of the shear-strain rate). This misconception apparently derives from numerical hydrodynamic models and calculations, where a constant viscosity is often assumed of the convenience of simplicity. As pointed out by Nemec (1995), the apparent viscosity of a current depends greatly on the volumetric concentration of sediment suspension, which depends directly on the intensity of turbulence (shear-strain rate) and hence varies both vertically and laterally within the turbidity current and inevitably varies also with time. In short, the viscosity of turbidity current is by no means constant, since it is both non-uniform (space-varied) and unsteady (time-varied). As the current decelerates and its sediment concentration increases towards the base, so does its viscosity – possibly until the extreme phase when the basal part begins to behave like non-turbulent plastic flow and undergoes rheological freezing (Lowe, 1982; Nemec and Steel, 1984; Postma et al., 1988; Vrolijk and Southard, 1997). Much confusion and controversy would be avoided if it was widely understood that turbidity current does not necessarily behave like a simple Newtonian fluid. For example, it has been argued by Shanmugam (op. cit.) that because the notion of HDTC implies non-Newtonian behaviour and allows for plastic freezing – such currents should preferably be classified as debris flows. In Nemec's (2002) words: "This is like saying that a snow scooter is not a scooter, because it has a pair of sleighs as runners, instead of the conventional two wheels. But that's exactly why we call it a 'snow' scooter. And, by analogy, that's why we distinguish the non-classical 'high-density' turbidity currents."

A mistake unwittingly made by Lowe (1982), on the other hand, was to narrow the definition of 'traction carpet' in a HDTC to a cohesionless, grainflow-like basal layer of colliding sediment particles, sheared and driven along by the overpassing turbulent phase of the turbidity current. The original definition of traction carpet, introduced by Dzułyński and Sanders (1962), was broader, referring to the turbidity current's basal layer with suppressed turbulence and plastic behaviour. Lowe apparently came to realize his error through the more recent study of the turbiditic Britannia Formation (Lowe and Guy, 2000; Lowe et al., 2003), but instead of revising his definition – he introduced the bizarre term 'slurry flow", somewhat misleading and poorly understood by most sedimentologists, not least because the same term was earlier used in Carter's (1975) classification as a synonym of cohesive debris flow. In Lowe's concept of 'slurry flow', the settling of sand grains from turbulent suspension involves clay clots with a corresponding settling velocity, and as these particles become disseminated in the sheared, high-concentration basal layer – the latter rapidly gains cohesive strength and freezes; the process of freezing of semi-discrete layers may be repeated many times over, so long as the fallout of similar sediment mixture persists.

Similarly, the formation process of Lowe's (1982) traction carpet can be repetitive within a single HDTC. The main difference would thus appear to be between the frictional plastic freezing in the latter case and the cohesive plastic freezing in former case.

Finally, there has been the poorly substantiated notion that the transport mode of sediment is one thing and the mode of its deposition is quite another thing, and that two separate classifications should preferably be used – one (physical) based on 'processes' and another (descriptive) based on 'deposits' (Fisher, 1986; Postma, 1986; Shanmugam, 1996). According to this dual concept, the mode of sediment deposition may have little to do with the mode of the sediment transport. However, it has been pointed out by Nemec et al. (1998) that virtually all depositional features arguably derive from transport. For example: every stratification type reflects a particular mode of tractional sediment transport (active bedform configuration) (Allen, 1982); normal grading in a non-stratified deposit reflects direct fallout of sediment from turbulent suspension (Lowe, 1988; Allen, 1991); and also the concentrated bed-load carpet is a mode of transport (Einstein, 1950), since the traction carpet must move and intensely shear for the characteristic inverse grading to develop (Lowe, 1982). Instead of a dual classification, a better insight in the sedimentary signatures of processes and a more rigorous use of sedimentological criteria are needed (Nemec et al., 1998).

Although some of the misconceptions reviewed above persist in the literature and have unwittingly been transmitted to more recent classifications (e.g., Mulder and Alexander, 2001; Gani, 2004), the distinction of sediment-gravity flow types based on rheology and sediment-support mechanism is now widely accepted. This conceptual framework provides a convenient basis to discuss the physics of sediment-gravity flows, and turbidity currents in particular (e.g., Kneller, 1995). Most of the mechanical aspects of flow behaviour can readily be recognized from the deposits, and our understanding of the sedimentary signatures of mass-flow processes has been consistently improving by the development of new sedimentological criteria based on laboratory experiments and detailed field studies (Lowe, 1982, 1988; Johnson and Rodine, 1984; Nemec and Steel, 1984; Postma et al., 1988; Savage and Lun, 1988; Campbell, 1989b, 1990; Savage and Hutter, 1989; Nemec, 1990; Nemec and Postma, 1991; Kneller et al., 1997; Kneller and Buckee, 2000; Lowe and Guy, 2000; McCaffrey et al., 2001; Mulder and Alexander, 2001; Tucker, 2001; Lowe et al., 2003).

2.2. The behaviour of sediment-gravity flows

Sediment-gravity flows, commonly referred to also as mass flows or density flows, are mixtures of sediment and fluid flowing down a slope by the virtue of gravity force (i.e., the mixture's mass, or own weight). In contrast to common water flows, such as rivers or sea

currents, the gravity in this case moves the sediment, which consequently drags the interparticle fluid along (while being also influenced by it). In subaqueous sediment-gravity flows, the fluid is water – either the saline seawater (as in flows triggered by common submarine slides) or freshwater (as in river-generated submarine hyperpycnal flows at their outset, or in sublacustrine settings). The physical behaviour of sediment-gravity flow, which ultimately determines much of the sedimentological character of the deposit, depends largely upon the following three factors (Lowe, 1979, 1982; Shanmugam, 1996): 1) flow rheology, itself dependent upon the composition (especially clay content) and volumetric concentration of sediment; 2) grain-support mechanism; and 3) flow state (turbulent vs. pseudolaminar). The last two factors, as well as the sediment concentration, depend directly on the flow's shear-strain rate – which itself is an important variable, indirectly affecting also the apparent (bulk) viscosity of the flowing sediment-water mixture.

Grain-support mechanisms (Middleton and Hampton, 1973; Pierson, 1981; Lowe, 1982) include: matrix strength (which may be predominantly frictional or cohesive), grain interactions (which may be limited to hindered settling or involve dispersive grain pressure arising from grain collisions), escaping pore fluid (which may be due to sediment liquefaction or fluidization), and fluid turbulence (which requires a sufficiently high volumetric percentage of fluid in the flow). In addition, buoyancy renders the grains lighter, according to the Archimedes principle, especially when the interparticle fluid is a relatively dense slurry, loaded with fines (clay, silt and very fine sand) (Hampton, 1975). Importantly, more than one grain-support mechanism may operate simultaneously in any particular sediment-gravity flow. Likewise, the flow state may change from laminar to turbulent and vice versa, depending on sediment concentration and substrate slope (or flow velocity).

The rheological behaviour of sediment-gravity flows can be categorized according to the constitutive stress-strain relationship describing the sediment-water mixture's response to applied shear stress (Fig. 3) (Tokaty, 1971; Barnes et al., 1989; Larson, 1999). *Fluids* lack yield strength and hence deform instantaneously when a stress is applied. If the rate of shear strain is linearly related to the applied shear stress, the fluid is said to have a constant (shear rate-independent) viscosity and is referred to as a *Newtonian fluid* (Fig. 3). Water is a classical example of such a fluid. Fluids which are changing their viscosity with the changes in shear-strain rate are called *non-Newtonian fluids* (Fig. 3). These fluids can be subdivided into *dilational* (if the fluid viscosity increases with an increasing shear-strain rate) or *contractional*, also referred to as *pseudoplastic* (if the fluid visciosity decreases with an increasing shear-strain rate). The adjectives 'dilational' (i.e., expanding, or shear-thickening) and 'contractional' (i.e., shrinking, or shear-thinning) pertain to the changes in fluid volume under an increasing shear strain. The alternative synonymous terms are 'shear-hardening' and 'shear-softening' fluids, which pertain to the changes in the fluid's internal resistance to

shear strain (i.e., viscosity) under an increasing shear strain. A generalized constitutive equation for rheological fluids is:

$$\tau = \eta \cdot \dot{e}^{n}$$

where: τ = shear stress (i.e., the downslope component of normal stress, or material weight); η = apparent viscosity; $\dot{e}$ = shear-strain rate (or vertical velocity gradient, du/dy); and n = dimensionless exponent specific to particular material (with n = 1 for Newtonian fluids; n < 1 for pseudoplastic fluids; and n > 1 for dilational fluids).

Plastics differ from fluids in that they have a finite yield strength, which must be overcome by the applied shear stress for deformation (shear strain) to occur. In other words, plastics begin to flow only when the applied stress is sufficient to overcome the yield strength of the material. The yield strength generally has a cohesive and a frictional component, and one of them normally predominates in particular sediment, depending upon its volumetric content of clay and water (Keedwell, 1984; Craig, 1987). Accordingly, plastic flows can be divided into *cohesive* and *cohesionless* (or *frictional*), as postulated by Nemec and Steel (1984) in their modification of Lowe's (1982) original classification of debris flows.

Irrespective of the nature of their yield strength, the rheological plastics – similarly as fluids (see above) – are divided on the basis of their viscosity response to an increasing shear stress. If the viscosity remains constant, independent of the rate of shear strain, the plastic material is referred to as a *Bingham plastic* (Fig. 3). A common mudflow or wet flowing concrete are considered to be typical examples of such a plastic flow. Plastics that are changing their viscosity with the changes in shear-strain rate are referred to *non-Bingham plastics*. These plastics can be divided further into *dilational* (if the viscosity increases with an increasing shear-strain rate) or *contractional* (if the visciosity decreases with an increasing shear-strain rate) (Barnes et al., 1989). Synonymous labels for these two categories are *shear-thickening* and *shear-thinning* plastics; or *shear-hardening* and *shear-softening* plastics, respectively. A generalized constitutive equation for rheological plastics can be written as follows (Johnson, 1970; Iverson, 1997):

$$\tau = k + \eta \cdot \dot{e}^{n}$$

where: τ = shear stress (i.e., the downslope component of normal stress, with the latter defined as the material weight reduced by buoyancy); k = yield strength; η = apparent viscosity; $\dot{e}$ = shear-strain rate (or vertical velocity gradient, du/dy); and n = dimensionless exponent specific to particular material (with n = 1 for Bingham plastics; n > 1 for dilatant fluids; and n < 1 for contractional fluids). Importantly, it is the presence of yield strength that defines rheological plastics and distinguishes them from rheological fluids (Fig. 3), and which thus also defines debris flows in Lowe's (1982) classification (Fig. 2).

Because the yield strength – according to the Coulomb criterion (Keedwell, 1984; Craig, 1987) – comprises cohesive and frictional components, the last equation can be written as:

$$\tau = (c + \tan\theta \cdot \sigma') + \eta \cdot \dot{e}^{n}$$

where the additional symbols are: c = cohesion (electrostatic particle-binding force; significant and particularly strong in clay, though dependent on the volumetric percentage of water); θ = the sediment angle of internal friction (chiefly a function of grain size); and σ' = normal stress (or sediment weight) corrected for buoyancy effect. The yield strength in a clay-rich mudflow will have $c >> \tan\theta \cdot \sigma'$ (cohesive debris flow), whereas that in a clay-free sandflow will have c = 0 (cohesionless debris flow).

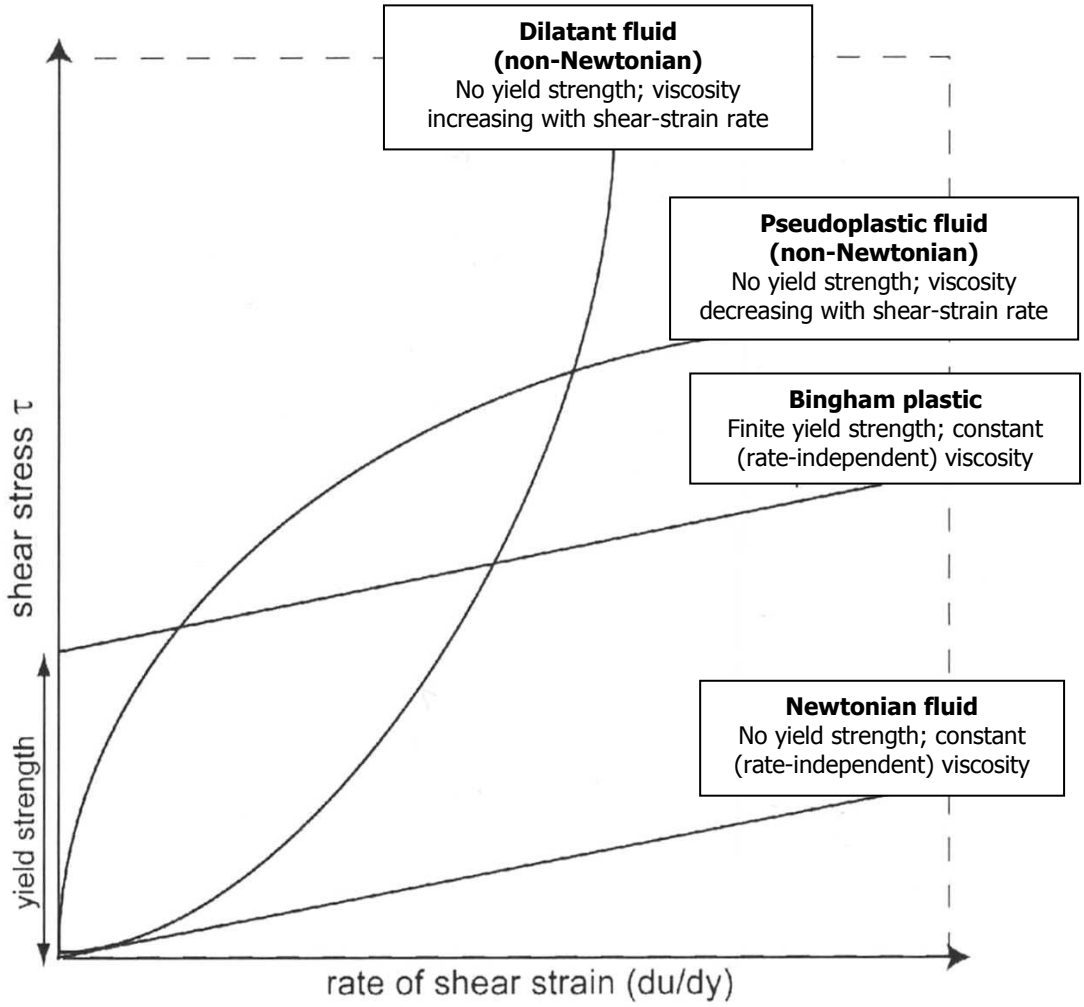

Fig. 3. Generalized rheological definitions (stress-strain relationships) of Newtonian fluid, non-Newtonian fluids and Bingham plastic. The line gradient in each case is the flow viscosity. Schematic, with no exact scale implied. Based on Shanmugam (2000).

The defining property of plastic flow is that – when the flow reaches gentler slope and decelerates – the shear stress decreases and eventually reaches a critical value equal to the yield strength, whereby the flow 'freezes' *en masse*. The freezing process, in reality, occurs

progressively from the flow top (where the strain rate is at a minimum, or virtually no strain occurs in the case of a non-shearing 'rigid plug') downwards, and the whole flow comes to a halt only when the zero-strain surface reaches the flow base. The rate of this downward freezing will determine the degree of the flow's distal spreading and thinning. If the downward freezing is rapid, we are dealing with the case of a 'simple-shear' debris flow, but if it is more gradual – we are dealing with a 'pure-shear' debris flow, which may show considerable downflow thinning (smearing-out effect).

Natural debris flows generally consist of poorly sorted sediment and contain a large proportion of sand and gravel. Most contain more than 5 vol.% of gravel, and may carry bedrock boulder blocks or large rafts of intraformational deposits in the non-shearing 'rigid plug' in the upper part of the flow (Johnson, 1970; Johnson and Rodine, 1984; Leigh and Hartley, 1992). Notably, many debris flows with a 'cohesive' appearance contain as little as 2-5 vol.% of mud (e.g., Sharp and Nobles, 1953), whereas some mud-richer but more watery debris flows may appear to be 'cohesionless', dominated by grain collisions (e.g., Lawson, 1982; Takahashi, 1991). This evidence points to the importance of the volumetric content of water to a debris-flow behaviour. Increased water content in a debris flow can lower its cohesive strength to a level where the flow is no longer cohesive, but becomes frictional (Fisher, 1971; Mulder and Alexander, 2001). Accordingly, a debris flow can change its behaviour underway, when becoming more dilute or more concentrated with the travel distance (Fisher, 1983).

Some debris flows are capable of travelling over the distances of tens to hundreds of kilometres (Gardner and Kidd, 1983; Campbell, 1989b; Simm et al., 1991; Gee et al., 1999), but – despite their reaching high speeds – are generally little erosive (e.g., Pickering et al, 1989; Gee et al., 1999). The deposits of individual debris flows are typically 1 to 2 m thick, but – depending on the sourcing system and depositional setting – their amalgamated packages may be tens to hundreds of metres thick (Hiscott and James, 1985).

In an attempt to subdivide the spectrum of subaqueous sediment-gravity flows on the basis of observed changes in flow behaviour at differing sediment concentrations (Hallworth and Huppert, 1998), Mulder and Alexander (2001) have distinguished three main classes of flow: 1) hyper-concentrated density flows; 2) concentrated density flows; and 3) turbidity currents. This simple classification (Fig. 4) seems to be conceptually useful as a guide, although it bears several weaknesses (see further below).

According to Mulder and Alexander (2001), the character of hyper-concentrated frictional flows depends on the proportion of cohesive and non-cohesive particles, water content and flow velocity. Since natural subaqueous flows completely devoid of cohesive particles are rare, it is likely that even some very low proportion (< 2 vol.%) of cohesive particles can instigate cohesive forces, but these are easily overcome by a relatively high water content

and flow dilution. The weak cohesive forces will thus not prevent grain collisions and development of turbulence (Kneller and Buckee, 2000), but may transform the flow when it decelerates and its concentration increases (Fisher, 1983).

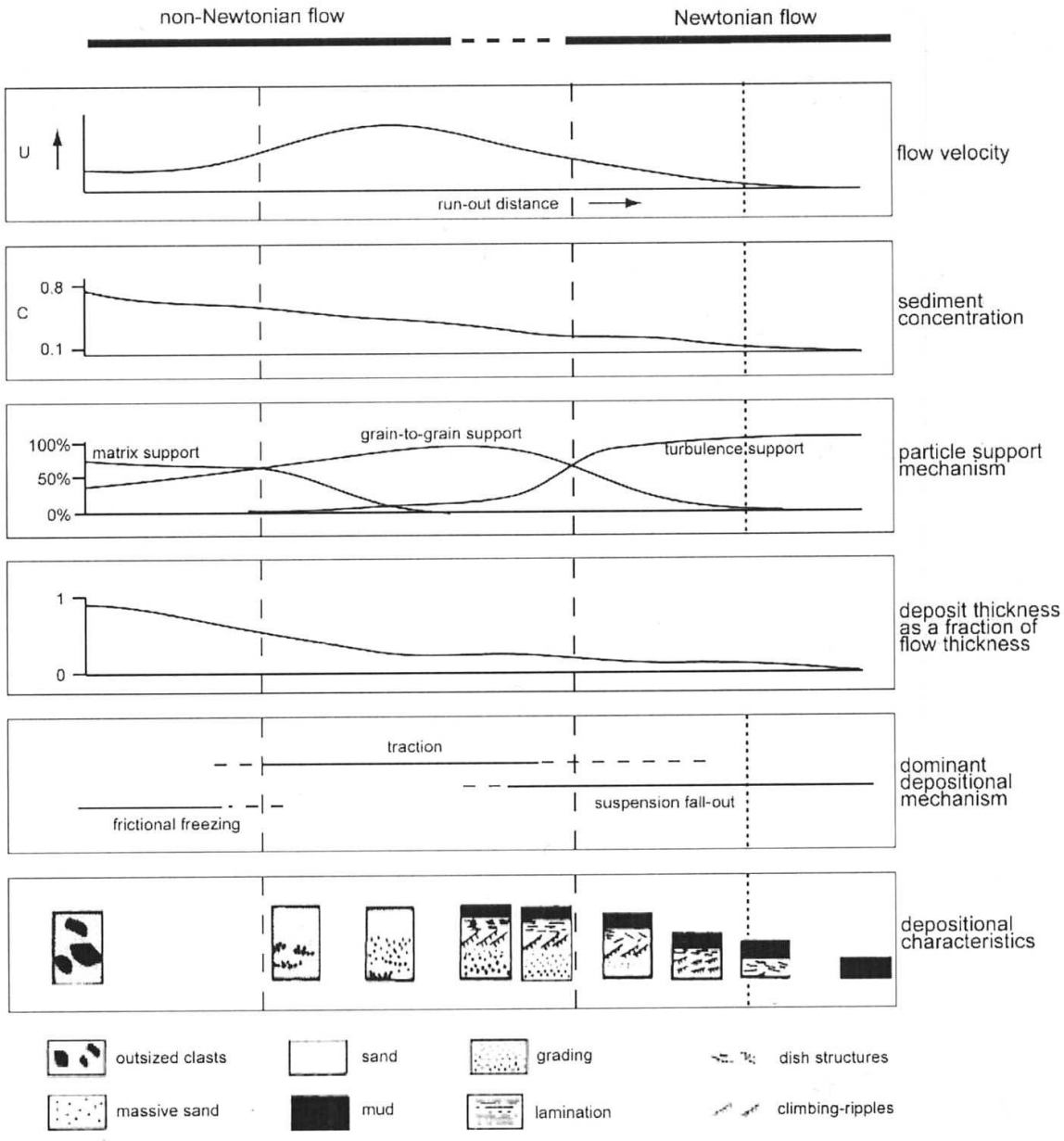

Fig. 4. Composite diagram illustrating the relationship between flow variables, flow behaviour and deposit type for 'frictional' flows; that is, non-cohesive, sediment-laden density flows (sandy debris flows, grain flows). After Mulder and Alexander (2001)

Turbulence is considered to be the dominant grain-support mechanism up to sediment concentrations of ca. 18 vol.% (McTigue, 1982; Campbell, 1989a), above which direct grain interactions become increasingly significant. At a concentration limit of 23 vol.%, fluids are considered to become fully non-Newtonian. Mulder and Alexander (2001) take this limit as an approximate boundary between 'concentrated' and 'hyper-concentrated' density flows

(Fig. 4), whereas Bagnold's (1962) concentration limit for turbulent suspension (9 vol.%) is used as an approximate boundary between the 'concentrated' density flows and 'turbidity currents'. Below this limit, the turbulence of interparticle fluid (water) is supposed to be the sole grain-support mechanism, even though low-frequency grain collisions probably still occur. However, the Bagnold limit is disputed, because many researchers believe that grain interactions may still be significant below a concentration of 9 vol.%.

The progressive entrainment of ambient water by a hyper-concentrated flow accelerating on a steep slope will lead to fewer grain collisions, whereby turbulence gradually replaces direct grain interaction as the main grain-support mechanism. When a density flow moves down on a very gentle slope, such as in a prodelta area or abyssal basin plain, the rate of water entrainment is low and the sediment concentration and grain interactions in the lower part of flow increase, which may lead to frictional freezing. Parker (1982) defined concentration and velocity optima, with respect to slope gradient, at which flows can move and entrain enough water to prevent freezing.

Concentrated density flows can achieve high velocities on steep slopes by virtue of the large density contrast with the ambient water. These flows can thus be strongly erosive. Erosion and entrainment of bed sediment contributes to the driving force of the flow and causes it to accelerate and grow in volume. Mulder and Alexander (2001) put high-density turbidity currents into the class of concentrated flows.

The grain-support mechanism in concentrated density flows involves both turbulence and direct grain interactions, operating simultaneously. Mulder and Alexander (2001) suggest that higher concentration prevents grain-size segregation, and hence normal grading, such as in the Bouma division A (see later Fig. 6), will not develop. This notion, however, is contradicted by laboratory experiments showing that a thick, non-stratified graded division can be deposited by a progressive upward freezing of sediment falling out directly from turbulent suspension (Kneller and Branney, 1995; Vrolijk and Southard, 1997). The duration of flow is an important factor. Sustained (long-duration) turbidity current may tend to be quasi-steady or involve waxing-waning pulses, and its behaviour will thus differ considerably from that of a simple surge-type (waning) turbidity current. Furthermore, concentrated density flows can be bipartite, or 'layered' – with the coarse-grained lower layer non-turbulent and dominated by grain collisions, and the fine-grained upper layer fully turbulent and moving at a considerably higher speed (Lowe, 1982; Postma, 1986; Postma et al., 1988) (Fig. 5). The lower part of the resulting deposit will lack stratification, but may show either normal or inverse grading (possibly with outsized clasts floating at the top), whereas the upper will be fine-grained, stratified and fining upwards.

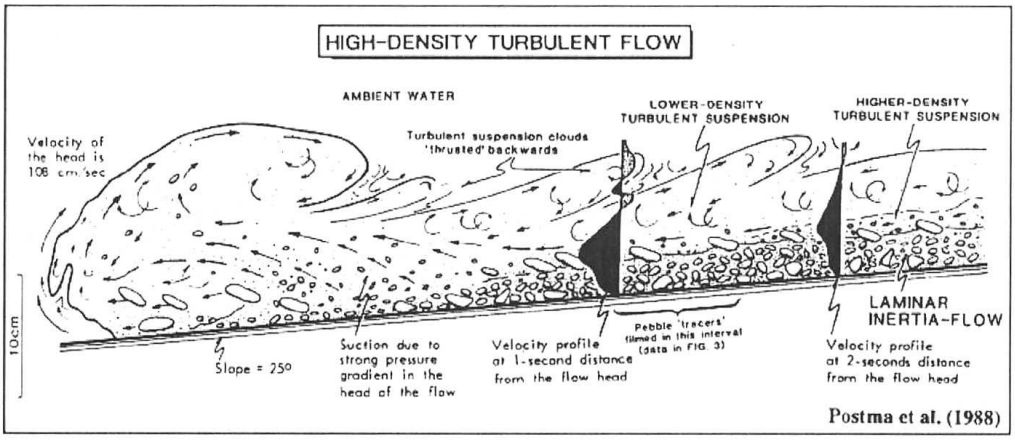

Fig. 5. Schematic illustration of an experimental concentrated density flow (high-density turbidity current), after Postma et al. (1988).

Mulder and Alexander's (2001) conceptual categorization of flows, though instructive, bears several other major weaknesses:

- The flow behaviour and deposit characteristics in reality depend on concentration in a continuous manner, so there is no discrete boundary between sediment-concentration ranges for the three classes (Fig. 4). Forcing such boundaries seems to be an artificial and possibly misleading exercise.
- The whole classification is limited to 'frictional (non-cohesive)' flows, whereas subaqueous sediment-gravity flows in reality are more commonly mud-bearing than mud-free.
- The hyperconcentrated density flows are said to be 'non-Newtonian' (Fig. 4) and to have 'no yield strength', whereas the authors' reference to 'sandy debris flows' and 'grain flows' implies rheologically plastics, rather than fluids. The proverbial apples should preferably not be mixed with oranges.
- The use of the term 'hyperconcentrated flow' is potentially misleading, because this term was originally introduced to denote a flow with 'behaviour intermediate between that of a mudflow [debris flow] and that of a common streamflow [water flow]' (Beverage and Culbertson, 1964; see also Wasson, 1979), whereas Mulder and Alexander (2001) apparently use it as a virtual synonym of debris flow.
- The authors' notion of 'flow density' is confusing, because on the one hand it refers to the flow's absolute density (sediment concentration) when it comes to the flow behaviour, but on the other hand refers to the relative density of different flows (more concentrated or less concentrated, on a comparative basis) and also to the absolute density difference between the flow and the ambient water. A particular flow may thus have a 'high density' when its turbulence is suppressed by sediment concentration, but be of 'low density'

compared to a hyper-concentrated flow and yet be of 'high density' when spreading as an underflow along the seafloor.

- The term 'turbidity current' in this classification has been limited to flows with a Newtonian behaviour, which means highly dilute, extremely low-density turbidity currents only.
- When it comes to the actual deposits of turbidity currents, the sequences of sedimentary structures and vertical grain-size trends drawn by Mulder and Alexander (2001) are purely hypothetical and, much like the grain-size trends in Kneller's (1995) model (see later Fig. 7), seem to be little-realistic, if not false and somewhat naïve. Simply, too little is known about the relationship between the changes in hydrodynamic behaviour of density flows – especially the sustained and the more concentrated ones – and the response mode of sediment deposition.

In the Mulder and Alexander (2001) classification, bedforms and related stratifications are expected to develop from concentrated density flows and turbidity currents, but not from hyper-concentrated flows (which, again, implies debris flows, rather than currents, for this latter category). However, the depositional models for bedforms suggested in the literature (Fig. 6) are hypothetical, surrounded by precaution that they are merely 'syntheses' of some 'wide spectra of field cases'. For example, Bouma (1962) himself admitted that his complete 'sequence' in the Annot Sandstone succession – where it was first defined – appeared to be relatively uncommon, if not rare.

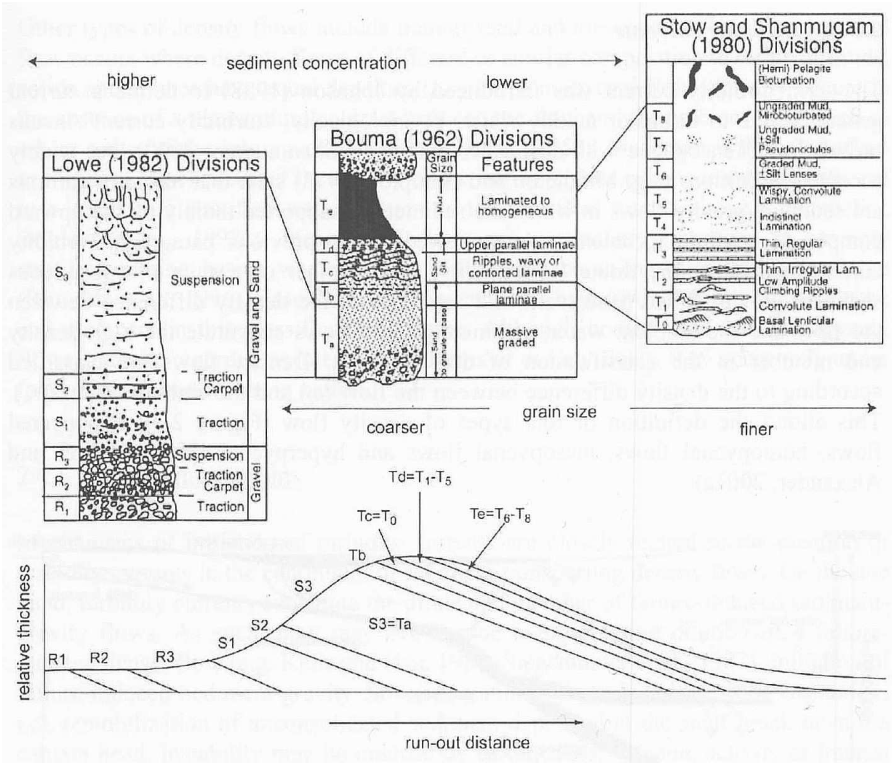

Fig. 6. Characteristic features of deposits of density flows in which turbulence is the primary grain-support mechanism. After Shanmugam (2000), based on Bouma (1962), Stow and Shanmugam (1980) and Lowe (1982).

The stability fields of hydraulic bedforms for high sedimentation rates are not well known (Allen, 1982; Lowe, 1988), and also the conditions for, and behaviour of, both traction carpet and 'moving bed' are debated (Hiscott, 1994a, b, 1995; Sohn, 1995, 1997, 1999). Bedform development is usually studied for laboratory conditions of quasi-steady flow. In flows where the basal part has a sufficiently low particle concentration, specific bedforms (such as plane bed configuration, ripples or dunes) can develop if flow conditions are maintained for long enough to achieve hydrodynamic equilibrium (Southard, 1971; Southard and Boguchwal, 1973). Climbing ripples, for example, are known to be associated with high sediment fallout rates from a quasi-steady turbulent flow, which implies that establishment of a hydrodynamic equilibrium is a requirement for the development of particular bedforms.

Many density flows are expected to be short-lived, waning and highly unsteady surges. Other density flows may be sustained and have pronounced phases of quasi-steady conditions, but yet others may be characterized by waxing/waning pulses of variable frequency and magnitude, and may also involve phases of erosion and/or sediment bypass (which effectively means gaps in depositional record). Therefore, it is a very difficult task to decipher reliably the flow's hydraulic history from its deposit, or to predict the depositional product for any particular flow. Accordingly, one has to concluded that turbidity currents are probably the most complicated and least understood flow phenomena, and hence the general importance of laboratory experiments and numerical simulations.

2.3. Turbidity currents – varieties, origin and behaviour

The term *turbidity current* was introduced by Johnson (1938) to define a current generated due to turbid or muddy water. Etymologically, 'turbidity current' means water flow driven by turbidity, or simply turbid flow (i.e., a water flow rendered opaque by suspended sediment) (Shanmugam, 2000). A widely accepted definition (Middleton and Hampton, 1973) says that 'turbidity currents are sediment-gravity flows in which the sediment is supported mainly by the upward component of fluid turbulence'.

As discussed in the preceding sections of this chapter, turbidity currents constitute the most dilute ('low-density' according to Mulder and Alexander, 2001) end-member of the natural spectrum of subaqueous sediment-gravity flows (Fig. 4). However, Mulder and Alexander (2001) simultaneously consider the density difference between the flow and the ambient water, and hence regard sediment-gravity flows as the 'high-density' end-member in the spectrum of density flows. On the basis of this latter criterion of flow/ambient density

difference, the density flows are categorized as (Fig. 7): 1) hypopycnal flows; 2) homopycnal flows; 3) mesopycnal flows; and 4) hyperpycnal flows.

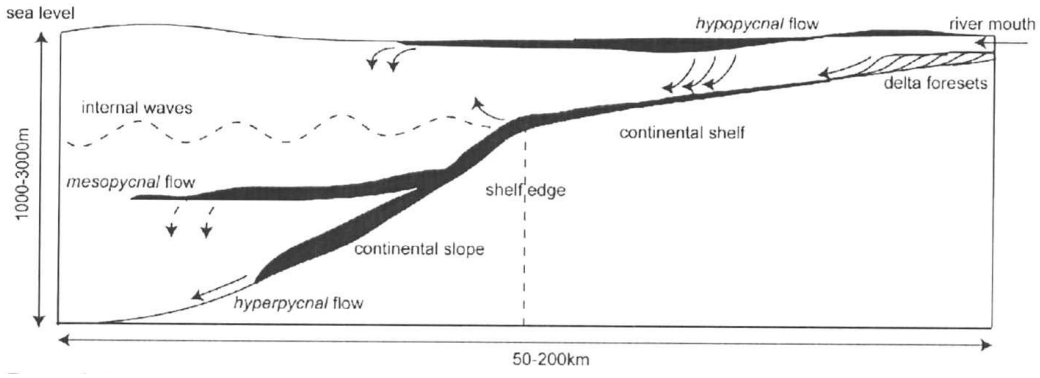

Fig. 7. Four types of density flow and their occurrence in a continental-margin setting (after Mulder and Alexander, 2001). Arrows are used to indicate direction of transport, settling and resuspension of sediment.

In accordance to the original terminology of Bates (1953), flows with a density lower than that of ambient water are called 'hypopycnal' flows (overflows). Hypopycnal flows occur primarily at river mouths, where sediment is dispersed as a buoyant plume (Nemec, 1995). The negative difference in density between the river effluent and the ambient water is usually caused by the differences in temperature and salinity between the river water and the seawater of the basin, which are in this case more significant than the positive difference in density caused by sediment suspension.

At some point off the river mouth, the hypopycnal plume may undergo transition and plunge to the seafloor as the flow density becomes higher than that of the ambient water. The transition is attributed to the mixing of saline ambient water into the flow and a temperature decrease of the river-derived water. The effluent in some cases may plunge directly at the river mouth. Such density flows, with a positive density difference relative to the ambient water, are called 'hyperpycnal' flows (underflows). The term hyperpycnal literally means 'above a density threshold'. In its modern usage, the term refers to sustained turbidity currents ('low-density' sediment-gravity flows *sensu* Mulder and Alexander, 2001) generated directly by the plunging of river effluent.

The other types of density flow are 'homopycnal' and 'mesopycnal' flows (Fig. 7). Homopycnal flow occurs where the flow density approximately equals the density of ambient water, which may mean a relatively low suspension load and an absence of temperature difference between the flow and the ambient fluid, such as where a river flows into a well-mixed lake (Bates, 1953). Mesopycnal flow (intraflow or intrusive flow) occurs when the density of flow is between the densities of the lower and upper layer in a stratified water column, such that the flow effectively spreads along a pycnocline. Mesopycnal flows are particularly important in strongly stratified marine basins where density differences between water layers are considerable (Rimoldi et al., 1996). The hypopycnal and hyperpycnal flows

can thus be regarded as the end-members and predominant varieties of density-flow behaviour. Homopycnal and mesopycnal flows are less common in deep-water basins and require rather special conditions, although a homopycnal stream effluent characterizes virtually all 'shoal-water' deltas, especially if wave-dominated.

As pointed out in the previous section, the duration of turbidity current is an important factor reflecting the intensity of sediment supply and affecting the current's depositional record – the character of the resulting turbidite. From the point of view of their duration, turbidity currents are divided into *surge-type* flows and *sustained* (long-duration) flows (Kneller and Branney, 1995). A sustained turbulent current is defined as a density flow in which the mean velocity at a point remains unchanged over a significant period of time, which means that sustained currents tend to be quasi-steady over significant time periods. In reality, all natural turbidity currents are unsteady on the full time-scale of their duration, although their mean local velocity may remain nearly constant for a period of hours to days (Shepard et al., 1979) or possibly even several weeks to a few months (Nakajima, 2006).

Kneller (1995) distinguished further five classes of depositional turbidity currents on the conceptual basis of flow-velocity steadiness and uniformity (Fig. 8). Depending on whether the flow velocity at a point decreases, remains constant or increases, the current is said – respectively – to be 'waning', 'steady' or 'waxing'. Likewise, depending on whether the flow velocity decreases, remains constant or increases with downflow distance, the current is said to be 'accumulative', 'uniform' or 'depletive', respectively.

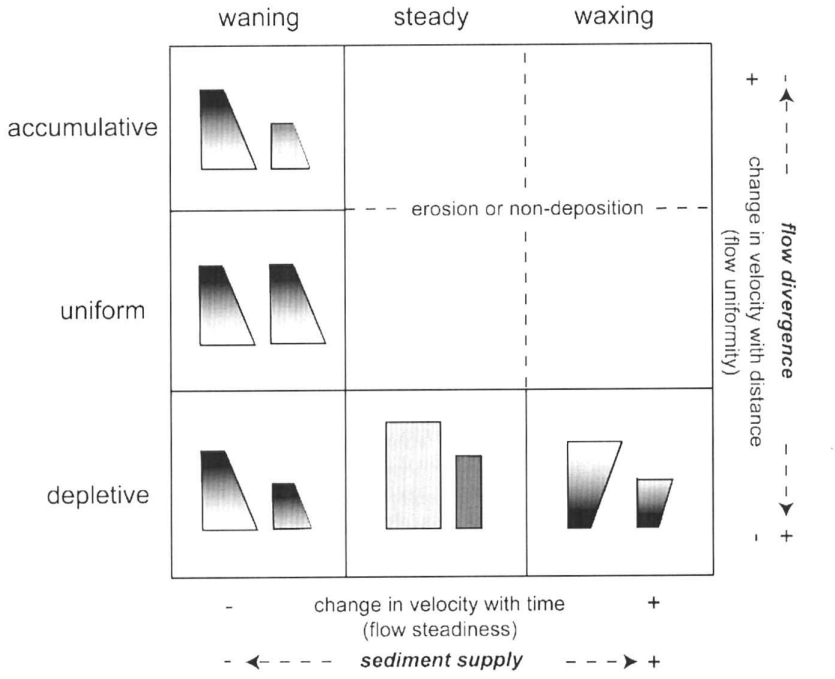

Fig. 8. The flow steadiness/uniformity matrix of Kneller (1995) predicting the depositional and non-depositional behaviours of turbidity current and the expected grain-size trend of the deposit.

According to Kneller (1995), only the waning and the depletive currents are depositional, whereas the steady or waxing uniform and accumulative currents cause erosion and/or sediment bypass (Fig. 8). An important implication of this conceptual scheme is that a surge-type (waning) flow will invariable be depositional, whereas the sustained currents may be subject to waning/waxing pulses and remain quasi-steady for considerable intervals of their duration, which allows for considerable episodes of non-deposition.

The triggering mechanisms — The triggering mechanisms for turbidity currents are closely related to the position of these currents in the continuum of sediment-transporting density flows (Mulder and Alexander, 2001). On the one hand, turbidity currents constitute the relatively dilute end-member of slope failure-generated sediment-gravity flows. As such, turbidity current may evolve by progressive dilution of a denser flow (Kelts and Hsű, 1980; Siegenthaler et al., 1987). The initiation of failure-produced sediment-gravity flows is commonly attributed to slope instability (i.e., remobilization of unconsolidated sediment deposited at the shelf break or in the submarine canyon head). Instability may be induced by earthquakes, volcanic activity or intense internal-wave action at or near the shelf break during storms (Mulder and Alexander, 2001). Turbidity currents may also arise directly from suspension clouds generated by storm activity on a shelf (Prior et al., 1989).

On the other hand, turbidity currents form at river mouths during periods of high discharge, when the sediment-laden effluent plunges directly to the seafloor or when a buoyant (hypopycnal) plume of river effluent transforms into hyperpycnal flow by increasing its density through temperature and salinity diffusion (Wright et al., 1986; Lambert and Giovanoli, 1988; Mulder and Syvitski, 1995, 1996; Nemec, 1995; Johnson et al., 2001). Many modern turbiditic fans show an obvious direct connection to river outlets (Bouma et al., 1985; Kneller and Buckee, 2000; Nakajima, 2006), and it is generally recognized that the growth of turbiditic systems occurs when fluvial systems can discharge their sediment load directly to the shelf break, notably during sea-level lowstands (Mutti, 1985; Shanmugam et al., 1985; Mutti and Normark, 1991; Posamentier et al., 1991; Normark et al., 1993), but possibly also during a highstand if the shelf is traversed by canyons (Nakajima, 2006) or the rate of delta progradation is sufficiently high to reach the shelf break (Burgess and Hovius, 1998). The river-generated turbidity currents are thought to be mainly of a ‘sustained’ (long-duration) type (Kneller and Branney, 1995; Kneller and Buckee, 2000; Nakajima, 2006).

Long-duration turbidity currents can also be generated by multiple, retrogressive slumping of sand bars at river mouths, even when the sediment concentration at the river outlet during a flood run-off is too low to produce directly hyperpycnal turbidity current (Mastbergen and van den Berg, 2003). Retrogressive slumping may also occur on non-deltaic subaqueous slopes if over-steepened by sediment deposition. Some sustained turbidity currents may

form by the confluence of flow surges descending from various parts of the basin slope (e.g., due to an earthquake) and coalescing into a pulsating flow in a basin-floor channel.

Surge-type turbidity currents — Flow surges are phenomena of relatively short duration with no persisting sediment supply. The flow is strongly non-uniform (i.e., its velocity varies with distance) and the development of a flow body is negligible (Middleton, 1966a). Surges are mainly depositional, and usually fail to transport sediment coarser than sand. Sediment is maintained in suspension through the upward component of turbulence and settles gradually, with a significant tractional movement along the bed and the development of bedforms (sedimentary structures) corresponding to the Bouma divisions B and C (Fig. 6) and possibly also including dunes (Allen, 1982). If decelerating too rapidly and temporarily overcharged with suspended load, the flow will dump the excessive load and form the Bouma division A (Allen, 1991) (Fig. 6). The head of the current is erosive, but the degree of substrate erosion generally declines with the flow distance. Erosion may be enhanced when the current reaccelerates due to a steeper slope or flow constriction (Mulder and Alexander, 2001). Surges generally have finite and relatively small volumes, and hence do not produce thick deposits. Most surges are probably triggered by subaqueous slope failures.

The duration of flow surge at a point depends on the scale of the slope-failure event. Small surges (flow thickness of centimetres to metres) have duration of seconds to minutes. Bedforms (sedimentary structures) tend to be rare in the deposits from such surges, because stable bedforms take time to develop, whereas the duration of bedform-generating stable conditions may be too short. In contrast, large surges (flow thickness of tens to hundreds of metres) may last for hours (e.g., the Grand Banks current had duration of over 9 hours; Hughes-Clarke et al., 1990) and develop long bodies, although their flow will be non-uniform and unsteady. The head and frontal part of the body are usually waxing and may be erosive, whereas the rest of the flow body and its tail are waning. These large surges tend to deposit well-developed Bouma turbidites T_{bcd} (Fig. 6)

Sustained turbidity currents — A sustained turbidity current is characterized by flow that persists for a time period over its entire route (i.e., the flow at the source continues, while the current's head has already reached the area of ultimate flow dissipation, which means behaviour comparable to that of an ephemeral river). Kneller and Branney (1995) defined sustained current of the basis of the flow velocity pattern, as a flow in which the mean velocity at a particular point remains unchanged over a significant period of time.

Mulder and Alexander (2001) defined sustained current as 'a steady motion of a particular body in which no boundary (head or tail) is observed' and considered the main difference between surge-type and sustained currents to be 'in the duration of the flow's waxing phase (i.e., the phase of velocity increase at a point)'. None of these notions is strictly true and shall be part of a definition, because: 1) a sustained flow does not necessarily need to be steady;

2) the flow is not infinite and hence will invariable have a head at the beginning and a tail at the end, and may also have several successive heads (volume pulses) ploughing at a higher speed through the preceding flow body; and 3) the waxing phase in sustained flow may not necessarily by longer than in a large surge-type current, depending on where the point of reference is located. As pointed out by Nakajima (2006), a sustained current may involve a series of successive flow pulses, which – if given sufficient distance – may outrun the current and form a powerful head, rendering the current similar in behaviour to a large surge.

In a sustained current, the duration of the passage of the head (or flow front) is very short compared to the passage of the body, which means that the head in such a case is relatively insignificant in determining the nature of the deposit (Kneller and Buckee, 2000). Hyperpycnal density flows are considered to be sustained and quasi-steady, at least for some significant periods, as the flow is fed by river flood discharge with a duration of hours to months. The deposit in such a case is expected to reflect mainly the body flow conditions.

Sustained turbidity currents develop frequently in lakes, where relatively little sediment suspension is needed to produce excess flow density and where the hyperpycnal flow can persist for days or several weeks, depending on the river-flood duration and seasonal weather conditions (Skene et al., 1997; Mulder et al., 1998; see also review by Nemec, 1995). To an observer at a particular point, the phenomenon appears to be steady for a prolonged period, particularly if the discharge varies gradually, although the flow may be uniform or non-uniform over a long distance, depending on the slope and initial momentum.

Sustained turbidity currents have attracted increased interest in the past decade (Nemec, 1990, 1995; Mulder and Syvitski, 1995; Skene et al., 1997; Mulder et al., 2001, 2003; Mutti et al., 2003; Baas et al., 2004), because it has been realized that these flows may be the most plausible explanation for the formation of meandering submarine channels and that the deposits of these flows may constitute large parts of many petroleum reservoirs. Little is known as yet – in terms of diagnostic sedimentological criteria – as to how the deposits of sustained currents can be recognized; how the deposits of hyperpycnal flow (‘hyperpycnites’) can be distinguished from the products of sustained flows of other origin; and to what extent the sustained current’s deposit may reflect the generator’s sediment-flux pattern (e.g., river flood hydrograph) and to what extent the latter can be obliterated in the depositional record by the flow’s own evalution in the basin (e.g., see discussion by Nakajima, 2006).

Mulder and Alexander (2001) have hypothetically suggested that the depositional signatures of sustained turbidity currents may vary from an inversely-graded unit overlain by normally-graded one to various sequences in which the inversely-graded unit is partly or completely eroded before the deposition of normally-graded unit (cf. Fig. 8). At locations where the flow is both steady and depletive, thick deposits with uniform grain size may form. Climbing ripples may develop when the flow velocity is low (i.e., ranging from a few

centimetres to about a metre per second, depending on the flow's Froude number). Climbing ripples may be a major sedimentary feature of sustained-flow turbidites, as they represent the steady migration of a typical hydraulic bedform with a relatively high rate of sediment fallout from suspension. However, all these are intuitive suggestions that need yet to be verified and possibly elaborated by field studies and by laboratory or numerical experiments.

The anatomy of turbidity current — Turbidity currents are described to have a well-defined head, body and tail, and in some cases also a thinner neck linking the head with the body (Middleton, 1966a, b; Simpson, 1987). The dynamics of the head are particularly important, because they set the boundary condition for the current as a whole (Britter and Simpson, 1978). Allen (1971) and Middleton (1993) have pointed out that the head is a locus for erosion, and hence of primary sedimentological importance. The head has an overhanging snout as a result of the no-slip condition at the lower boundary and frictional resistance at the upper boundary (Fig. 9). The no-slip condition requires that the velocity must decrease to zero at the boundary between the fluid and the stationary substrate. At the rear of the head, a series of transverse vortices (billows) develop, identified as a product of the Kelvin-Helmholtz instabilities (Britter and Simpson, 1978).

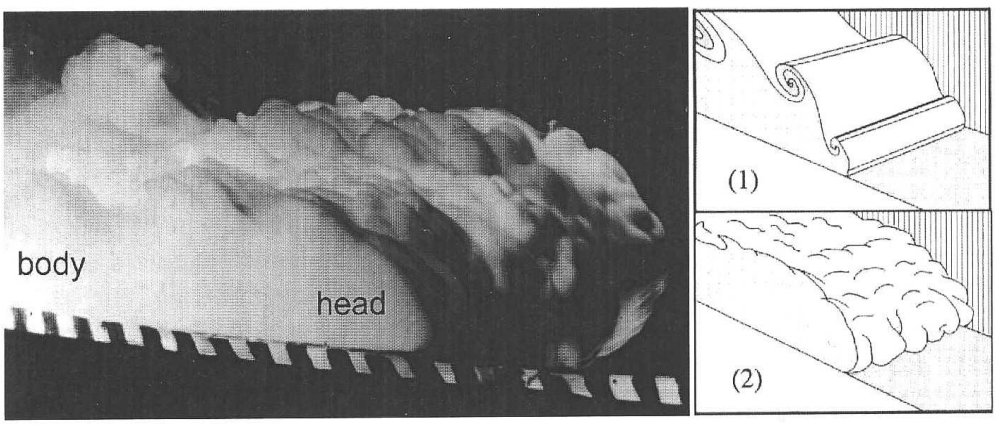

Fig. 9. Laboratory flume photograph showing the frontal part of an experimental turbidity current, with sketches showing the Kelvin-Helmholtz billows (1) and frontal lobes and clefts (2). From Simpson (1987).

Middleton (1966b) performed the first comprehensive set of laboratory experiments on the heads of brine currents and turbidity currents, investigating the effects of slope on the velocity and shape of the head. The downstream velocity in the body of the current, which depends on the slope, has been shown to be up to 30-40 % faster than the head velocity (Middleton, 1966b; Kneller et al., 1997, 1999). Consequently, the head height increases with the slope angle, as the body velocity increases and material moves rapidly from the body into the head (Hopfinger and Tochon-Danguy, 1977; Britter and Linden, 1980; Simpson, 1987). The turbulence structure in the current head (Fig. 10) is dominated by backward shearing at the upper interface against the ambient water, as documented recently in considerable detail

by Kneller et al. (1997, 1999) and Parson (1998). Time series of instantaneous downstream velocity show a clear record of the arrival of the head and the passage of large, low-frequency Kelvin-Helmholtz billows superimposed on a period of quasi-steady motion. Entrainment of ambient water into the head is a function of the densimetric Froude number (Ellison and Turner, 1959), and hence the initial reduced gravity Kneller et al. (1999).

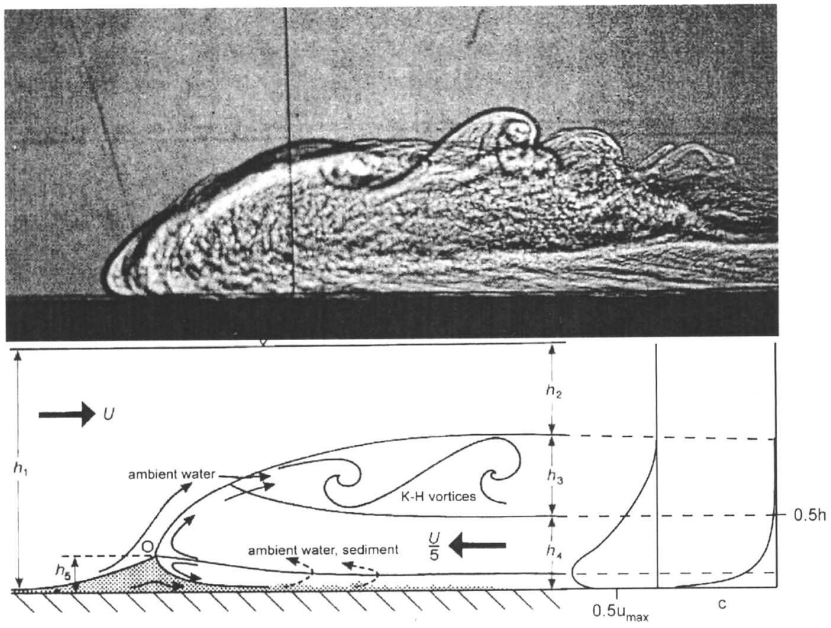

Fig. 10. Laboratory flume photograph and corresponding sketch showing the frontal part of an experimental turbidity current. From Allen (1982).

Few physical descriptions of the body and tail of turbidity currents are available in the literature. Ellison and Turner (1959) describe the body as a region of steady downstream velocity which has a thin, dense layer of fluid near the base of the current. The flow in this region, with an increasing downstream velocity, mixes with the ambient fluid at the upper boundary as an irregular succession of large eddies. In general, the body of turbidity current can be divided into two distinct regions: the lower, dense layer and the region of less-dense fluid that has been mixed out of the head of the current (Britter and Simpson, 1978; Simpson and Britter, 1979). Time series of downstream velocity in the body of quasi-steady gravity currents reveal the presence of large coherent eddy structures which are associated with internal-wave action and advect with the current (Kneller et al., 1997; Best et al., 2001). Instantaneous velocities in the body may be up to 40 % higher than the time-averaged downstream velocity in the body (Buckee et al., 2001) and, therefore, be equivalent to or higher than the instantaneous velocities in the head. This suggests that the body of the current may play a significant role in sediment entrainment, not only its downflow transfer.

The vertical profile of turbidity current is described to have an inner and an outer region, divided by the horizontal velocity maximum. The inner region is bounded at the base by the substrate-flow interface and has a positive velocity gradient, whereas the outer region has a

negative velocity gradient and is bounded at the top by the interface with the ambient water. The inner (lower) region is generally less than half the thickness of the outer (upper) region. The height of the velocity maximum is controlled by the ratio of the drag forces at the upper and lower boundaries. Gravity currents are density stratified; that is, they have a vertical concentration gradient, with a dense, poorly-mixed heterogeneous basal layer and a less dense, mixed homogeneous region above.

Two main types of sediment concentration profiles have been observed in laboratory turbidity currents: 1) a smooth profile is commonly seen in low-concentration, weakly depositional currents (Altikanar et al., 1996; Garcia, 1990, 1994) and in saline gravity currents (Ellison and Turner, 1959); and 2) a steepened concentration profile is commonly observed in erosive currents (Garcia, 1993) or currents interpreted to have a high entrainment rate at the upper boundary (Peakall et al., 2000). Experiments in which the vertical grain-size distribution has been measured (Garcia, 1994) show that fine-grained sediment is more uniformly concentrated in the lower part of the current. From laboratory and field measurements, it is possible to define a standard velocity and concentration profile for equilibrium turbidity currents (e.g., Sloff, 1997; see Fig. 11).

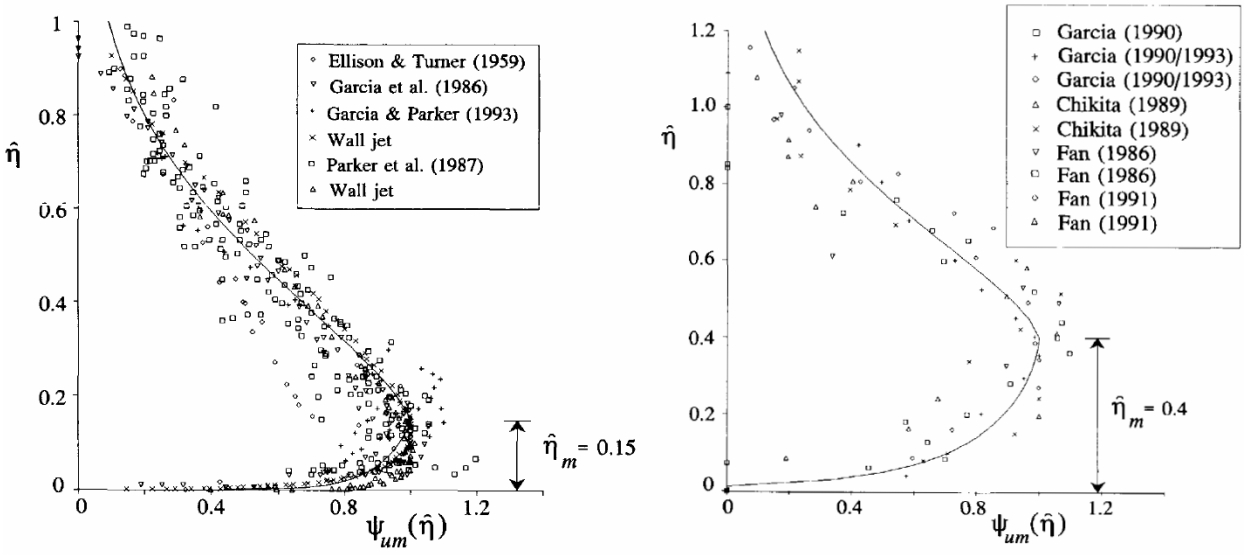

Fig. 11. Measurements of flow velocity in experimental supercritical (left) and subcritical (right) turbidity current, with fitted velocity profiles (Sloff, 1997).

3. METHODOLOGY

3.1. Research methods

Since Kuenen (1937) and Kuenen and Migliorini (1950) first demonstrated experimentally that turbidity currents were the single most important mechanism for the dispersal and deposition of clastic sediment into the deep sea, the corresponding world-wide research has followed three main lines of scientific approach: 1) outcrop-based studies; 2) laboratory experiments; and 3) numerical simulations based on mathematical models of physical processes (Fig. 12).

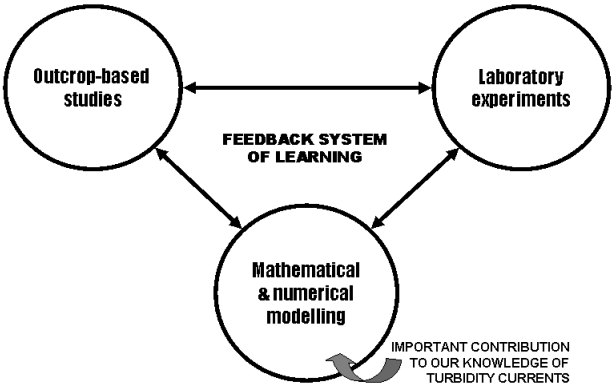

Fig. 12. The main methodological approaches to improving our understanding of turbidity currents.

The research on turbidity currents has been limited by the difficulties of studying them in nature. Turbidity currents may reach velocities of tens of metres per second and heights of hundreds of metres (Heezen and Ewing, 1952), and such giant phenomena are not easy to monitor. Even some modest currents have damaged equipment deployed for the purpose of studying them (Shepard et al, 1979; Zeng et al., 1991; Xu et al., 2004). Therefore, much of what is known about large natural turbidity currents (i.e., those that are really significant in terms of sediment transport to the deep sea) has been inferred from indirect sources, such as submarine cable breaks (Heezen and Ewing, 1952).

The three methodological lines of research on turbidity currents (Fig. 12) are reviewed briefly below, as they form an interlinked feedback system of our growing knowledge on these processes and hence are inseparable from one another. The present study focuses on the mathematical modelling of physical processes and their numerical simulation, and this approach not only supplements the two other lines of research, but necessarily relies on them when it comes to the construction and verification of models.

Outcrop-based studies — Outcrop studies can provide valuable sedimentological data at various scales. After all, the discovery of ’turbidity current’ was based on the rock record

(Sheldon, 1928), and so was also the Bouma sequence defining typical turbidity-current behaviour (Bouma, 1962) (Fig. 6). On a large scale, the vertical successions of turbidites, the lateral changes in the sedimentological characteristics of turbidite beds and their depositional (bedding) architecture can be studied to recognize and understand such stratigraphic elements as depositional lobes, palaeochannels and associated levee/overbank deposits (e.g., Janbu et al., 2007). Similar research, focused on the palaeogeomorphology of turbiditic systems, is being increasingly done on the basis of 3D seismic sections. Hydrodynamic inferences are based on the small-scale observations of turbidite bed characteristics in outcrops and drilling cores. The results of outcrop studies are both revealing and important, providing the crucial link with stratigraphic reality. However, the outcrop-based process interpretations are often hypothetical, speculative and unverifiable. To be reliable, this methodological approach requires a solid theoretical and experimental basis (Fig. 12).

Laboratory experiments — Small-scale laboratory experiments are an alternative and widely used method to study turbidity-current dynamics. Laboratory research has a long tradition and a long list of important studies, beginning with Kuenen's (1937) classic work and and Middleton's (1966a, b, 1967) seminal flume experiments. Some of the most recent experimental studies are compiled by McCaffrey et al. (2001).

Advances in experimental technology in the last decade have increased our insight from broad descriptions of turbidity-current behaviour to details of the turbulence structure in these flows (Kneller et al., 1997, 1999; Parsons, 1998; Best et al., 2001; Buckee et al., 2001). Furthermore, it is the physical laboratory data – along with outcrop evidence – that are needed for the calibration and verification of numerical models (Fig. 12). However, the advantages of laboratory experiments are offset by the scaling problems. The scaling of natural turbidity currents to laboratory level, or vice versa, is a major problem that has been extensively discussed and variously handled in fluid dynamics (e.g., Prandtl, 1952; Duncan, 1953; Middleton and Southard, 1984; French, 1985).

There are basically four different approaches to the scaling of physical models: 1) one-to-one replicas of the field prototype; 2) distorted-scale modelling; 3) non-scaled experimental analogues; and 4) Froude number similarity. The large scale of turbidity currents in the world's oceans renders them impossible to reproduce at a one-to-one basis. Consequently, scaled laboratory experiments are the preferred way to study turbidity currents. The results of non-scaled experimental analogue models of large turbidity currents (Alexander and Morris, 1994), though qualitatively informative, are difficult to apply quantitatively. Distorted-scale experiments with unrealistically steep slopes, for example, have been used to obtain appropriate bed shear stresses (Postma et al., 1988) and may be the best way of reproducing specific aspects of natural currents, although the results necessarily require some caution when it comes to their application.

Froude-scale modelling is based on a similarity approach in which the gravity current is fully characterized by a range of dimensionless variables. As long as the values of these dimensionless variables in laboratory currents are known to be comparable to those in natural currents, the experiment is considered to be adequately scaled and allows the large-scale natural currents to be modelled in the laboratory (Middleton, 1966a). Dimensional analysis depends upon identification of the controlling variables, which are then grouped into a smaller number of dimensionless parameters such as the Froude number. In the Froude-scale modelling of turbidity currents, the densimetric Froude number is used, since the action of gravity depends upon the fractional density difference between the sediment-laden current and the ambient water. In addition, the laboratory turbidity currents must be scaled to the natural system. Under the assumption that the settling velocity adequately describes the particle hydrodynamics, a dimensionless settling velocity is used, which is defined as the ratio of the terminal settling velocity of sediment particles to some velocity scale that is considered characteristic of the current (Middleton, 1966a; Laval et al., 1988).

Electrostatic forces may change the correctly-scaled settling velocity of very fine sediment in experimental studies, and this problem can be solved by using glass beads or silica flour (Parker et al., 1987; Garcia, 1993). Another potential problem is due to the fact that fine sediment is subject to capillary forces once settled. The capillary forces arise from the adhesive intermolecular forces between sediment particles and water, which – in the case of fine-grained sediment – are larger than the cohesive forces between the water molecules (Atkins, 1990). The impact of the capillary forces on substrate erodibility can only be reduced by using larger grain sizes. The settling velocity can also be scaled by using grains of reduced density, but the consequent reduction in the bulk density of the current necessitates an increase in the sediment concentration, which may no longer scale with the whole current behaviour (Middleton, 1966a; Peakall et al., 1996). Therefore, problems invariably arise in reproducing natural-scale flows in a laboratory.

Mathematical modelling and numerical simulations — Mathematical models, if skilfully designed, can provide considerable insights into turbidity-current dynamics. This approach is particularly valuable when it comes to an understanding of the complex system of the controlling variables and their feedback mechanisms operating in turbidity currents. Analytical solutions have been proposed for some aspects of turbidity-current behaviour (Chu et al., 1979), but numerical techniques are by far the most promising tool to understand and predict three-dimensional turbidity currents and their deposits.

Turbidity currents are highly complex phenomena. In most cases, there are more variables than governing equations, and many models thus rely heavily on various simplifying assumptions to circumvent this problem. Observational data from experiments and outcrops provide a means of constraining some of the variables and also allow

calibration and verification for mathematical models (see the learning feedback in Fig. 12). Numerical modelling of turbidity currents spans the full range from simple hydraulic equations and box models to highly complex turbulence models. Numerical models may be used for a wide range of purposes, from the prediction of turbidite geometries and grain-size distribution to the modelling of the vertical structure of turbulence in turbidity current.

Mathematical models may be process-based (deterministic), rule-based (empirical), or a combination of both. A major drawback in the building of a fully dynamic, process-based model is the complexity involved in breaking down the interacting processes into elementary objects and continua to which the Newton laws can be applied exactly: the deductive or process-based approach (Paola, 2000). Yet another, related issue is the large amount of computer power required to run the complex physically-based algorithms that are needed to present the interaction of sediment transport processes with external forces. To limit the complexity, and thus the amount of computing power needed, many models either reduce the number of dimensions or use a rule-based design. The extent to which a 2-D or 2.5-D (depth-averaged or shallow-water) representation may be considered a valid simplification of natural conditions depends largely on the system that is to be modelled.

In the case of turbidity currents, in which turbulent fluxes in the direction transverse to flow play a significant role in the hydrodynamics of the current, a fully three-dimensional representation is preferable. Characteristic of the rule-based and process-response models is a relatively simple description of the processes involved. Instead of a detailed physical description of the processes, their behaviour is translated into rules that capture merely the essence of the processes. The essence in this context refers to these properties of the process that are responsible for the expected response. The expected response is obtained from a combination of field/laboratory observations and detailed knowledge of the physics of the processes involved. Consequently, a quantitative verification (to small-scale experiments) is difficult in many such models, because the very basic translation of the elementary laws of physics includes an implicit up-scaling step, in which the influence of small-scale processes on sedimentation is assumed to be negligible.

3.2. Computational fluid dynamics

The foundations for experimental fluid dynamics were laid in the 17th century France and England (Tokaty, 1971). As a result, the study and practice of fluid dynamics throughout most of the 20th century involved the use of pure theory on the one hand and pure experiment on the other hand. However, this practice changed with the advent of the digital computer in the 1960s, combined with the development of accurate numerical algorithms for solving

physical problems with the use of these computers. This progress has led to a fundamentally new numerical approach in fluid dynamics – the computational fluid dynamics (CFD).

The term 'computational fluid dynamics' refers to the broad topic encompassing the numerical solution – by computational methods – of the governing equations that describe fluid flow: 1) the conservation of momentum (known as the Navier-Stokes equations); 2) the conservation of fluid mass; and 3) any additional conservation equations that may be relevant (Wesseling, 2001). It nicely and synergistically complements the other approaches, but it will never replace any of them, because there will always be a need for theory, facts from nature and laboratory experiments. The future advancement of fluid dynamics rests upon a proper balance of all three methodological approaches (Fig. 12), with computational fluid dynamics helping to interpret and understand the results of theory and experiment, and vice versa. The acronym CFD is now universally accepted and will be used further below.

3.3. Flow-3D™

The CFD has grown over the years from a mathematical curiosity to become an essential tool in almost every branch of fluid dynamics. In its design and development, CFD is considered to be a standard numerical method, widely utilized today in the industrial and academic research. There are many CFD software programs available, and several of them have been evaluated for the present study.

Flow-3D™ is a general purpose CFD software program that employs specially developed numerical techniques to solve the equations of motion for fluids to obtain transient, three-dimensional solutions to multi-scale, multi-physics flow problems. Fluid motion is described with non-linear, transient, second-order partial differential equations. The fluid equations of motion must be employed to solve these equations. A numerical solution of these equations involves approximating the various terms with algebraic expressions. The resulting equations are then solved to yield an approximate solution to the original problem, and this process is called a simulation. The Flow-3D™ approach is to subdivide the flow domain into a computational mesh, or grid of rectangular cells, sometimes called brick elements. The mesh is effectively the numerical space that replaces the original physical one. It provides the means for defining the flow parameters at discrete locations, setting boundary conditions and for developing numerical approximations of the fluid motion equations. Finite difference and finite volume methods form the core of the numerical approach used in Flow-3D™ and they are applied to obtain numerical solutions to differential equations on such meshes (Ames, 1992). The finite difference method is based on the properties of the Taylor expansion and on the straightforward application of the definition of

derivatives. The finite volume method derives directly from the integral form of the conservation laws for fluid motion and, therefore, naturally possesses the conservation properties. In addition, Flow-3D™ is equipped with a range of physical models that expand its capabilities beyond those of many other CFD software programs.

Flow-3D™ has been adopted, because the main physical models needed to simulate turbidity-current dynamics are available in this CFD software, namely: 1) the renormalization-group (RNG) turbulence model; 2) the drift-flux model; 3) the particle model; and 4) the sediment scour model.

RNG turbulence model — Flow-3D™ has implemented a more recent turbulence model based on renormalization-group methods (Yakhot and Orszag, 1986; Yakhot and Smith, 1992). This approach applies statistical methods for a derivation of the averaged equations for turbulence quantities, such as turbulent kinetic energy and its dissipation rate. The RNG-based models rely less on empirical constants, while setting a framework for the derivation of a range of models at different scales. The RNG model uses equations similar to the equations for the k-ε turbulence model (Harlow and Nakayama, 1967), but the equation constants that are found empirically in the standard k-ε model are derived explicitly in the RNG model. Therefore, the RNG model has wider applicability than the standard k-ε model. In particular, the RNG model is known to describe more accurately low-intensity turbulence flows and flows having strong shear regions.

Drift-flux model — In the fluids consisting of multiple components (e.g., fluid/solid particles, fluid/bubbles, fluid/fluid mixtures), where the components have different densities, it is observed that the components can assume different flow velocities. Velocity differences arise because the density differences result in non-uniform body forces. The differences in velocities can often be very pronounced (e.g., large raindrops falling through air or gravel clasts sinking in water). Under many conditions, however, the relative velocities are small enough to be described as a ‘drift’ of one fluid component through the other. Examples are dust in air and sediment in water. The ‘drift’ distinction depends on whether or not the inertia of a dispersed component moving in a continuous component is significant. If the inertia of relative motion can be ignored, and the relative velocity reduced to a balance between a driving force (e.g., gravity force or a pressure gradient) and an opposing drag force between the components, then it is a ‘drift-flux’ approximation. Drift velocities are primarily responsible for the transport of mass and energy. Some momentum may be transported as well, but this is usually quite small and has been neglected in the Flow-3D™ drift model. The idea behind the drift model is that the relative motion between the fluid components can be approximated as a continuum, rather than by discrete elements (e.g., sediment particles). This enhances computational efficiency, as there is no need for a computational tracking of the motion and interaction of discrete elements.

Particle model – The particle model implicitly couples the momentum of discrete-mass particles with a continuous fluid. Particles may have individual masses, which are computed to move under the action of forces that include body forces (gravity), viscous and form drag, and buoyancy forces computed from the local pressure gradient. Particles may bounce or stick to rigid surfaces according to a coefficient of restitution and are transmitted or reflected from granular surfaces with a probability proportional to the fraction of open area. In addition, particles can move in both void and liquid regions and particles may have a variable distribution of density or size. The particle motion is influenced by fluid flow through the drag forces. A fully coupled particle/fluid interaction model is included in the Flow-3D™ to account for interactions between the continuous and dispersed materials that arise due to the drag experienced by the dispersed particles as they move through the continuous fluid. The displacement of fluid volume by particle volume is not taken into account in the particle model, because the particle-fluid momentum exchange is considered to be a more important factor, as it can be significant even when the volume of particles is small. The momentum change in the fluid resulting from the interaction with a particle is expressed as a drag coefficient multiplying the relative velocity between the fluid and the particle. An implicit numerical method is used in the Flow-3D™ to couple the momentum of the particles and fluid together.

Sediment scour model — The sediment scour model predicts the behaviour of packed and suspended sediment within the three-dimensional computational capabilities of Flow-3D™. This model is based on the drift-flux model and presumes that most of the sediment transport is by suspension (Van Rijn, 1987) and advection due to the influence of the local pressure gradient. Suspended sediment originates from inflow boundaries or from erosion of packed sediment. Packed sediment can only move if it becomes eroded into suspended sediment at the packed sediment – fluid interface. Suspended sediment can become packed sediment if the fluid conditions are such that the sediment drifts towards the packed bed more quickly than it is eroded away. At the surface of the packed bed of sediment, the fluid shear stress acts to remove sediment; the empirical Shields number (e.g., Guo, 2002) is used to correlate the minimum shear stress required to lift a sediment particle away from the packed bed interface for various particle diameters and densities. A drag model is used to mimic the solid-like behaviour of sediment particles in regions where the particle concentration exceeds a cohesive solid fraction. The angle of repose controls how steep a slope can be supported by the packed sediment in a quiescent flow region. Where the angle is zero (i.e., a horizontal surface with respect to gravity), the effective critical shear stress is equal to the critical shear stress.

In the present study, these four models have been used in various combinations to simulate turbidity currents on both small (laboratory) and large (natural) scale.

4. RESULTS OF THE PRESENT STUDY

4.1. Small-scale simulations

Most of the numerical simulations have been performed on a scale of laboratory currents, because such small-scale experiments require less computational capacity and — once properly designed — can be run on a laptop computer.

Specific aims — The small-scale numerical experiments performed by the author have had two basic aims: 1) to imitate some pre-selected laboratory experiments and compare the results in order to evaluate as to how realistic the numerical simulations with Flow-3D™ are; and 2) to demonstrate further the software's capacity to simulate a wide range of hydrodynamic aspects of the behaviour of laboratory-type turbidity currents. The design involved a surge-type turbidity current passing through an inclined, channel-like confinement onto an open-space horizontal floor, thus imitating a canyon- or slope channel-confined current expanding upon entering a wide and flat basin floor. The following hydrodynamic aspects of turbidity current have been selected for simulation, using models with mono- or poly-sized sediment-water mixtures:

- a 2D display — in flow-parallel axial section — of the main hydraulic characteristics (bulk density, shear-strain rate, dynamic viscosity, velocity magnitude and its x-y-z components) of a channel-confined current;
- a display of the shear stress, sediment concentration and velocity magnitude for several 'probing stations' in a channel-confined current expanding abruptly on an open-space flat floor;
- the response of the confined and unconfined parts of a current (in terms of its velocity magnitude, turbulent shear stress and sediment concentration) to changes in such principal controlling parameters as the channel slope angle, sediment grain size, bed (floor) roughness and initial sediment concentration;
- a display of sediment grain-size segregation of a current (using a flow run with poly-sized sediment suspension);
- the velocity time series for a surge-type and a sustained turbidity current; and
- the responses of turbidity current to obstacles and to a hydraulic jump at the channel outlet (using flow runs with sediment scour model).

The experimental setup adopted for the small-scale simulations is as described below (Fig. 13), and the basic physical conditions assumed for the flow-simulation runs referred to further in the thesis are listed in Table 1.

Table 1. Initial conditions of the experimental flow-simulation runs discussed in the present thesis.

Run	Channel slope (°)	Grain size (mm)	Sedim. concentr. (vol.%)	Bed roughness	Flow-3D™ models employed
2	1	0.15	25	clay	Drift-flux, RNG and particle
6	5	0.15	25	clay	Drift-flux, RNG and particle
9	10	0.15	25	clay	Drift-flux, RNG and particle
11	20	0.15	25	clay	Drift-flux, RNG and particle
12	5	0.6	25	clay	Drift-flux, RNG and particle
14	5	0.15	25	clay	Drift-flux, RNG and particle
16	5	0.0375	25	clay	Drift-flux, RNG and particle
28	5	0.15	5	clay	Drift-flux, RNG and particle
29	5	0.15	15	clay	Drift-flux, RNG and particle
35	5	0.15	25	smooth	Drift-flux, RNG and particle
37	5	0.15	25	medium silt	Drift-flux, RNG and particle
39	5	0.15	25	v. fine sand	Drift-flux, RNG and particle
47	5	0.15	25	clay	Sediment scour and RNG

The experimental setup — The experimental setup has been designed to imitate the laboratory flow experiments performed by Baas et al. (2004) in a flume facility of the Utrecht University's Department of Earth Sciences. The laboratory setup consisted of a straight, inclined channel leading from the feeder tank to a horizontal expansion table, all submerged in freshwater (Fig. 13). The channel was 4 m long, 0.22 m wide and 0.50 m deep, and had a variable, adjustable inclination. The expansion table was 3.5 m long, 3 m wide and free of sidewalls to minimize flow reflections, and was located in a walled tank 1 m deep and 4x4 m^2 in area (Fig. 13). The laboratory setup had three flow-probing stations (see Ott locations in Fig. 13), but only a few of the flow runs provided data sufficiently 'pure' (non-averaged) and of a sufficient time span to be used for comparative purposes.

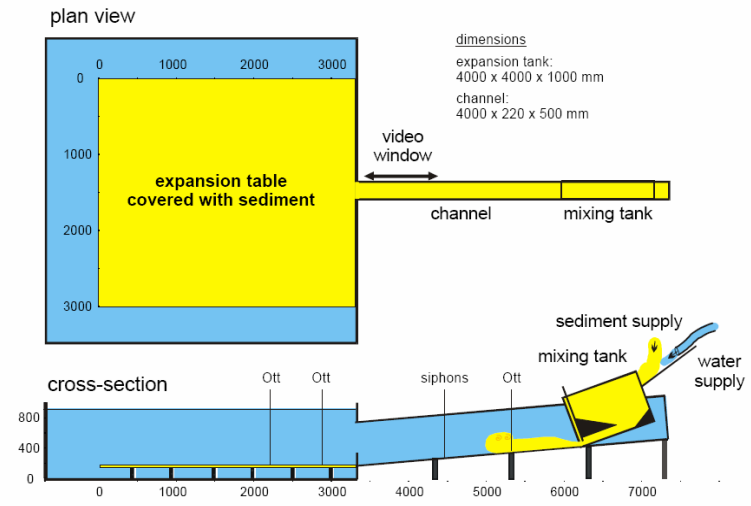

Fig. 13. The laboratory experimental setup in plan view (top) and in longitudinal cross-section (bottom); Ott = position of current-meter. From Baas et al. (2004).

In the laboratory experiments, sediment was mixed with fresh water in a specially constructed mixing tank at the upstream end of the channel (Fig. 13). The water was supplied to the mixing tank by a slurry pump at a constant discharge of 5.2 or 7.8 dm^3/s. The sediment was supplied to the mixing tank by means of a conveyor belt, which allowed for up to 15 seconds of constant slurry discharge. Three types of sediment were used in the laboratory experiments: 1) a moderately well-sorted, coarse silt composed of spherical glass beads (mean size 0.040 mm); 2) a well-sorted, very fine-grained sand composed of spherical glass beads (mean size 0.069 mm); and 3) a moderately sorted, fine-grained natural sand (mean size 0.235 mm).

The downstream wall of the mixing tank had a basal gate with adjustable height. The gate in all experiments was opened to a height of 3.5 cm, which provided a cross-sectional outflow area of 63 cm^3. The outflow was balancing the inflow of sediment and water to the mixing tank, with a steady hydraulic pressure head in the tank. The constant head assured practically a quasi-steady slurry yield for a period of 11-14 seconds, because about 1-4 seconds were needed to fill up the mixing tank and stabilize the pressure head. The initial flow surge with up to 15 second duration was followed by a waning flow with approximately similar time span, when the slurry level and pressure head in the mixing tank were falling and the outflow was progressively slower and less dense.

The channel had its walls and floor covered with Perspex™ plates, and a default inclination of the channel floor was 5^o. In the experiments with fine-grained sand, the floor plate had a smooth surface and was hoisted on sockets to increase the slope angle to 8.6^o. In this way, deposition in the channel was kept at a minimum. The plate was placed directly on the channel bottom in the experiments with very fine-grained sand and coarse silt, to decrease the slope angle to 3.7^o and reduce the buoyancy flux. A further reduction of the latter factor was achieved by decreasing the water supply from 7.8 to 5.2 dm^3 and by gluing fine-grained sand onto the Perspex™ plate to increase the flow drag. The expansion table (Fig. 13) was covered with a 3-cm layer of loose sediment to allow for possible erosion by the turbidity current. For a particular run, this layer consisted of the same sediment as used in the mixing tank.

Flow velocities were measured at three probing stations along the path of the turbidity currents, using Ott-type current-meters. The Ott-meters consist of simple propellers (diameter 2.5 cm) connected to a counter registering the number of rotations in a predefined time interval. One current-meter was positioned in the channel, about 60 cm downflow from the mixing tank's gate, and two others measured the flow velocity in the expansion tank at 46 and 126 cm away from the channel outlet (Fig. 13). These last two locations corresponded roughly to the position of hydraulic jump and the area of maximum deposition, respectively.

The flows in the channel were fully confined (< 50 cm thick), and all the current-meters were recording the downflow velocity at a height of 3 cm above the floor. The counters were monitored by video recording, which allowed calculation of mean flow velocities for time periods down to 0.5 seconds to be made and velocity time series to be obtained.

The suspensed sediment concentration in the mixing tank ranged from 14 to 35 vol.%. The sediment concentration in the turbidity currents was lower due to the vertical expansion of the flow upon its release from the mixing tank. A vertical array of four vacuum-operated siphon tubes was used to measure sediment concentration in the steadily-supplied first half of turbidity current. The siphon tubes were located at a distance of 144 cm from the mixing-tank gate (Fig. 13), at equally-spaced heights within 6 cm above the floor. The tubes had a diameter of 1 cm, which was sufficient to measure sediment concentrations of up to 15 vol.%. At higher concentrations, the sediment particles began to clog the tubes and the concentration measurements became unreliable. The grain-size distribution of sediment in every tube-derived sample was estimated by using a Malvern laser particle sizer. These data allowed the sediment grain-size distribution within the turbidity current to be estimated.

Before and after a flow run, the topography of the sediment surface on the expansion table was measured using automated laser and acoustic bed profilers. The horizontal relief resolution was chosen at 2 cm and the vertical resolution was at 0.4 mm. The topographic data provided information on the thickness of the turbidity-current deposit, and on the shape, size and orientation of the resulting morphological features. These data also allowed an estimation of the volume of eroded and deposited sediment.

Standard lacquer peels were used to preserve vertical cross-sections of the fine-sand deposits of turbidity currents, and these samples allowed the vertical and horizontal changes in sedimentary structures to be recognized. Samples of deposit were collected for grain-size analysis with the use of Malvern laser particle sizer. The samples typically had a thickness of 0.5-1.0 cm and a volume of 1-2 cm^3. The grain-size data were used to construct 2D contour plots of the vertical and horizontal distribution of mean grain sizes in the deposit.

Simulation of the Utrecht laboratory flows — Only a few of the laboratory datasets were sufficient to simulate particular turbidity currents for comparative purposes, and the only non-averaged flow characteristic measured in the laboratory was the downflow (x-direction) velocity component. The first attempt was to simulate faithfully the whole laboratory setup, including the supply of water and sediment and their blending in the mixing tank. The drift-flux, RNG and particle models (see earlier section 3.3) were employed in the simulations. The results of these simulations came out to be close to the laboratory data in terms of their pattern (see examples in Figs. 14 and 15), but appeared to be insufficiently 'identical' in terms of the magnitude (value range). The likely reason of this discrepancy is that laboratory setup is difficult to simulate in an exact manner (e.g., mixing tank pressure conditions).

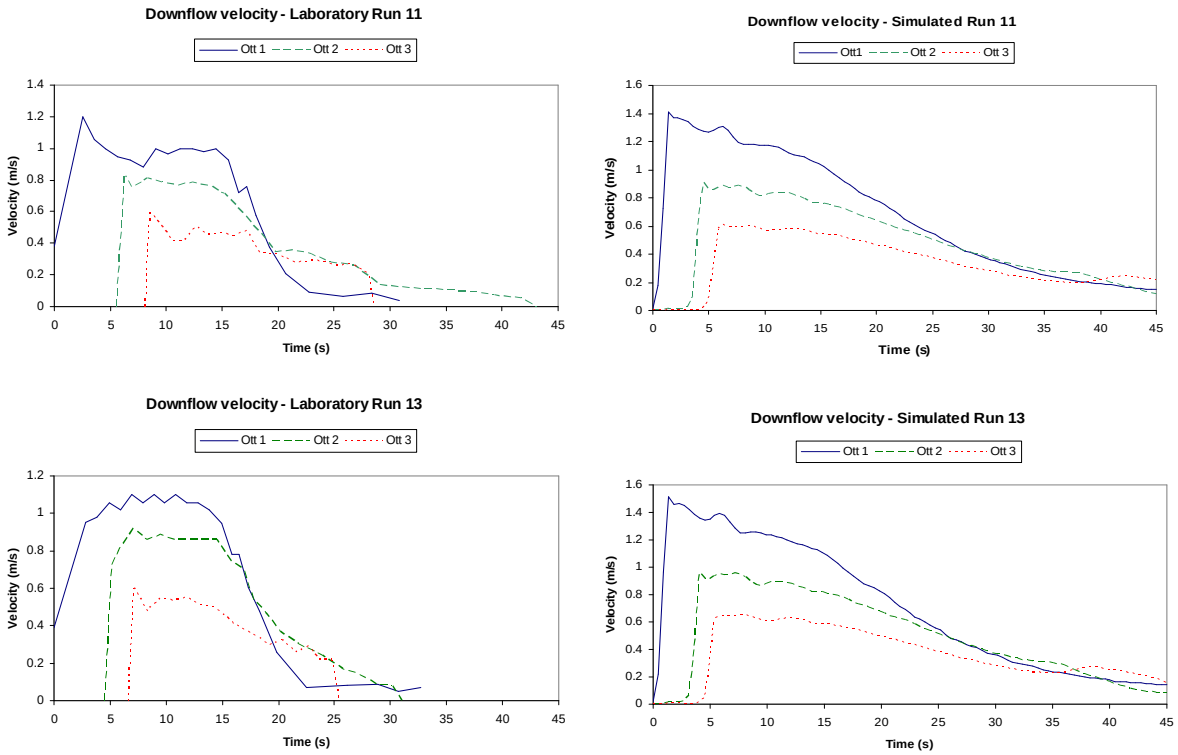

Fig. 14. Plots of the downflow (x-direction) velocity component measured in the laboratory Run 11 (Baas et al., 2004) and calculated in a numerical simulation of the same laboratory run, including the sediment-water mixing in the feeder tank.

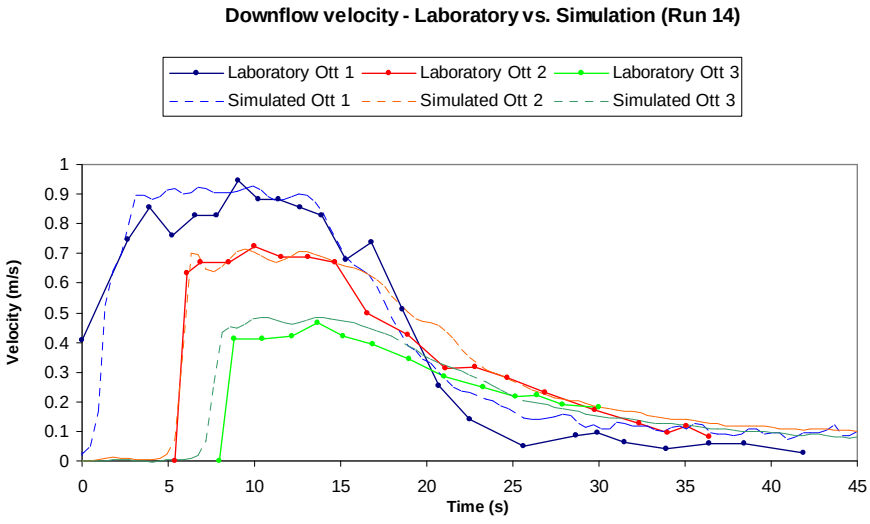

Fig. 15. Plots of the downflow (x-direction) velocity component measured in the laboratory Run 13 (Baas et al., 2004) and calculated in a numerical simulation of this laboratory run, with the sediment-water mixing process in the feeder tank disregarded and the outflow taken directly as the initial boundary condition.

Simulations were then repeated without imitating the tank mixing and slurry-release phase and by taking the 15-second slurry discharge from the tank directly as the inflow boundary condition. The results came out to be nearly identical with the laboratory measurements in terms of both the pattern and the value range (see example in Fig. 15).

Taking into account the problem with the simulation of mixing-tank conditions, it is concluded that the numerical flow simulations imitate the laboratory flows quite satisfactorily and that the Flow-3D™ software can be used to perform realistic flow simulations. The following several series of simulations were then intended to demonstrate some of the insights in flow dynamics that the Flow-3D™ can provide.

Display of flow characteristics — There are several possible ways of displaying and monitoring the hydraulic characteristics of a turbidity current, and the one most commonly used is a vertical section parallel to the flow axis. Examples of such a display for a wide range of flow characteristics of channel-confined turbidity current (see setup in Fig. 13) are shown as time series in Figures 16-23. The data are from Run 47 (Table 1), which is basically identical to Run 6, but employing the sediment scour model (see section 3.3).

The current's characteristics displayed include: flow velocity components in the x, y and z directions (Figs. 16-18); velocity magnitude (Fig. 19) also known as speed, is defined as the quadratic mean of the three-dimensional x-y-z velocity components; macroscopic (bulk) density variation in the current (Fig. 20 and 21); and the current's dynamic viscosity (Fig. 22) and shear-strain rate (Fig. 23). The values of any particular variable can be displayed as a spectrum of colours or as discrete isolines, as shown for the flow bulk density in Figures 20 and 21, respectively.

The Flow-3D™ allows similar displays to be made at any pre-selected time interval, and such cartoon strips can readily be converted into animations. The accuracy of the calculation of flow characteristics and hence also the quality of display obviously depend on the resolution of the computational grid employed. In the present examples (Figs. 16-23), a resolution of 5 cm in all three directions has been used to optimize the computer capacity required. If necessary, the colour spectrum of display can be altered; its values can be kept constant or – as in the present case – allowed to change with the range of values in each successive display; and also either the horizontal or the vertical dimension of the display can be exaggerated relative to the other.

Velocity can alternatively be displayed in the form of vectors (arrows), and more than one flow characteristics can simultaneously be displayed as a combination of colour spectrum, coloured points (markers or tracer particles), isolines and vectors.

Multi-location display of flow characteristics — A Flow-3D™ simulation can be designed in such a way that any of the flow characteristics is monitored, as a time series, at a number of pre-selected locations. This kind of flow display – for a channel-to-plain experimental design (Fig. 24) and three selected variables (flow velocity magnitude, turbulent shear stress and sediment concentration) probed 7.5 cm above the floor – is shown in Figure 25.

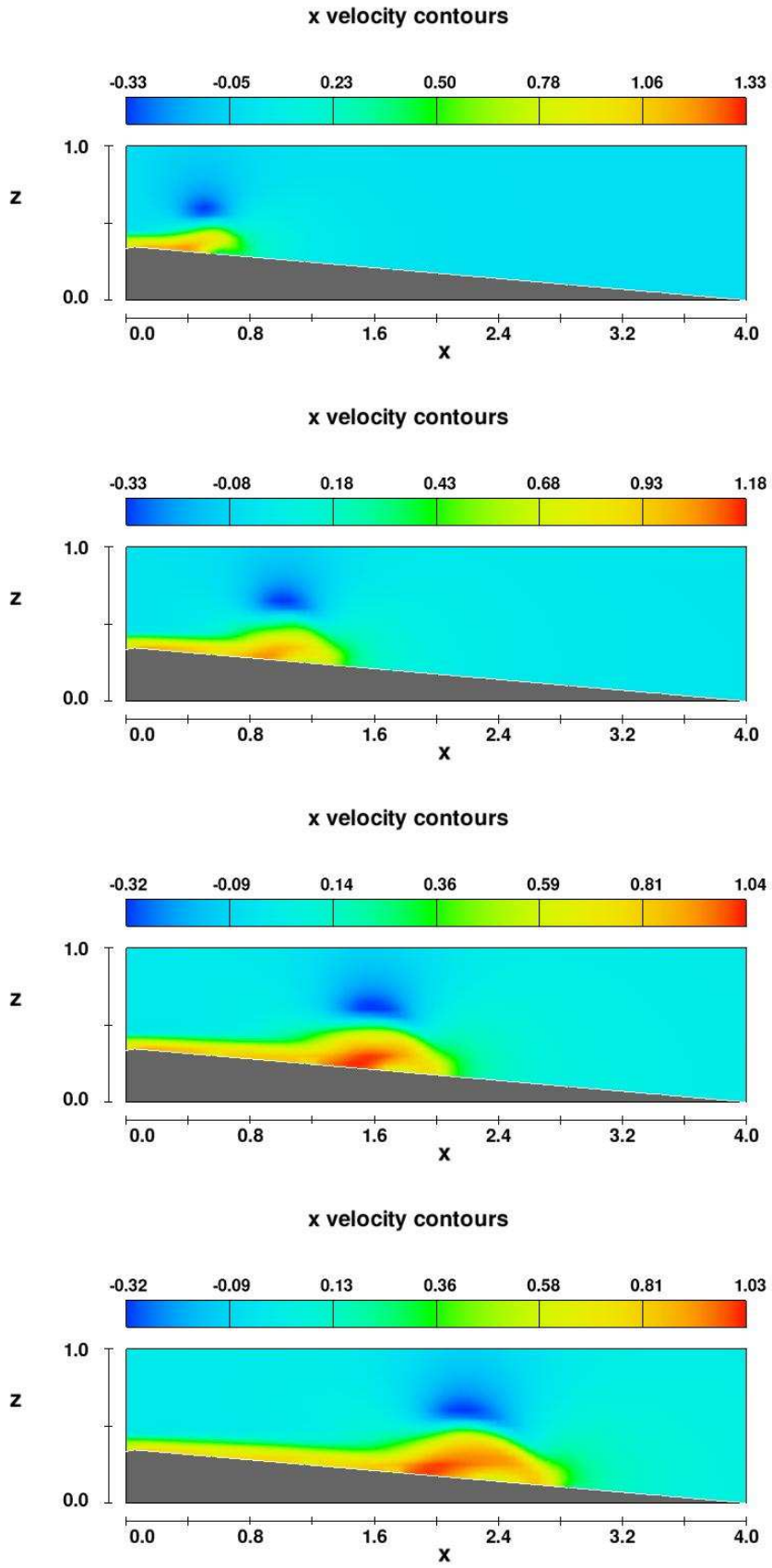

Fig. 16. Time series of the flow velocity component in x-direction (downflow) in Run 47. The eight snapshots correspond to flow time of 1 to 8 sec. The channel has an inclination of 5^{o}. The scales units on x and z axes are metres and the velocity is m/sec (note that the scale values change from snapshot to snapshot).

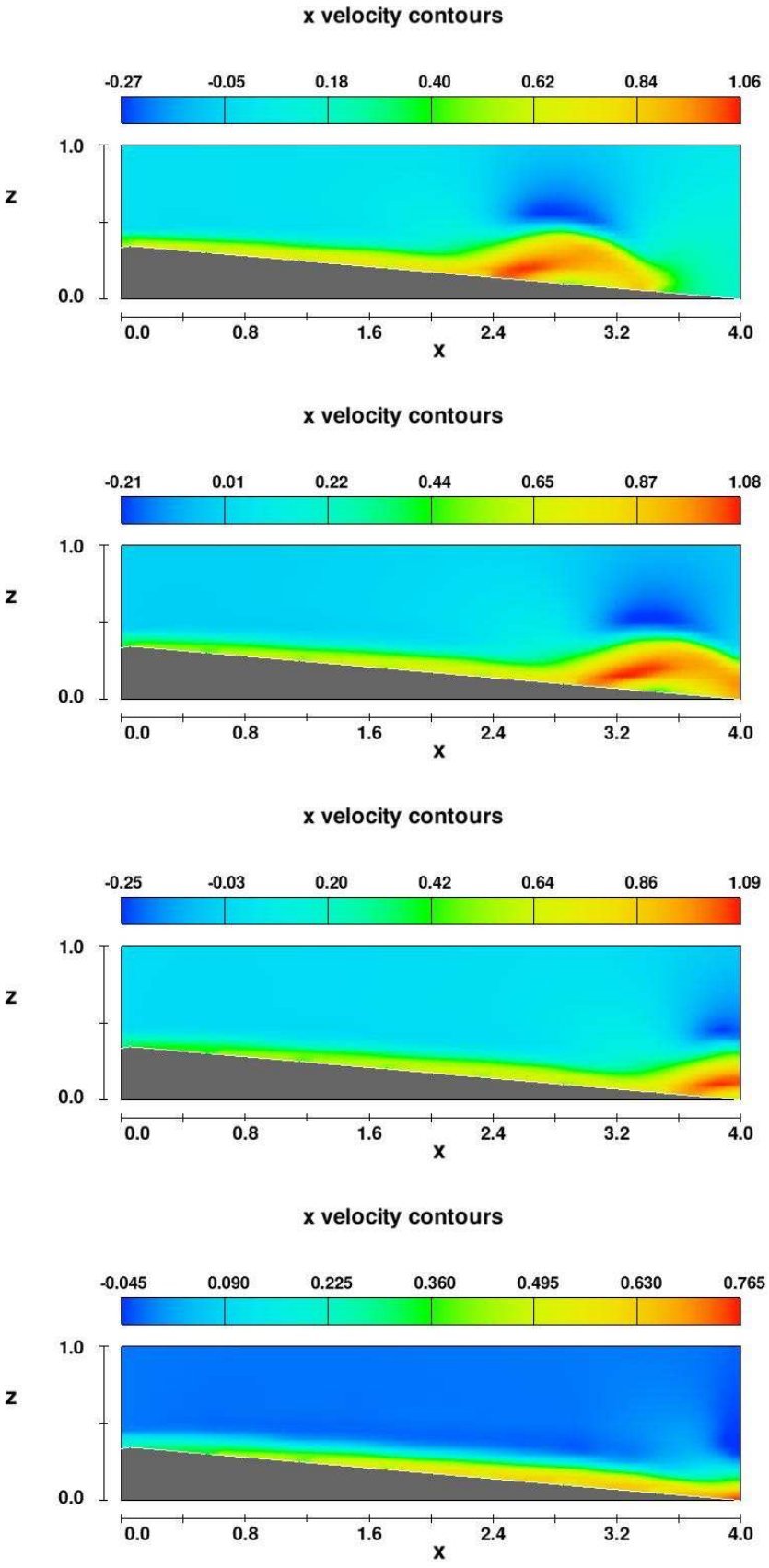
x velocity contours
-0.27 -0.05 0.18 0.40 0.62 0.84 1.06
1.0
z
0.0
0.0 0.8 1.6 2.4 3.2 4.0
x
x velocity contours
-0.21 0.01 0.22 0.44 0.65 0.87 1.08
1.0
z
0.0
0.0 0.8 1.6 2.4 3.2 4.0
x
x velocity contours
-0.25 -0.03 0.20 0.42 0.64 0.86 1.09
1.0
z
0.0
0.0 0.8 1.6 2.4 3.2 4.0
x
x velocity contours
-0.045 0.090 0.225 0.360 0.495 0.630 0.765
1.0
z
0.0
0.0 0.8 1.6 2.4 3.2 4.0
x

Fig. 16 (cont.)

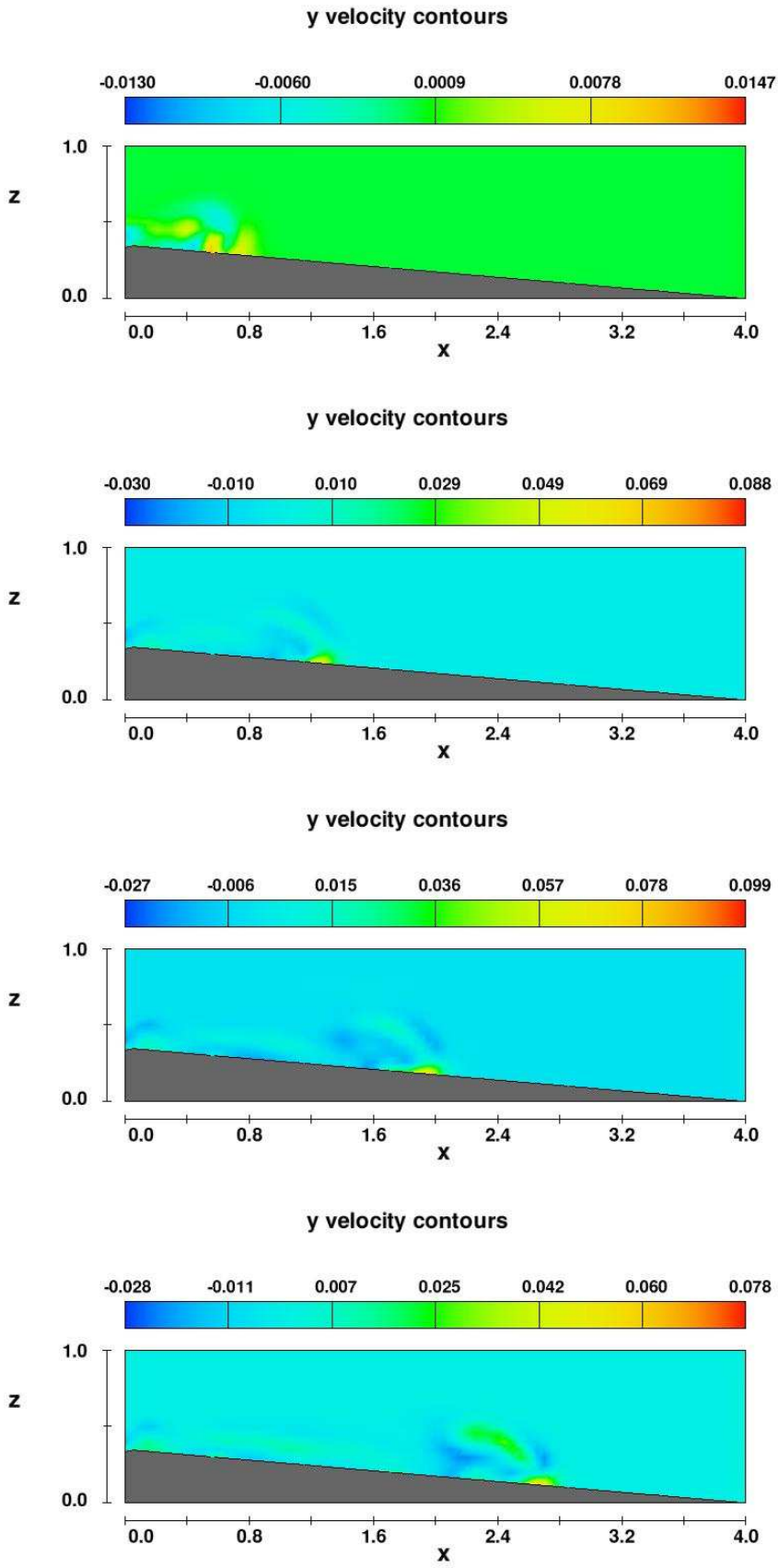

Fig. 17. Time series of the flow velocity component in y-direction (transverse to flow) in Run 47. The eight snapshots correspond to flow time of 1 to 8 sec. The channel has an inclination of 5°. The scales units on x and z axes are metres and the velocity is m/sec (note that the scale values change from snapshot to snapshot).

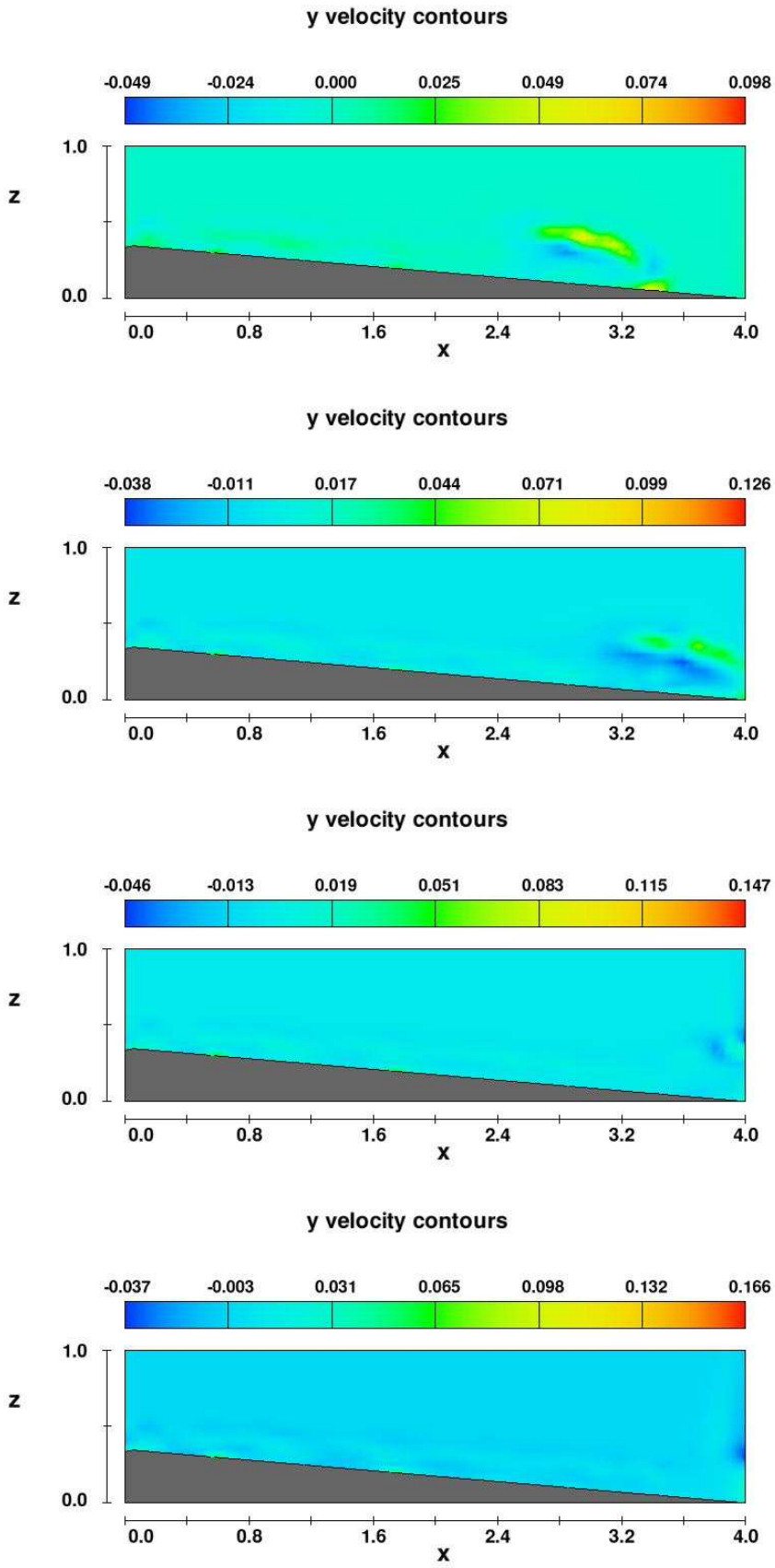
y velocity contours
-0.049 -0.024 0.000 0.025 0.049 0.074 0.098
1.0
z
0.0
0.0 0.8 1.6 2.4 3.2 4.0
x
y velocity contours
-0.038 -0.011 0.017 0.044 0.071 0.099 0.126
1.0
z
0.0
0.0 0.8 1.6 2.4 3.2 4.0
x
y velocity contours
-0.046 -0.013 0.019 0.051 0.083 0.115 0.147
1.0
z
0.0
0.0 0.8 1.6 2.4 3.2 4.0
x
y velocity contours
-0.037 -0.003 0.031 0.065 0.098 0.132 0.166
1.0
z
0.0
0.0 0.8 1.6 2.4 3.2 4.0
x

Fig. 17 (cont.)

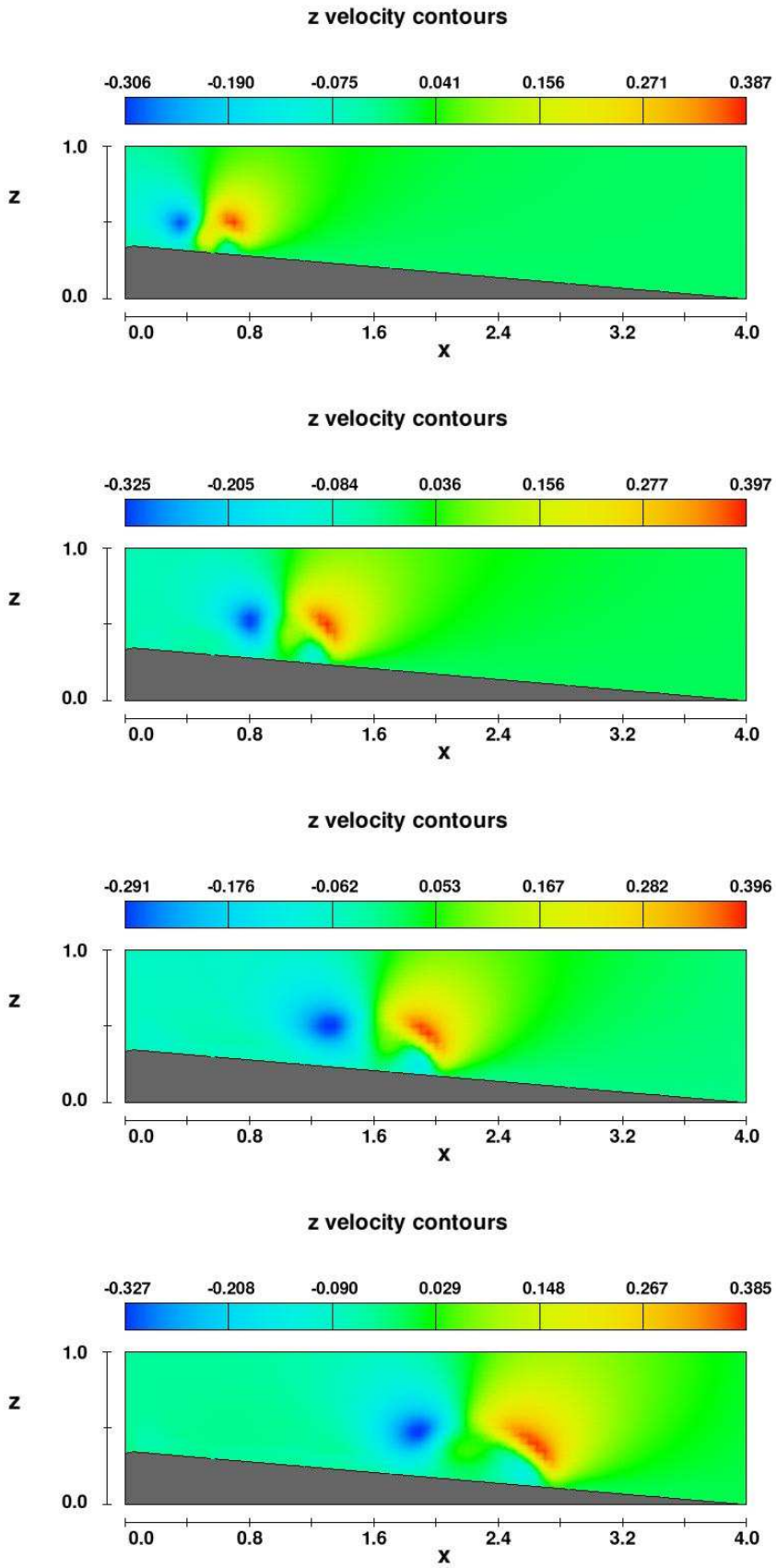

Fig. 18. Time series of the flow velocity component in z-direction (vertical) in Run 47. The eight snapshots correspond to flow time of 1 to 8 sec. The channel has an inclination of 5^{o}. The scales units on x and z axes are metres and the velocity is m/sec (note that the scale values change from snapshot to snapshot).

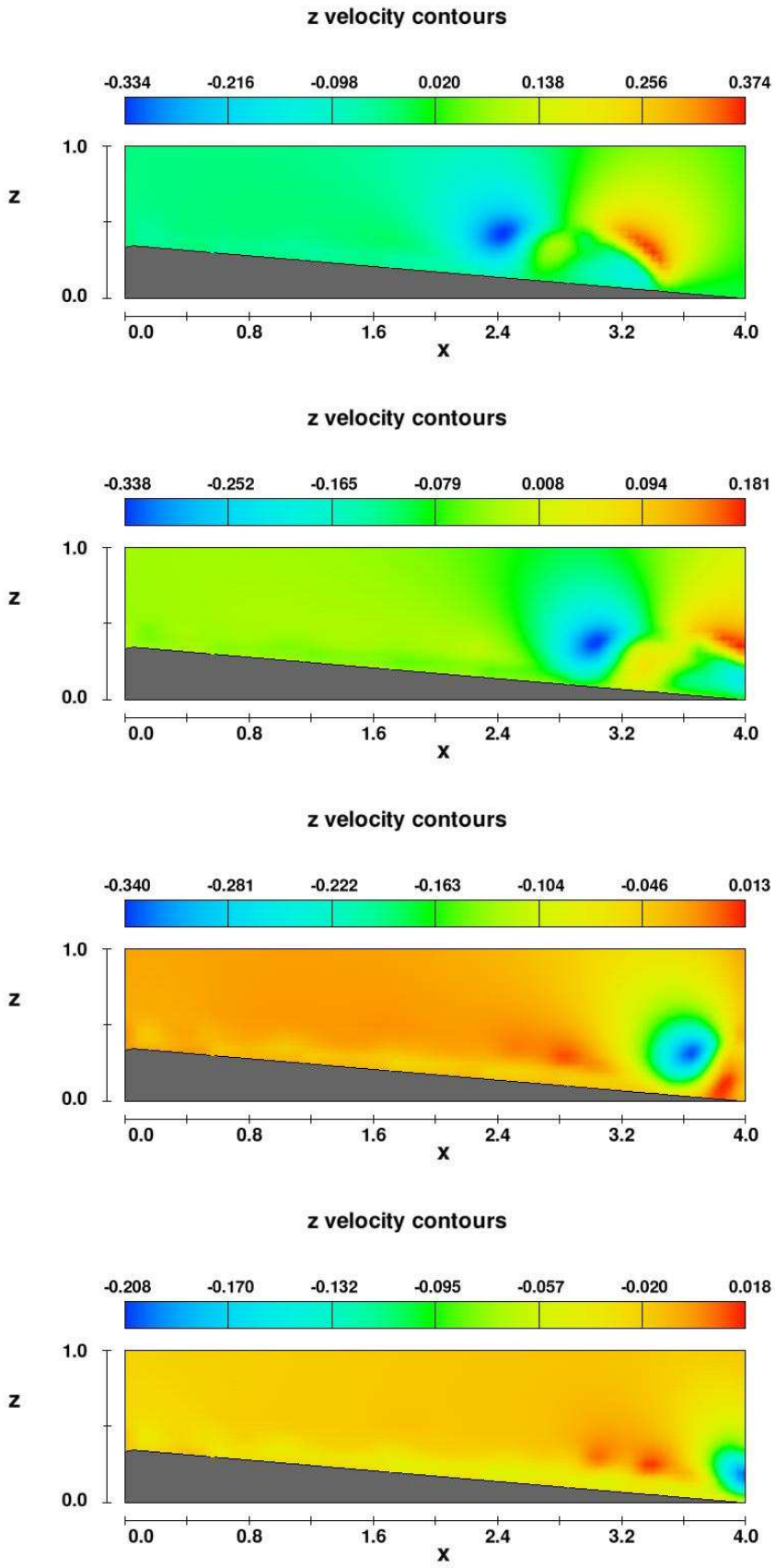
z velocity contours
-0.334 -0.216 -0.098 0.020 0.138 0.256 0.374
1.0
z
0.0
0.0 0.8 1.6 2.4 3.2 4.0
x
z velocity contours
-0.338 -0.252 -0.165 -0.079 0.008 0.094 0.181
1.0
z
0.0
0.0 0.8 1.6 2.4 3.2 4.0
x
z velocity contours
-0.340 -0.281 -0.222 -0.163 -0.104 -0.046 0.013
1.0
z
0.0
0.0 0.8 1.6 2.4 3.2 4.0
x
z velocity contours
-0.208 -0.170 -0.132 -0.095 -0.057 -0.020 0.018
1.0
z
0.0
0.0 0.8 1.6 2.4 3.2 4.0
x

Fig. 18 (cont.)

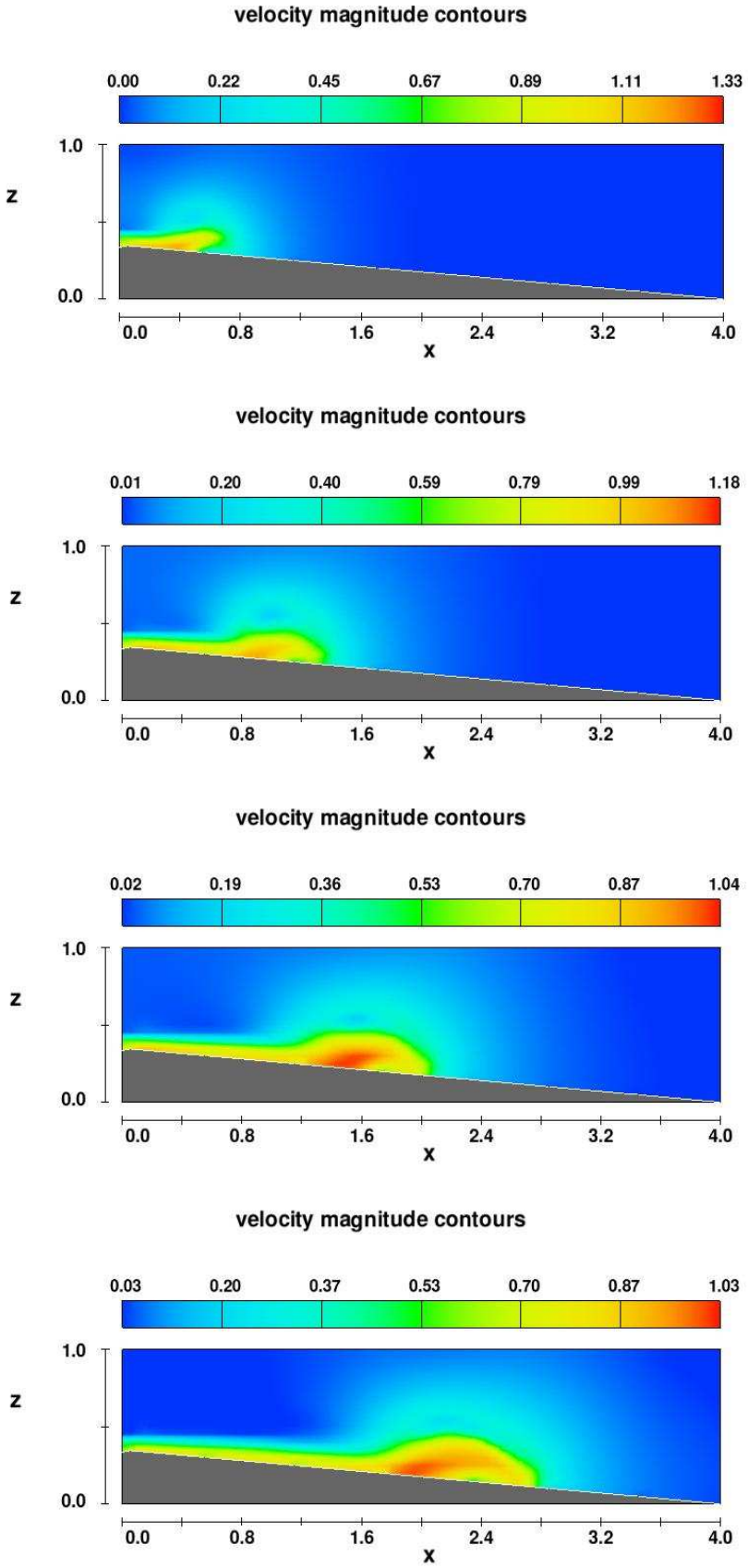

Fig. 19. Time series of the flow velocity magnitude in Run 47. The eight snapshots correspond to flow time of 1 to 8 sec. The channel has an inclination of 5^{o}. The scales units on x and z axes are metres and the velocity is m/sec (note that the scale values change from snapshot to snapshot).

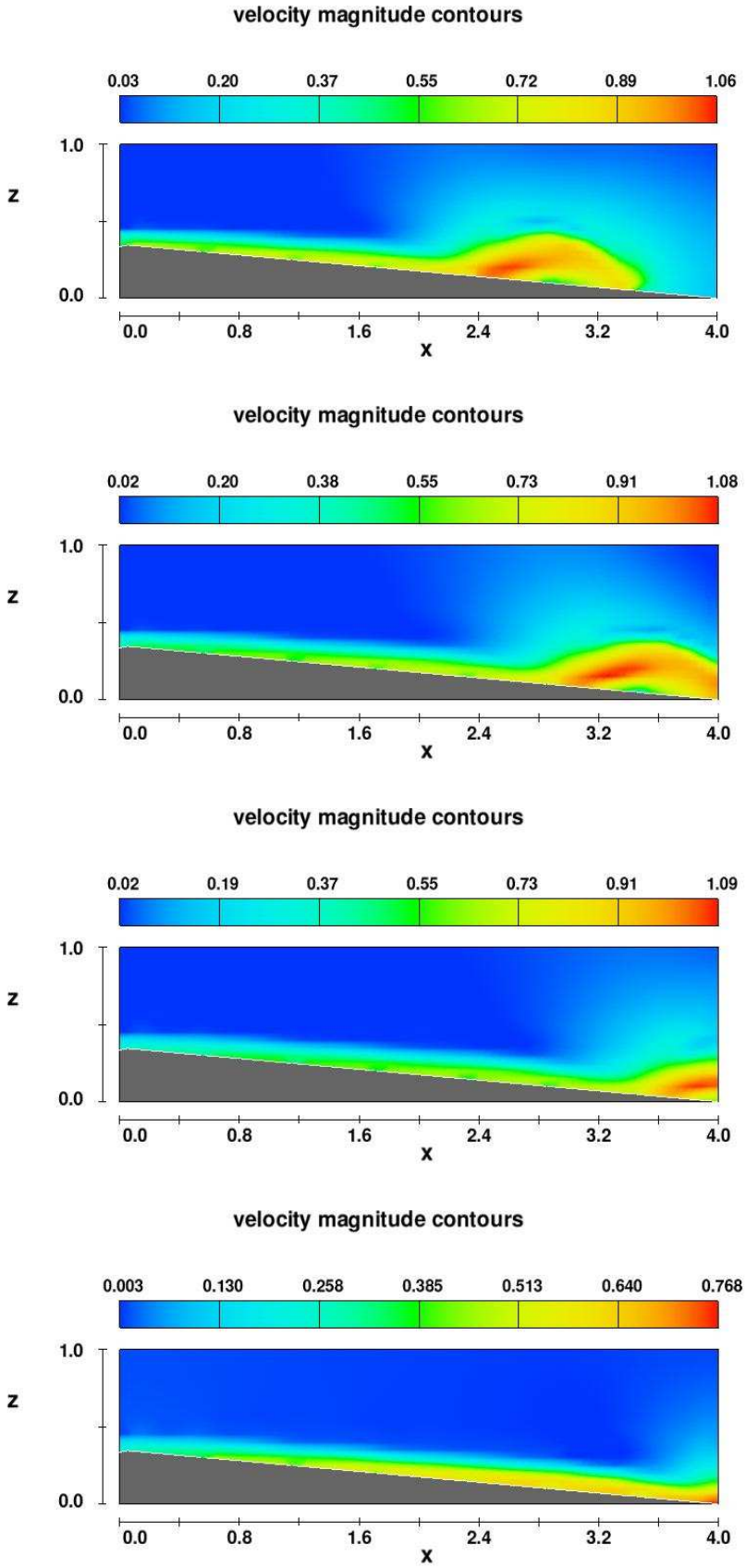
velocity magnitude contours
0.03 0.20 0.37 0.55 0.72 0.89 1.06
1.0
z
0.0
0.0 0.8 1.6 2.4 3.2 4.0
x
velocity magnitude contours
0.02 0.20 0.38 0.55 0.73 0.91 1.08
1.0
z
0.0
0.0 0.8 1.6 2.4 3.2 4.0
x
velocity magnitude contours
0.02 0.19 0.37 0.55 0.73 0.91 1.09
1.0
z
0.0
0.0 0.8 1.6 2.4 3.2 4.0
x
velocity magnitude contours
0.003 0.130 0.258 0.385 0.513 0.640 0.768
1.0
z
0.0
0.0 0.8 1.6 2.4 3.2 4.0
x

Fig. 19 (cont.)

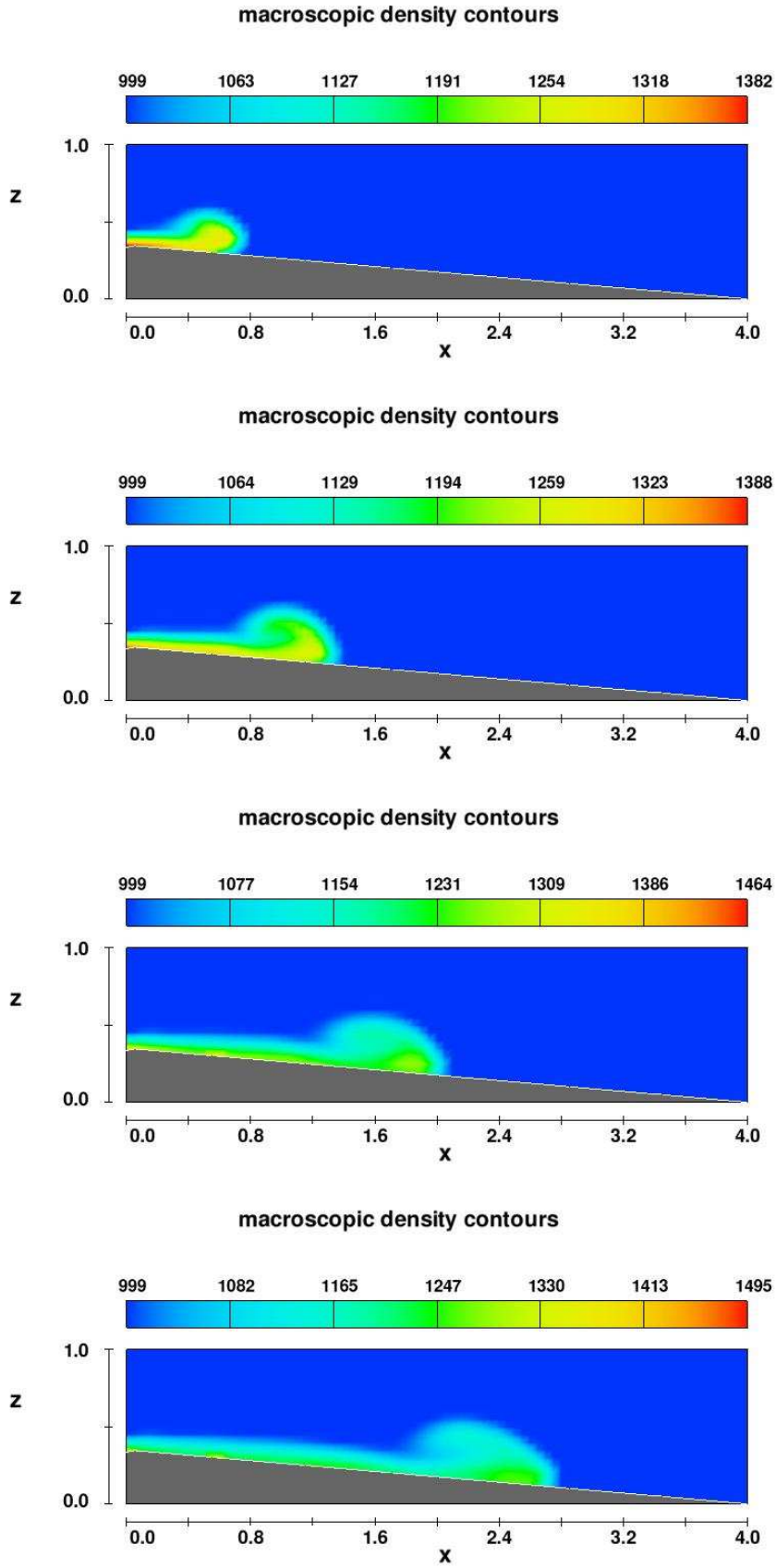

Fig. 20. Time series of the current's macroscopic (bulk) density in Run 47. The eight snapshots correspond to flow time of 1 to 8 sec. The channel has an inclination of 5^{o}. The scales units on x and z axes are metres. The density is in kg/m^3 and its values are displayed as a colour spectrum (note that the scale values change from snapshot to snapshot).

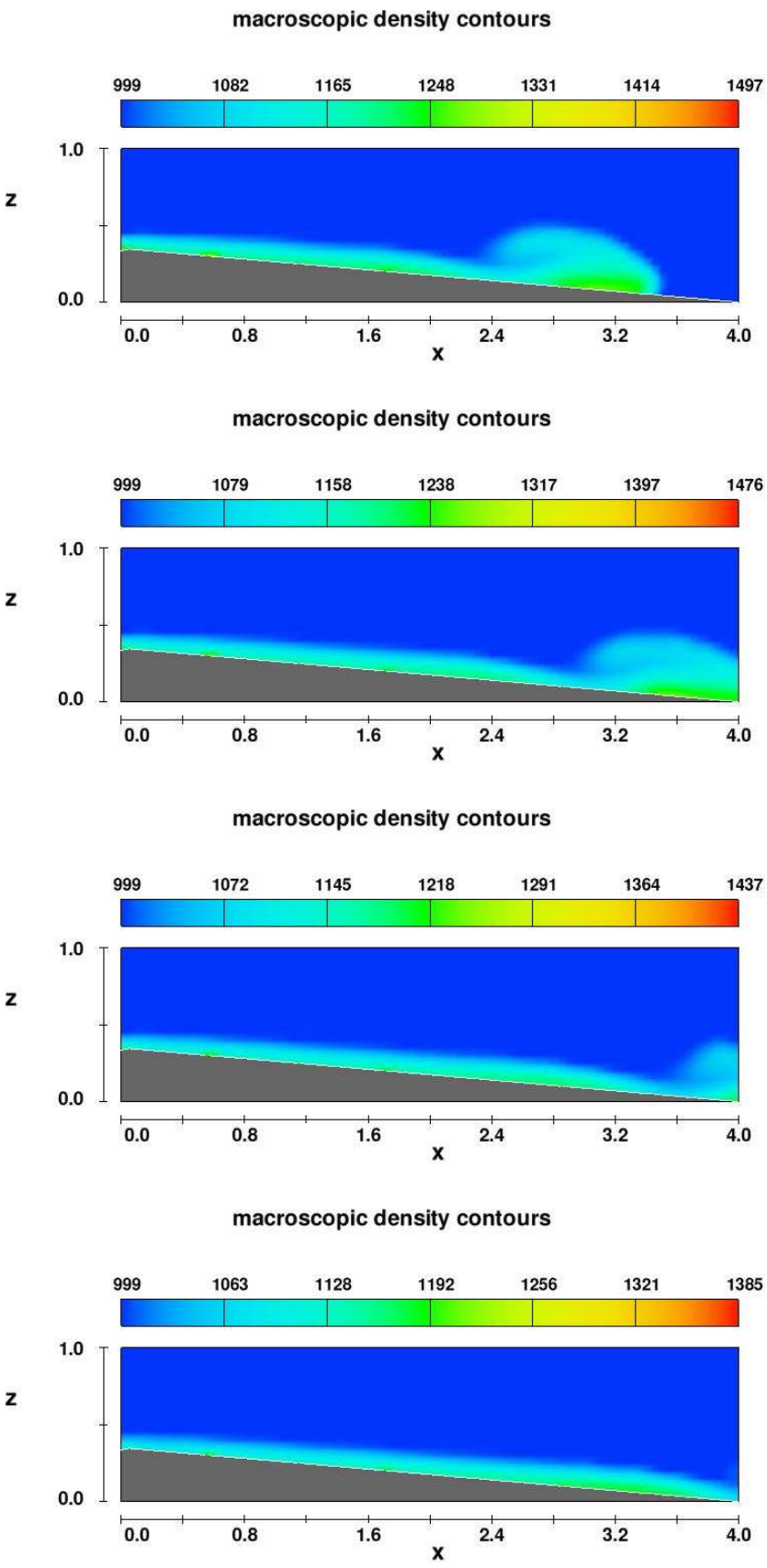
macroscopic density contours
999 1082 1165 1248 1331 1414 1497
1.0
z
0.0
0.0 0.8 1.6 2.4 3.2 4.0
x
macroscopic density contours
999 1079 1158 1238 1317 1397 1476
1.0
z
0.0
0.0 0.8 1.6 2.4 3.2 4.0
x
macroscopic density contours
999 1072 1145 1218 1291 1364 1437
1.0
z
0.0
0.0 0.8 1.6 2.4 3.2 4.0
x
macroscopic density contours
999 1063 1128 1192 1256 1321 1385
1.0
z
0.0
0.0 0.8 1.6 2.4 3.2 4.0
x

Fig. 20 (cont.)

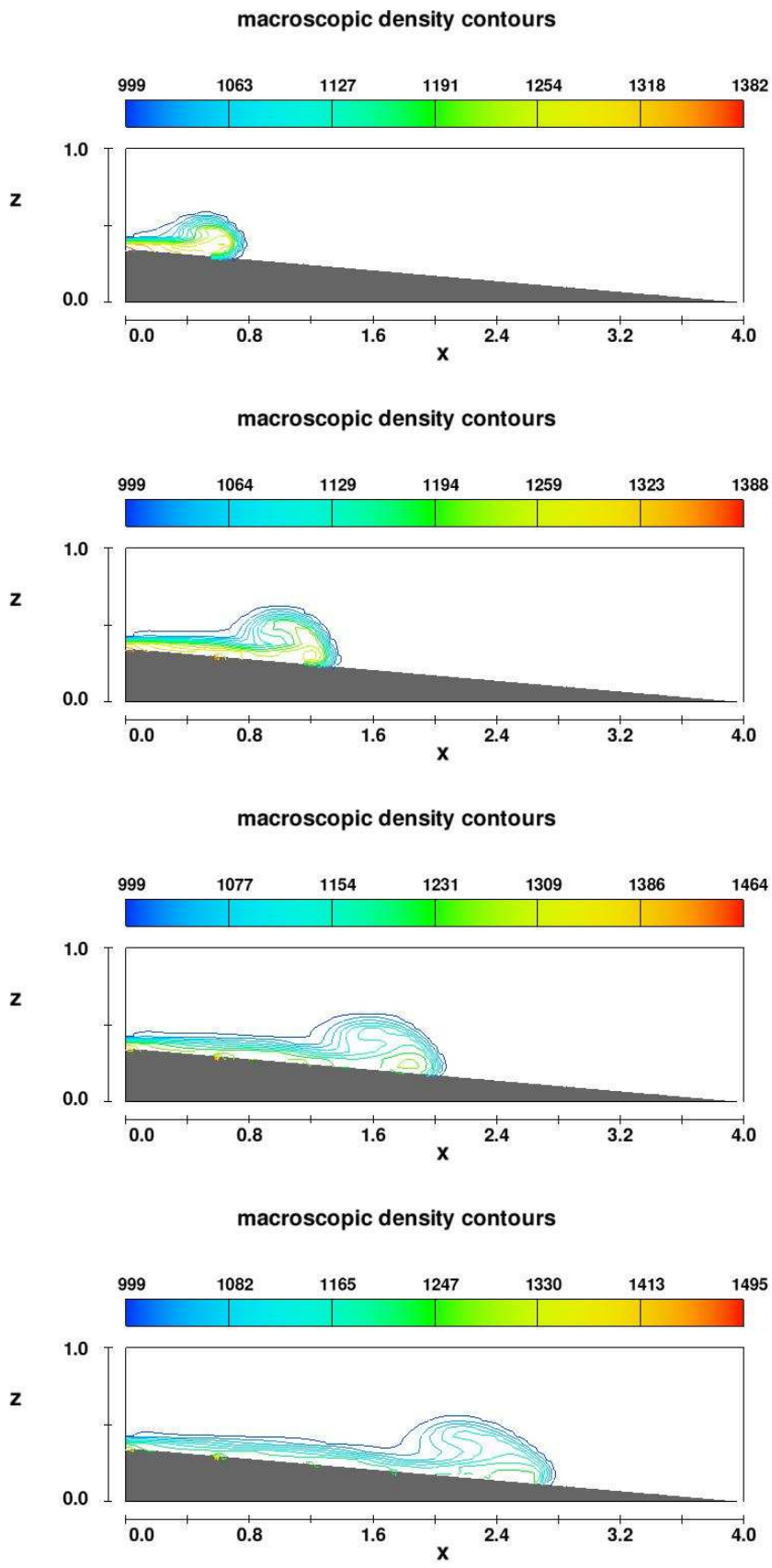

Fig. 21. Time series of the current's macroscopic (bulk) density in Run 47. The eight snapshots correspond to flow time of 1 to 8 sec. The channel has an inclination of 5°. The scales units on x and z axes are metres. The density is in kg/m^3 and its values are displayed here as discrete isolines (note that the scale values change from snapshot to snapshot).

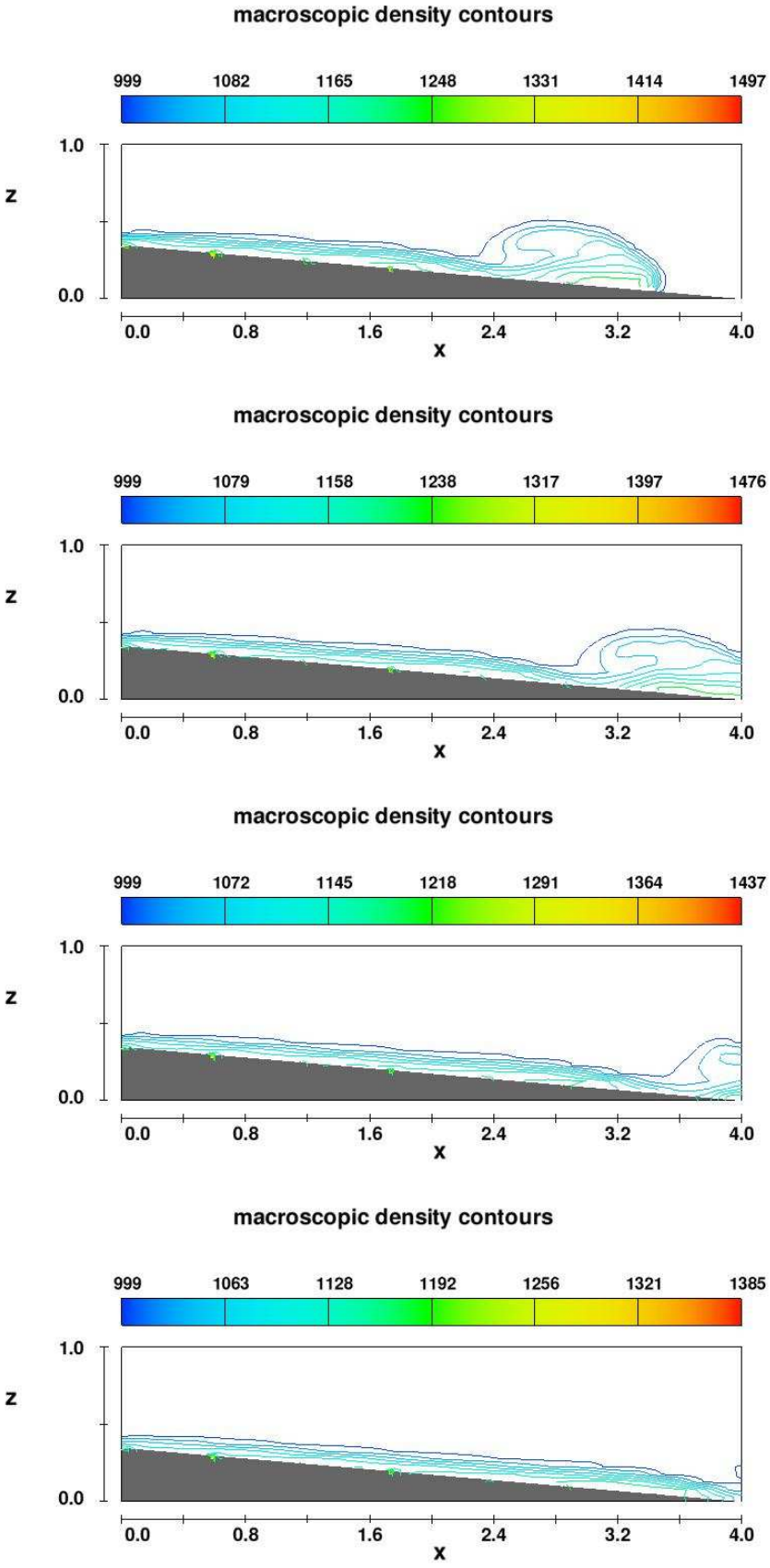
macroscopic density contours
999 1082 1165 1248 1331 1414 1497
1.0
z
0.0
0.0 0.8 1.6 2.4 3.2 4.0
x
macroscopic density contours
999 1079 1158 1238 1317 1397 1476
1.0
z
0.0
0.0 0.8 1.6 2.4 3.2 4.0
x
macroscopic density contours
999 1072 1145 1218 1291 1364 1437
1.0
z
0.0
0.0 0.8 1.6 2.4 3.2 4.0
x
macroscopic density contours
999 1063 1128 1192 1256 1321 1385
1.0
z
0.0
0.0 0.8 1.6 2.4 3.2 4.0
x

Fig. 21 (cont.)

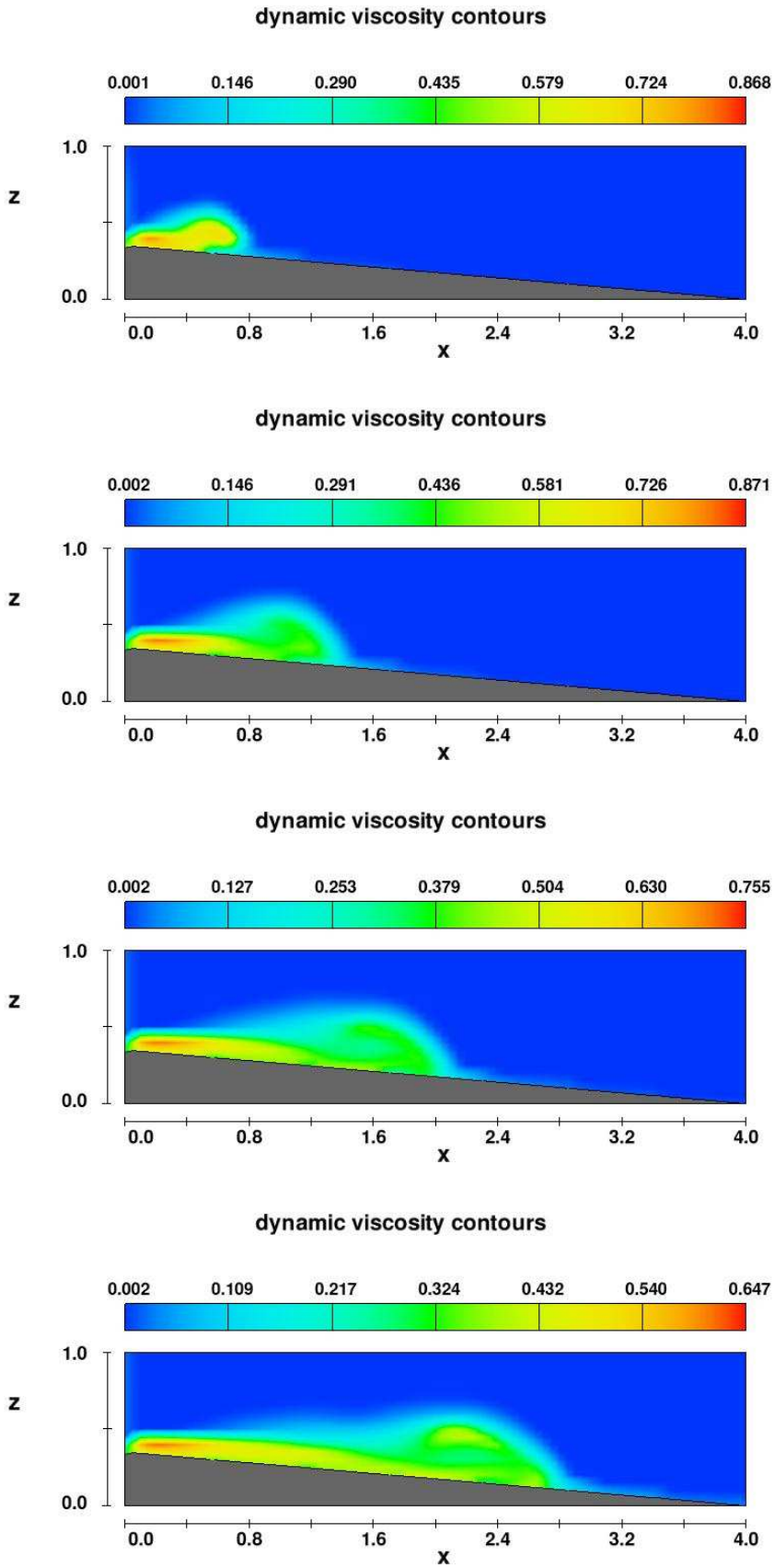

Fig. 22. Time series of the current's dynamic viscosity in Run 47. The eight snapshots correspond to flow time of 1 to 8 sec. The channel has an inclination of 5^{o}. The scales units on x and z axes are metres. The viscosity is in kg/m/s (1 kg/m/s = Pa·s = 10 poise) and its values are displayed as a colour spectrum (note that the scale values change from snapshot to snapshot).

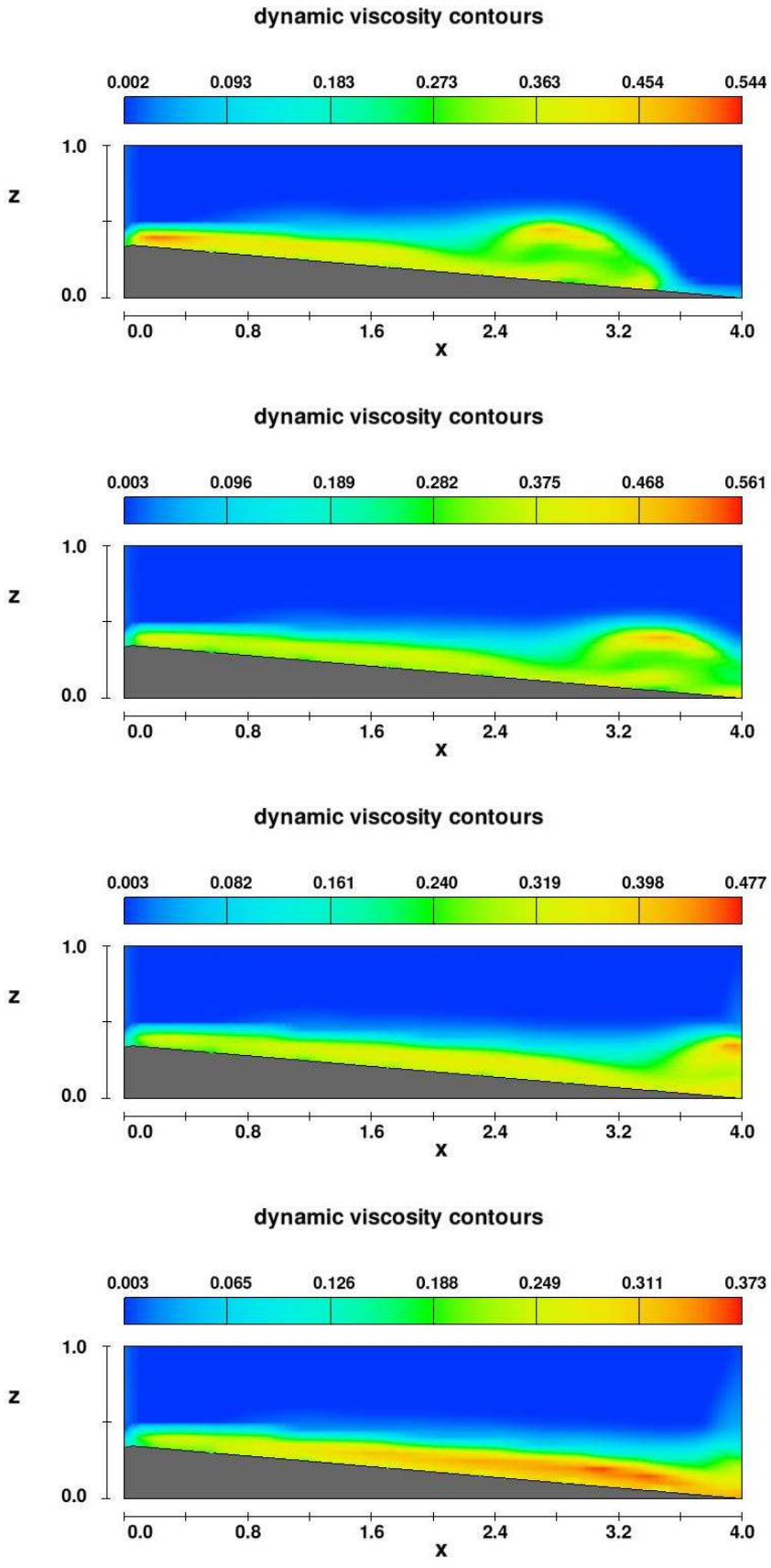
dynamic viscosity contours
0.002
0.093
0.183
0.273
0.363
0.454
0.544
1.0
z
0.0
0.0
0.8
1.6
2.4
3.2
4.0
x
dynamic viscosity contours
0.003
0.096
0.189
0.282
0.375
0.468
0.561
1.0
z
0.0
0.0
0.8
1.6
2.4
3.2
4.0
x
dynamic viscosity contours
0.003
0.082
0.161
0.240
0.319
0.398
0.477
1.0
z
0.0
0.0
0.8
1.6
2.4
3.2
4.0
x
dynamic viscosity contours
0.003
0.065
0.126
0.188
0.249
0.311
0.373
1.0
z
0.0
0.0
0.8
1.6
2.4
3.2
4.0
x

Fig. 22 (cont.)

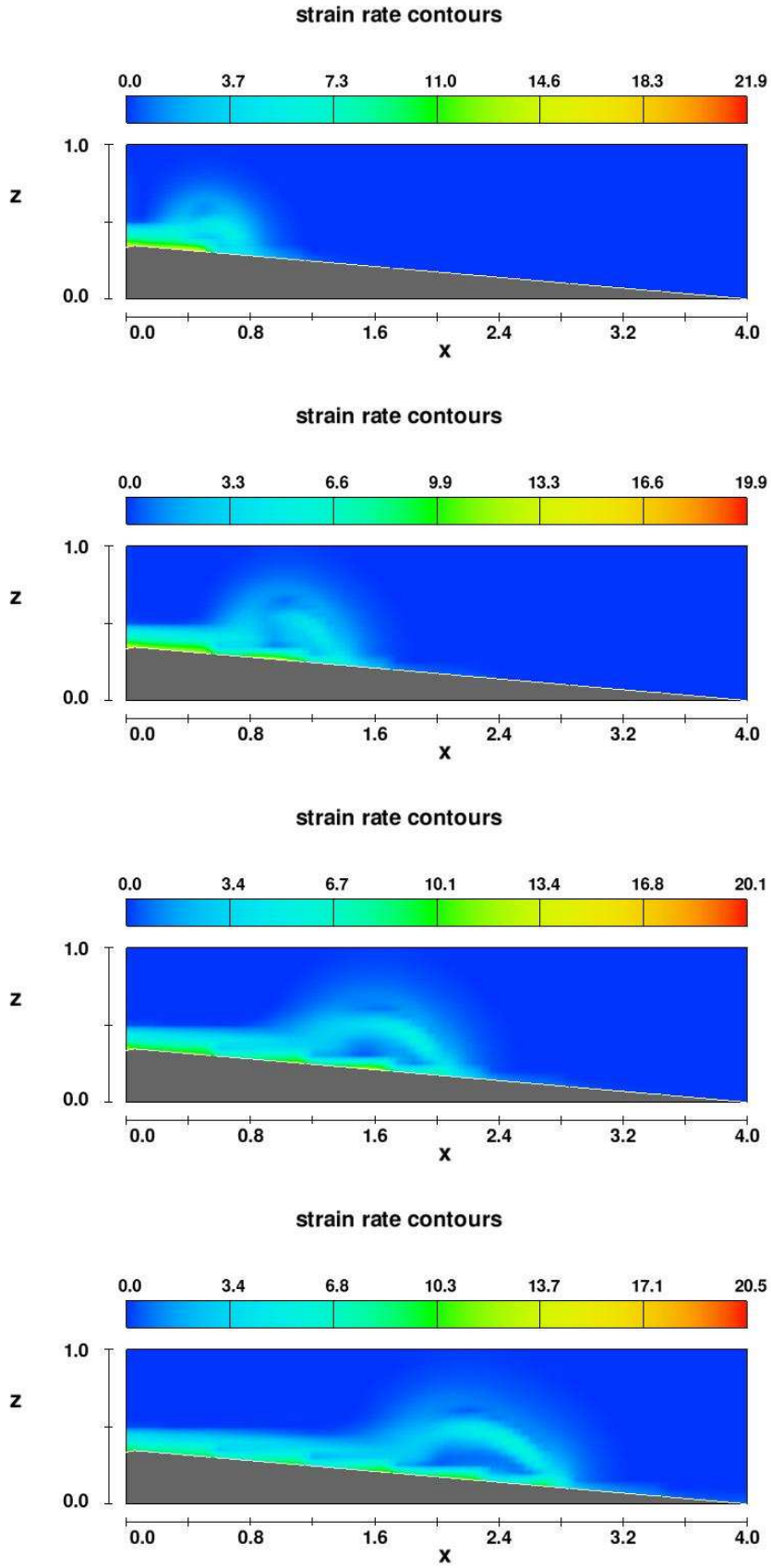

Fig. 23. Time series of the current's shear-strain rate in Run 47. The eight snapshots correspond to flow time of 1 to 8 sec. The channel has an inclination of 5^{o}. The scales units on x and z axes are metres. The strain rate is in s^{-1} units and its values are displayed as a colour spectrum (note that the scale values change from snapshot to snapshot).

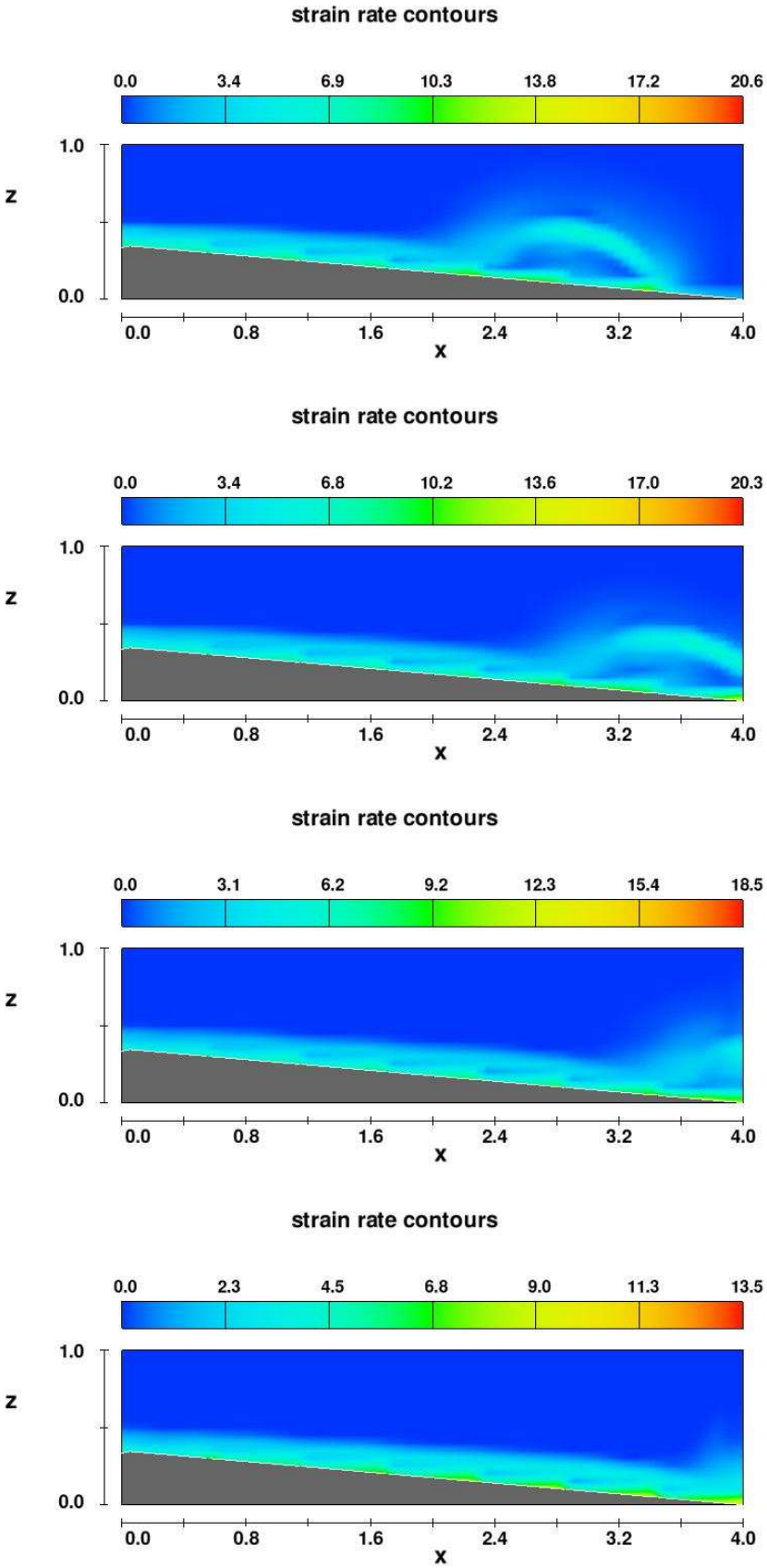
strain rate contours
0.0 3.4 6.9 10.3 13.8 17.2 20.6
1.0
z
0.0
0.0 0.8 1.6 2.4 3.2 4.0
x
strain rate contours
0.0 3.4 6.8 10.2 13.6 17.0 20.3
1.0
z
0.0
0.0 0.8 1.6 2.4 3.2 4.0
x
strain rate contours
0.0 3.1 6.2 9.2 12.3 15.4 18.5
1.0
z
0.0
0.0 0.8 1.6 2.4 3.2 4.0
x
strain rate contours
0.0 2.3 4.5 6.8 9.0 11.3 13.5
1.0
z
0.0
0.0 0.8 1.6 2.4 3.2 4.0
x

Fig. 23 (cont.)

In this flow example (Run 6, Table 1), it is worth noting the velocity waves (Fig. 25, top) and the corresponding pulses in turbulent shear stress (Fig. 25, middle) in the tail part of the current at the probing stations 1 and 2 within the channel. These waves of flow acceleration and deceleration apparently occur at the flow upper surface, since they are recorded by probes at a height of 7.5 cm and the flow tail here is only about 8-9 cm thick. However, the velocity fluctuations are most pronounced near the base of the flow (Fig. 26). It is possible that these are internal shock waves generated by the bottom roughness effect on the highly dilute (Fig. 25, bottom) and thin tail of the turbidity current. Similar shock waves can be observed, for example, in the shallow flow of rainwater running off on an inclined, rough asphalt road.

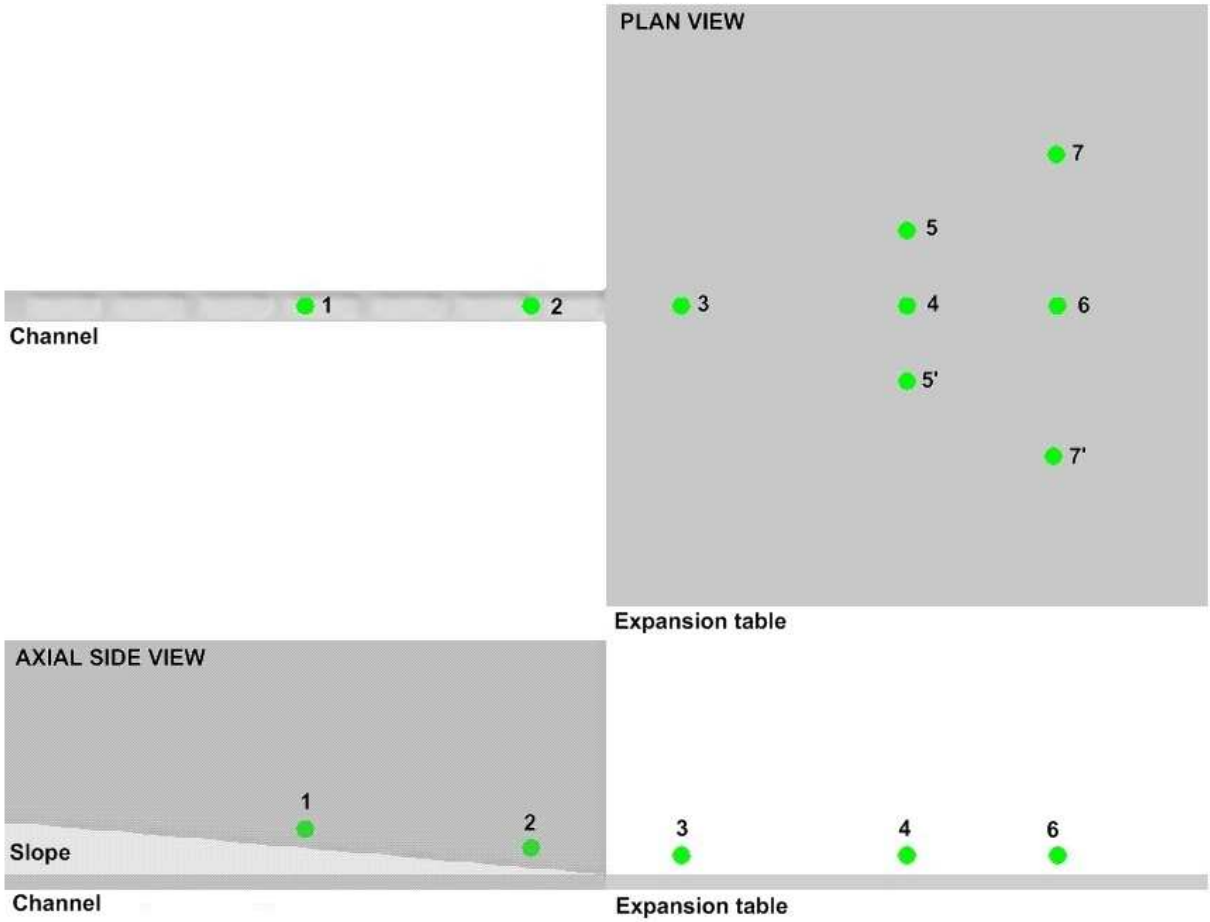

Fig. 24. The experimental setup used in Run 6 (Table 1) is based on the Utrecht laboratory flume (Fig. 13). The channel is 4 m long, 0.2 m wide and up to 1.5 m deep, inclined at 5^{o}. The wall-less expansion table is 4x4 m^2 and has an outflow boundary condition on its three outer sides. The green points indicate the location of probes (7.5 cm above the floor). The current is considered to be axisymmetrical, so that probes 5' and 7' in numerical terms are mirror-images (replicas) of probes 5 and 7, respectively.

Turbidity current response to changes in controlling parameters — By changing the initial conditions, the Flow-3D™ can be used to simulate the responses of the channel confined and unconfined parts of a turbidity current to changes in such principal controlling parameters as the channel slope angle (Fig. 27), initial sediment concentration (Fig. 28), sediment grain size (Fig. 29) and bed roughness (Fig. 30). The simulations show that turbidity currents are highly sensitive to subtle variations in the initial conditions and that the results are quite realistic.

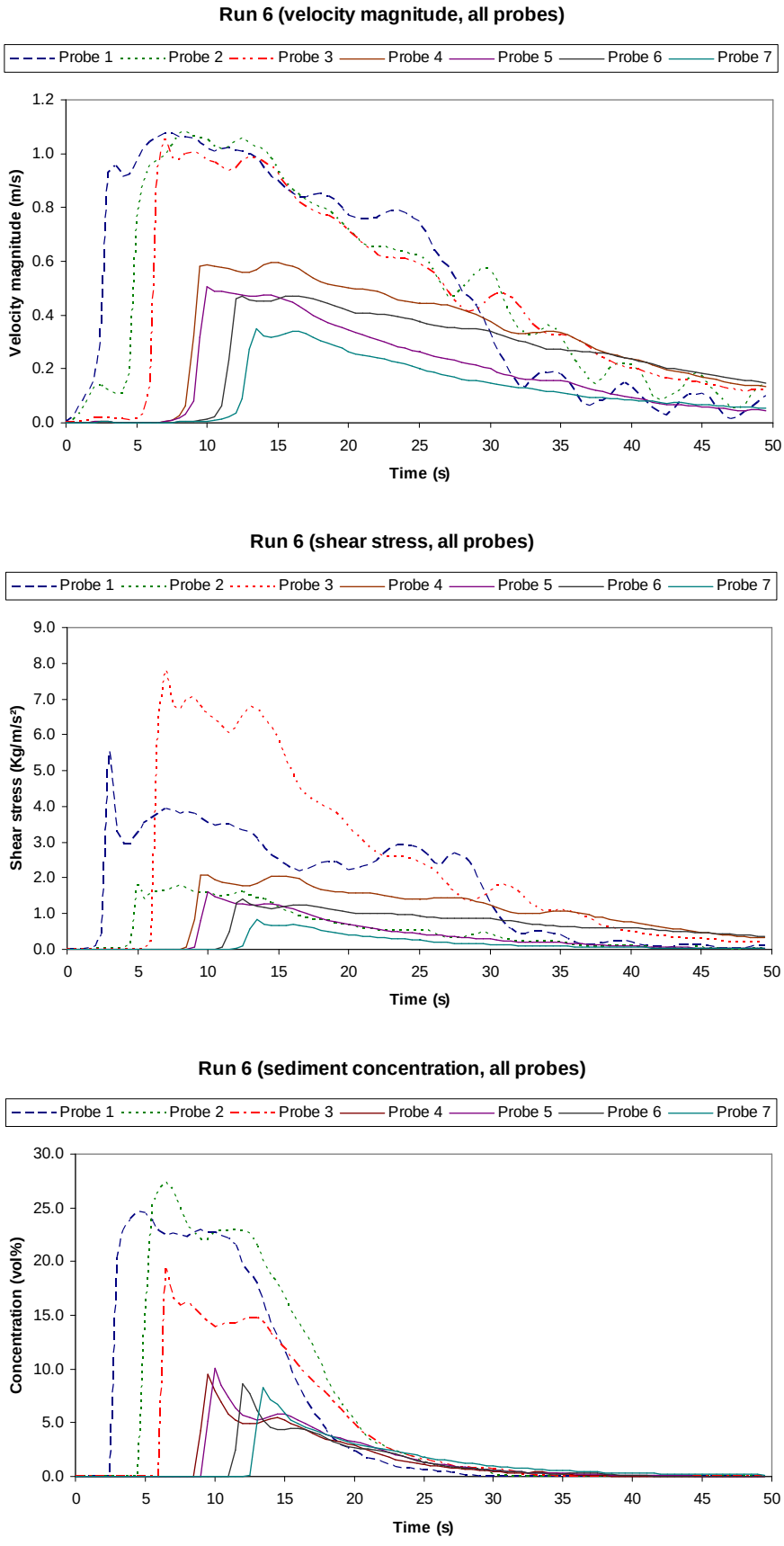

Fig. 25. The time series of flow velocity magnitude, turbulent shear stress and sediment concentration monitored simultaneously at seven probing stations for Run 6 (experimental setup as shown in Fig. 24).

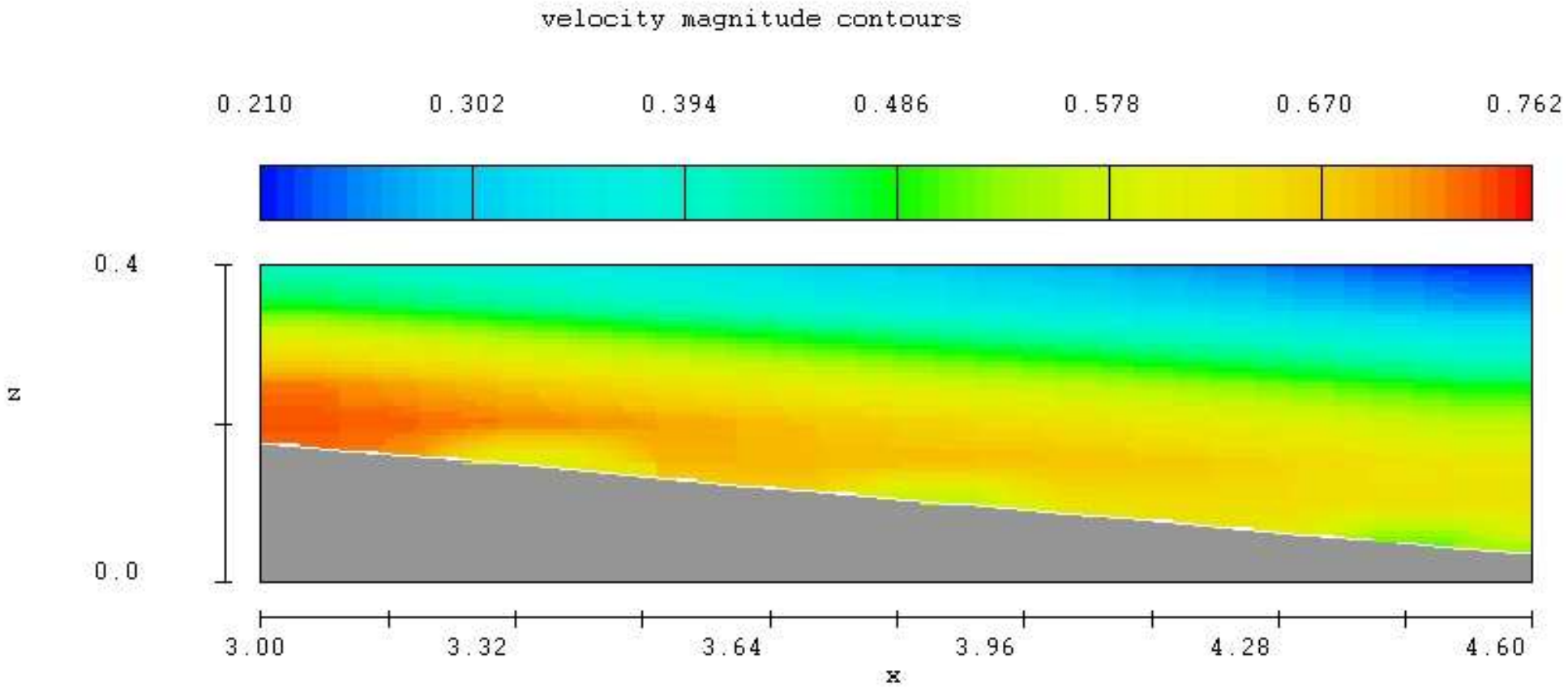

Fig. 26. Velocity fluctuations at the bottom of turbidity-current tail between probing stations 1 and 2 in simulation Run 6, at the time flow of 25 s (comp. Fig. 25, top). The x and z scales are in metres and the velocity is in m/sec. The distance shown is from the backwall of the mixing tank and corresponds to the channel segment between the two probes.

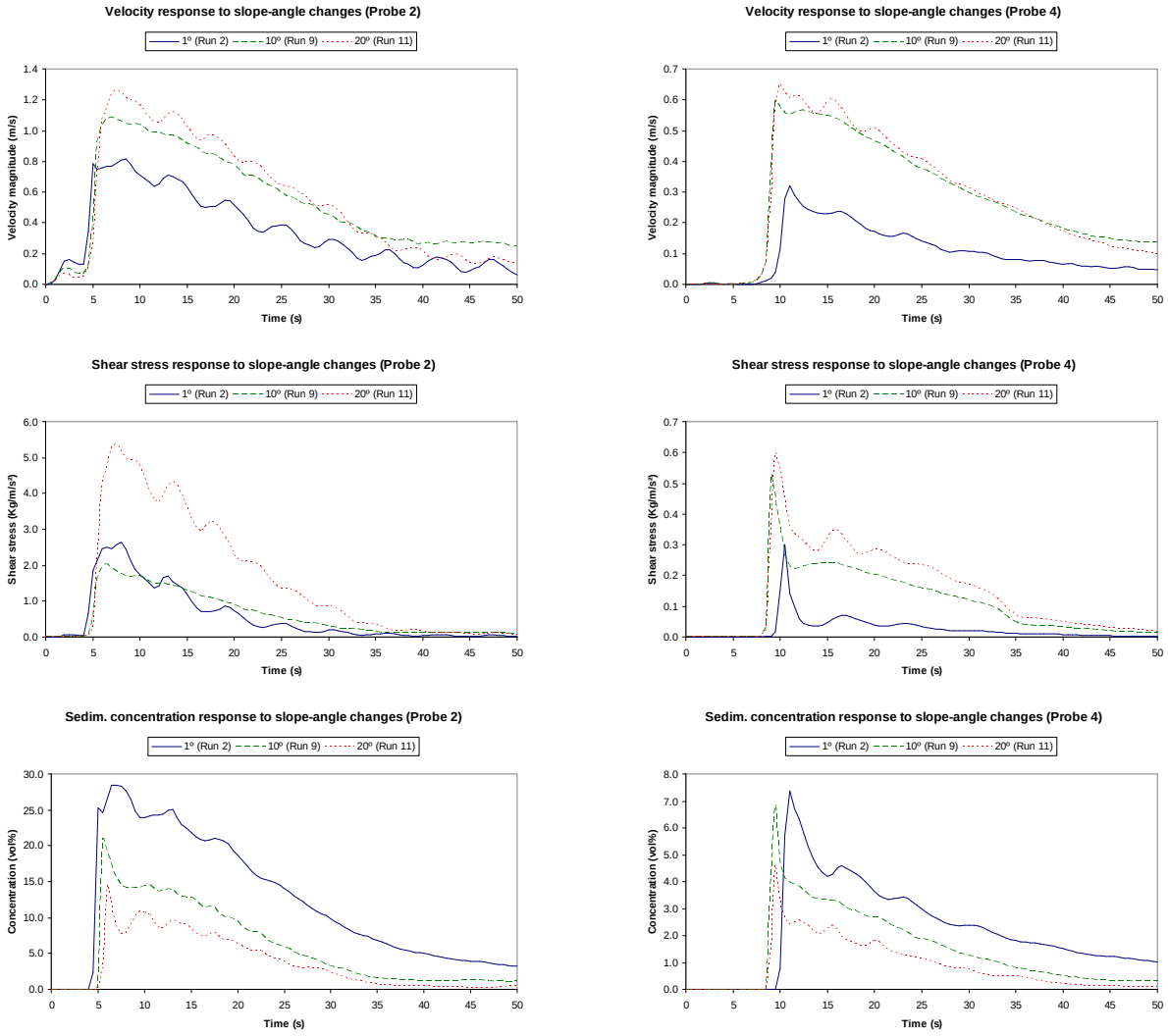

Fig. 27. The effects of slope-angle changes on the flow velocity, turbulent shear stress and sediment concentration in the channel-confined (probe 2) and unconfined (probe 4) parts of turbidity current. Simulation runs 2, 9 and 11 (Table 1); setup as shown in Fig. 24.

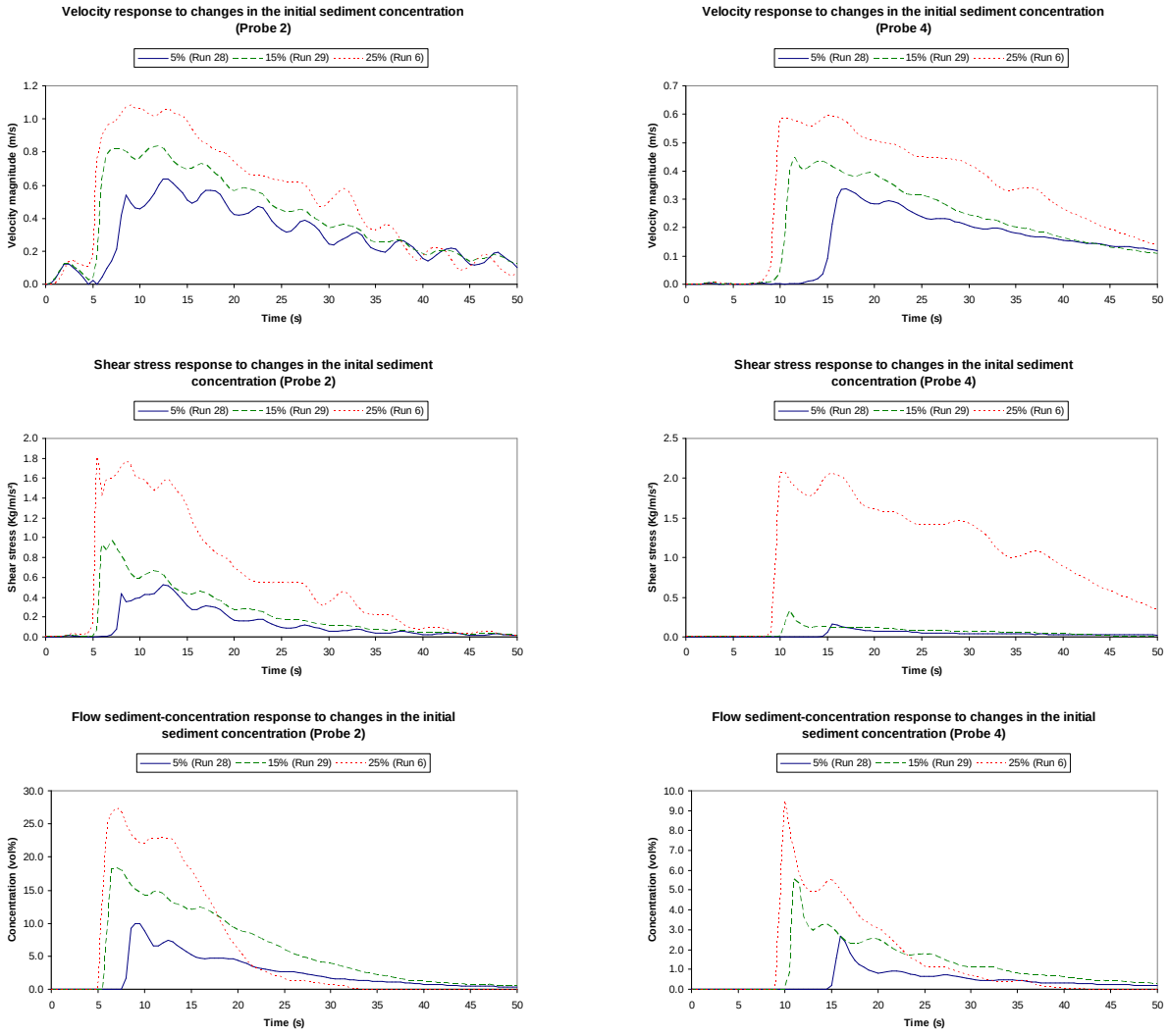

Fig. 28. The effects of changes in initial sediment concentration on the flow velocity, turbulent shear stress and sediment concentration in the channel-confined (probe 2) and unconfined (probe 4) parts of turbidity current. Simulation runs 6, 28 and 29 (Table 1); setup as shown in Fig. 24.

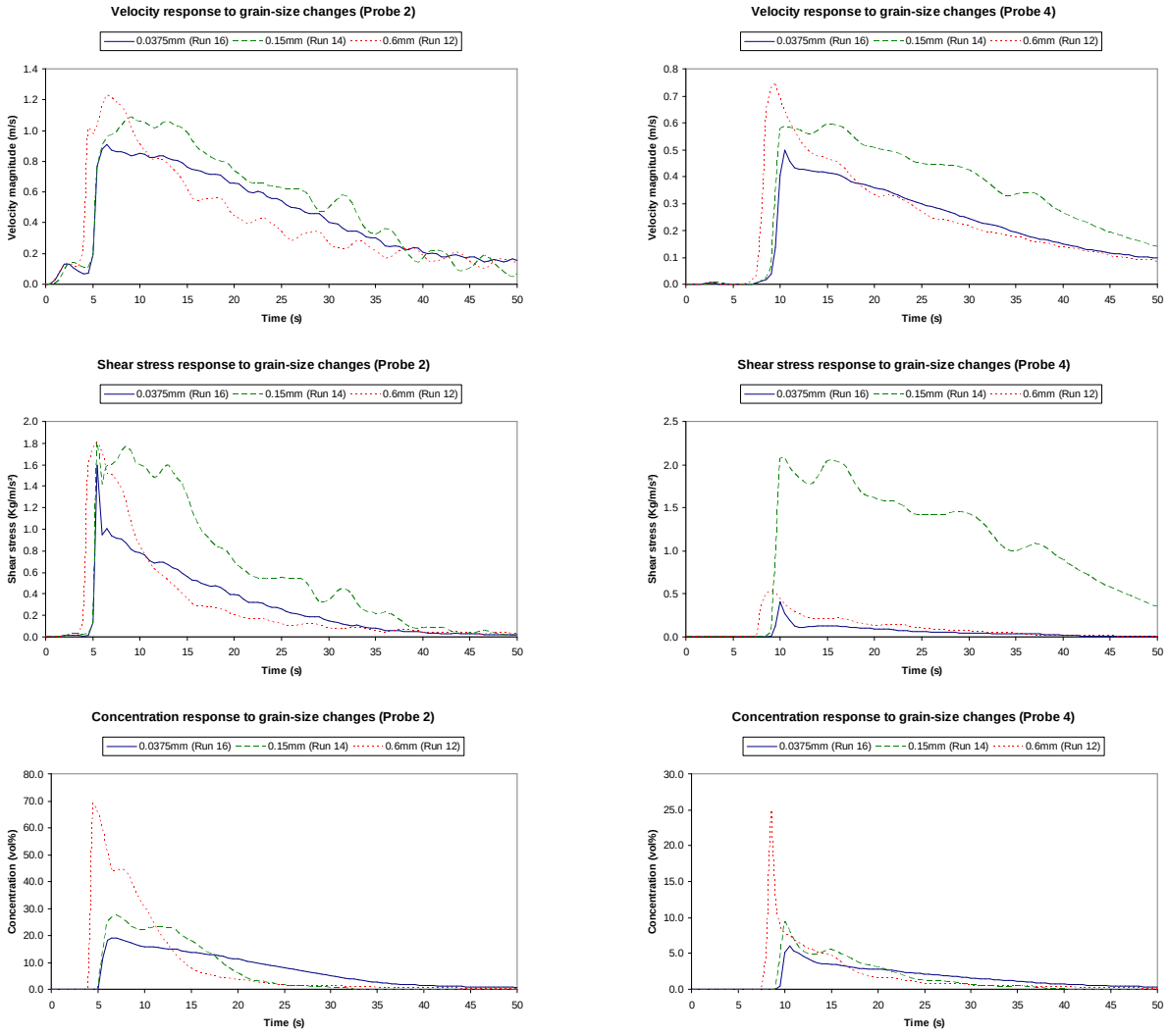

Fig. 29. The effects of grain-size changes on the flow velocity, turbulent shear stress and sediment concentration in the channel-confined (probe 2) and unconfined (probe 4) parts of turbidity current. Simulation runs 12, 14 and 16 (Table 1); setup as shown in Fig. 24. The three mono-sized sediment types used are coarse silt (Run 16), fine sand (Run 14) and coarse sand (Run 12).

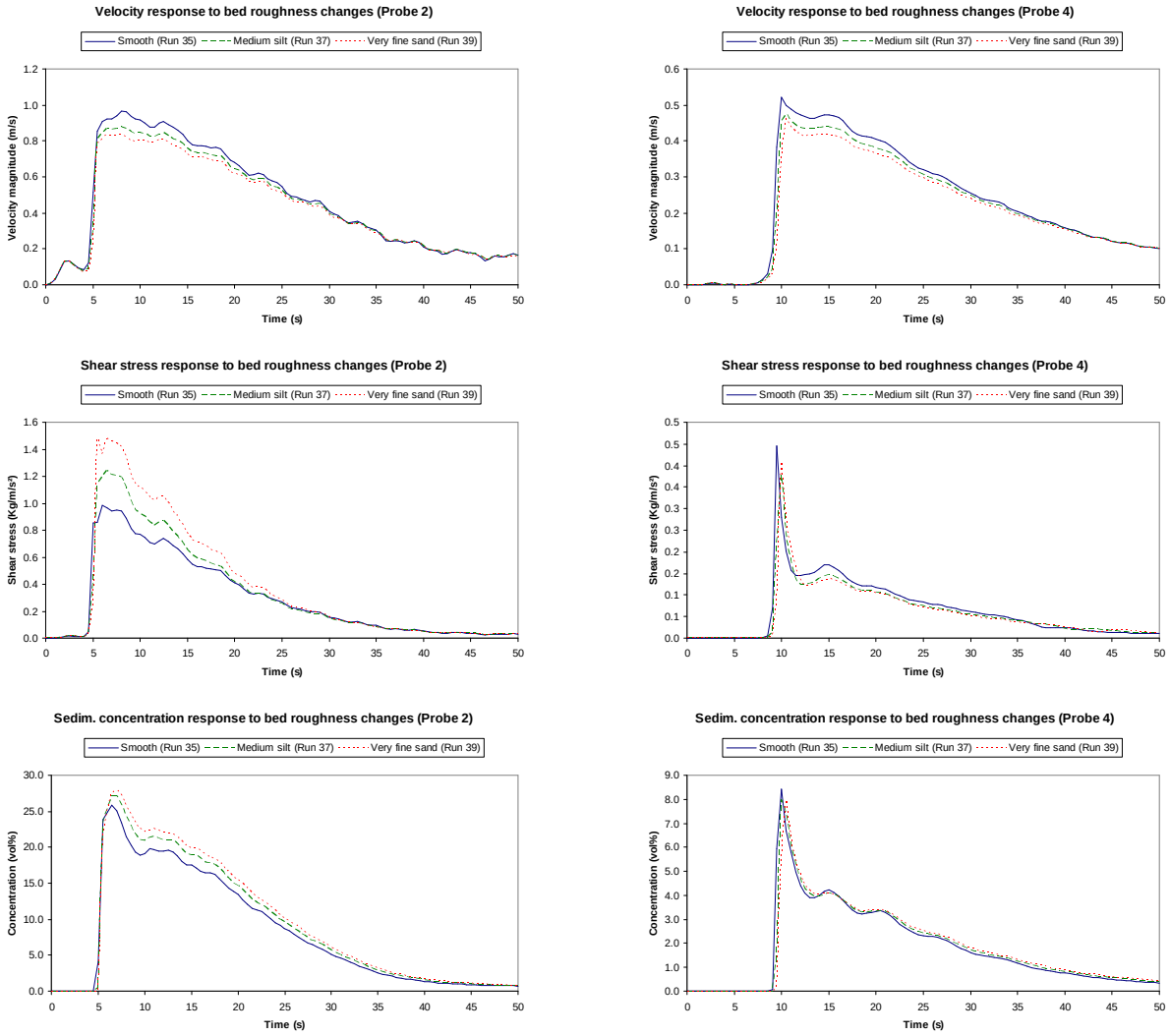

Fig. 30. The effects of bed (floor) roughness changes on the flow velocity, turbulent shear stress and sediment concentration in the channel-confined (probe 2) and unconfined (probe 4) parts of turbidity current. Simulation runs 35, 37 and 39 (Table 1); setup as shown in Fig. 24. The three bed-roughness types used are smooth floor (Run 35), floor cover with medium silt (Run 37) and v. fine sand (Run 39).

Simulation of basic flow types – By selecting different initial boundary conditions (inflow mode), the Flow-3D™ can be used to simulate both surge-type and sustained turbidity currents. An example for such simulations, displayed as flow velocity time series, is shown in Figure 31. The surge in this case shows a gradual waning directly after the passage of the flow front, whereas the sustained flow shows a constant velocity for a period of 15 seconds – when the inflow ended and the flow velocity rapidly declined. The difference in the rates of flow waning reflects the two different modes of inflow used: the surge was generated by the emptying of a tank containing finite slurry volume, which took 15 seconds, whereas the sustained flow was produced by a constant inflow for 15 seconds and its abrupt closure.

The example demonstrates that the Flow-3D™ models are capable of revealing differences between turbidity currents generated with different inflow conditions.

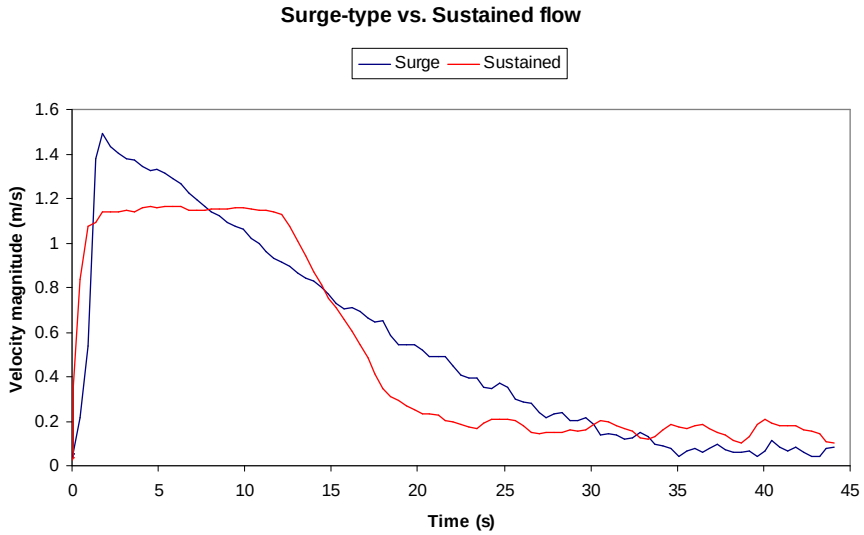

Fig. 31. Simulated velocity time series of flows generated with different modes of inflow

Flow runs with poly-sized sediment mixtures – The Flow-3D™ with the use of particle model (see section 3.3) allows simulation of flows carrying poly-sized sediment mixtures. An example of such a simulation is shown in Figure 32. The setup in this case was the same as in Run 6 (Table 1 and Fig. 24), but with poly-sized particles. A mixture of 100,000 particles ranging from very fine to medium sand (0.075-0.275 mm in diameter) has been selected, with the corresponding grain-size spectrum divided into four classes with equal weight (mass) proportions. The simulation time series shows how the grain sizes become segregated in the turbidity current passing through the channel. A clear downflow and upward fining is recognizable within the flow body, whereas the flow head shows well-mixed particles with the finest ones stripped from the top of the head and thrown behind it (Fig. 32).

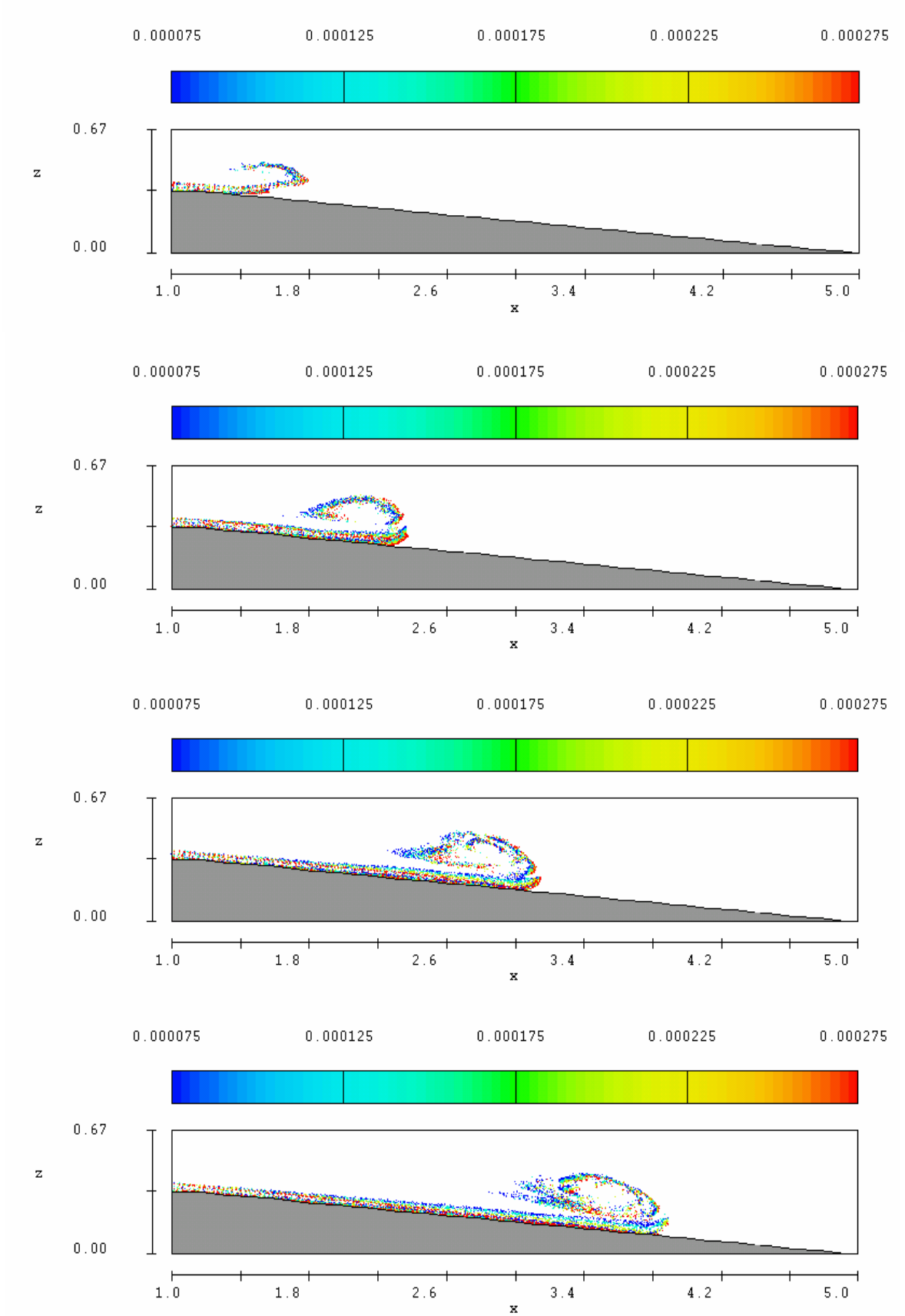

Fig. 32. Time series of a turbidity current transporting poly-sized sediment particles. The eight snapshots correspond to flow time of 1 to 8 sec. The channel has an inclination of 5°. The scales units on x and z axes are metres and the particle sizes are in metres.

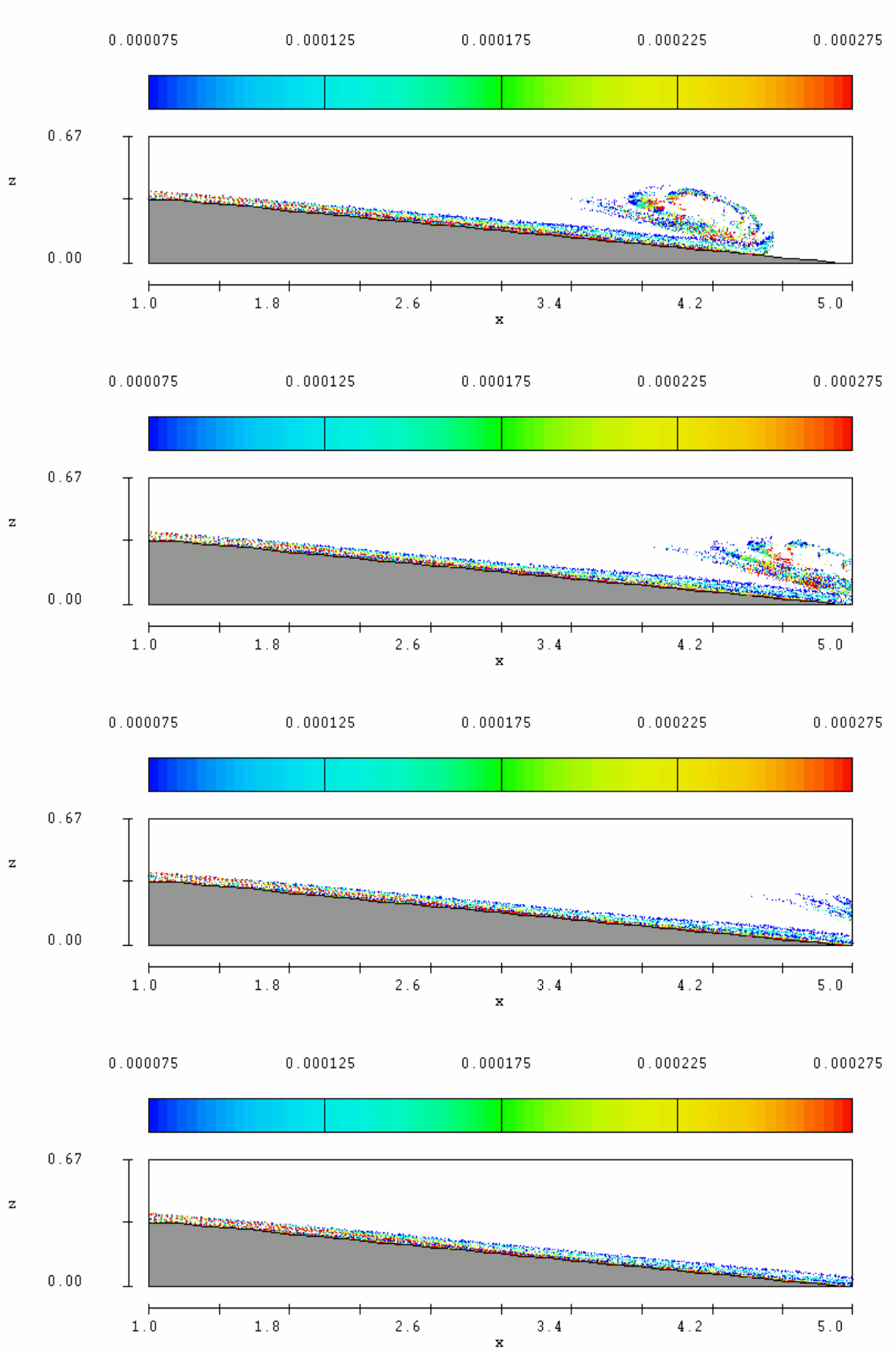
0.000075
0.000125
0.000175
0.000225
0.000275
0.67
z
0.00
1.0
1.8
2.6
3.4
4.2
5.0
x

Fig. 32 (cont.)

Turbidity current reaction to topographic obstacles – A few simple simulations have been performed also to show flow reaction to obstacles such as a low-relief transverse ridge, with overflowing (Fig. 33), and a high-relief pillar (Fig. 34) without overflowing. The results are comparable to laboratory observations reported, for example, by Alexander and Morris (1994) and Morris and Alexander (2003). This evidence indicates that flow responses to pre-defined topographic obstacles can readily be simulated with the Flow-3D™ software.

Turbidity current response to hydraulic jump – A response to turbidity current to hydraulic jump has been simulated with the same setup as shown in Figure 24, but with the expansion table covered with a 10-cm static layer of fine-grained sand, same as transported by the current (Run 47, Table 1). The distribution of flow velocity magnitude in the uppermost part of the current shows wave-like pulses of higher velocity descending along the channel and similar, but broader shock waves propagating outwards in the expanding current (Fig. 35A-D). When the current's tail eventually begins to descend through the channel, it meets waves of counter-flow reflected from the topographic erosional relief created by the hydraulic jump (Fig. 35E-J). An evidence of these reflected tail-flow waves is described below, whereas the 3D velocity field in the hydraulic-jump area is shown in Figure 36.

The time series in Figure 37 shows the development of the topographic relief in the hydraulic-jump area, in the form of an elliptical scour, by means of substrate erosion and sediment redeposition – accompanied by a backfilling of the lowest part of the channel (see Fig. 37F-H). Erosional chutes transverse to the channel axis appear in the vicinity of the scour depression (see Fig. 37G-H), and their origin is attributed to the lateral drainage of the tail flow waves reflected backwards by the downstream relief of the depression (Fig. 38). The evidence of such reflections is shown in Figure 39, where two backflow waves (displayed in blue colour) can be seen entering the lower segment of the channel and colliding with a descending flow wave (displayed in red/orange).

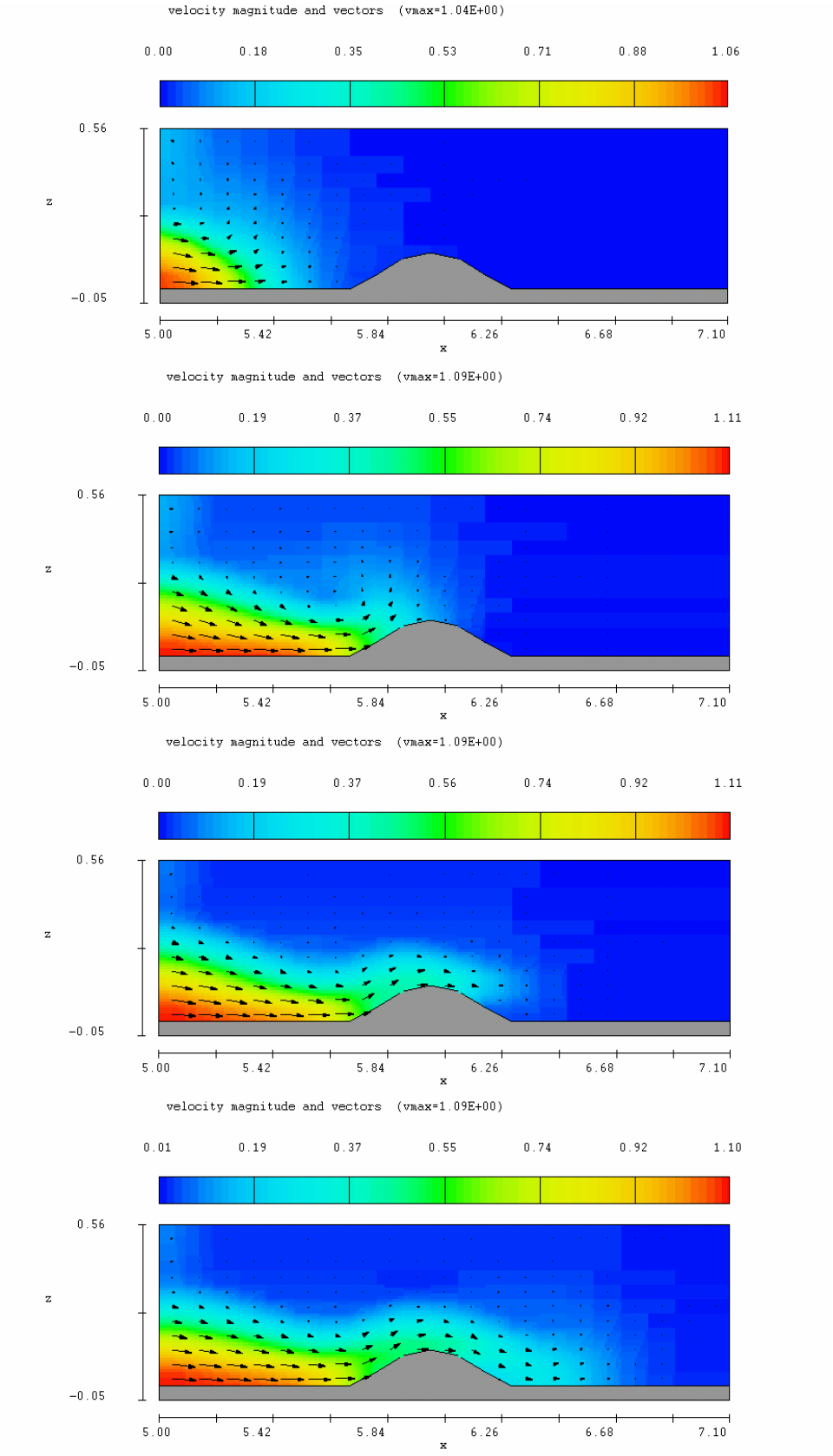

Fig. 33. Time series of a turbidity current's reaction to transverse topographic ridge (side view showing velocity magnitude as both colour spectrum and vectors). The eight snapshots correspond to flow time of 6 to 13 sec. The scales units on x and z axes are metres and the velocity scale is in m/s (note that the scale values change from snapshot to snapshot).

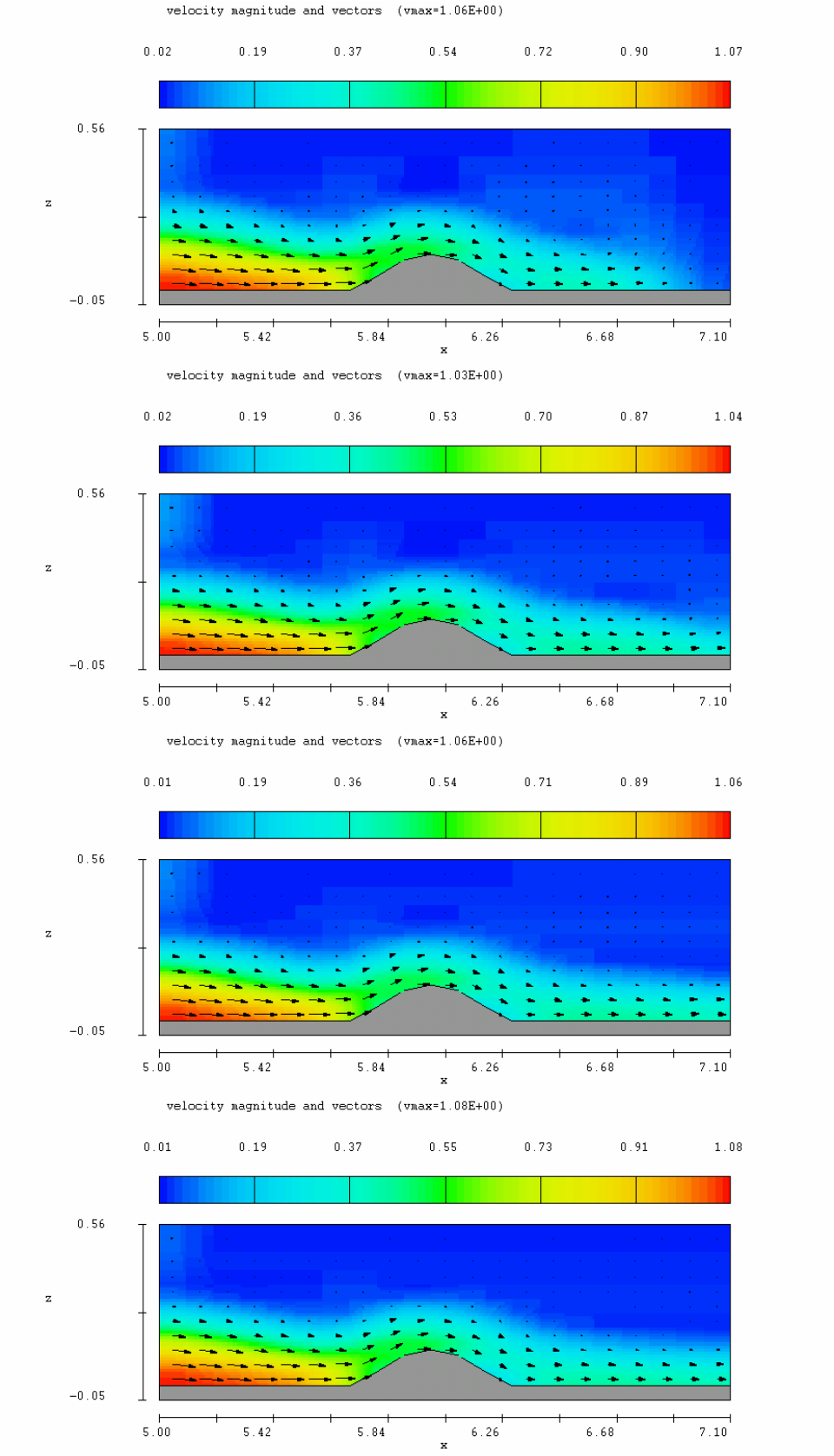
velocity magnitude and vectors (vmax=1.06E+00)
0.02 0.19 0.37 0.54 0.72 0.90 1.07
0.56
z
-0.05
5.00 5.42 5.84 6.26 6.68 7.10
x
velocity magnitude and vectors (vmax=1.03E+00)
0.02 0.19 0.36 0.53 0.70 0.87 1.04
0.56
z
-0.05
5.00 5.42 5.84 6.26 6.68 7.10
x
velocity magnitude and vectors (vmax=1.06E+00)
0.01 0.19 0.36 0.54 0.71 0.89 1.06
0.56
z
-0.05
5.00 5.42 5.84 6.26 6.68 7.10
x
velocity magnitude and vectors (vmax=1.08E+00)
0.01 0.19 0.37 0.55 0.73 0.91 1.08
0.56
z
-0.05
5.00 5.42 5.84 6.26 6.68 7.10
x

Fig. 33 (cont.)

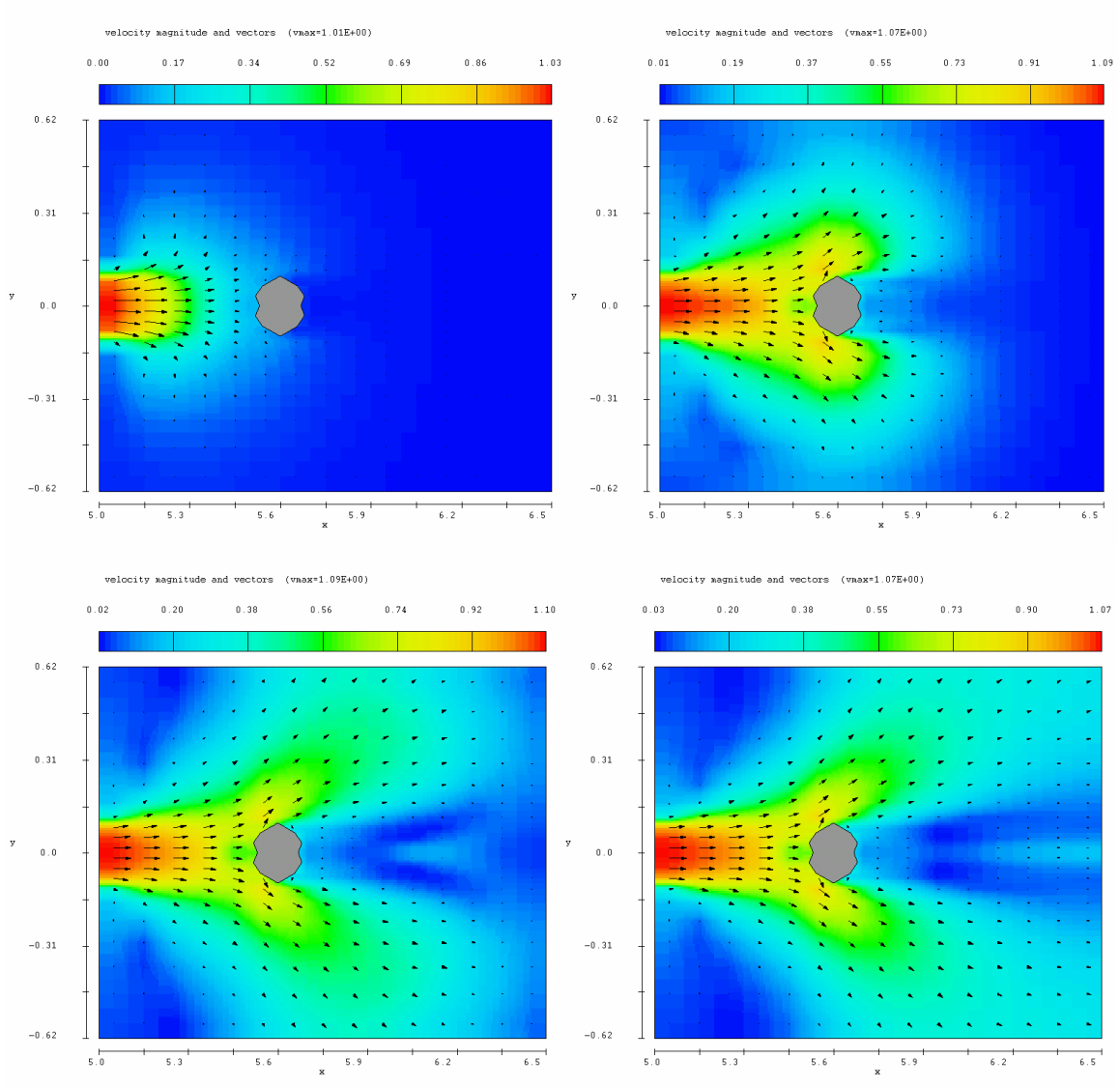

Fig. 34. Time series of a turbidity current's reaction to vertical topographic pillar (plan view showing velocity magnitude as both colour spectrum and vectors). The eight snapshots correspond to flow time of 6 to 13 sec. The scales units on x and z axes are metres and the velocity scale is in m/s (note that the scale values change from snapshot to snapshot).

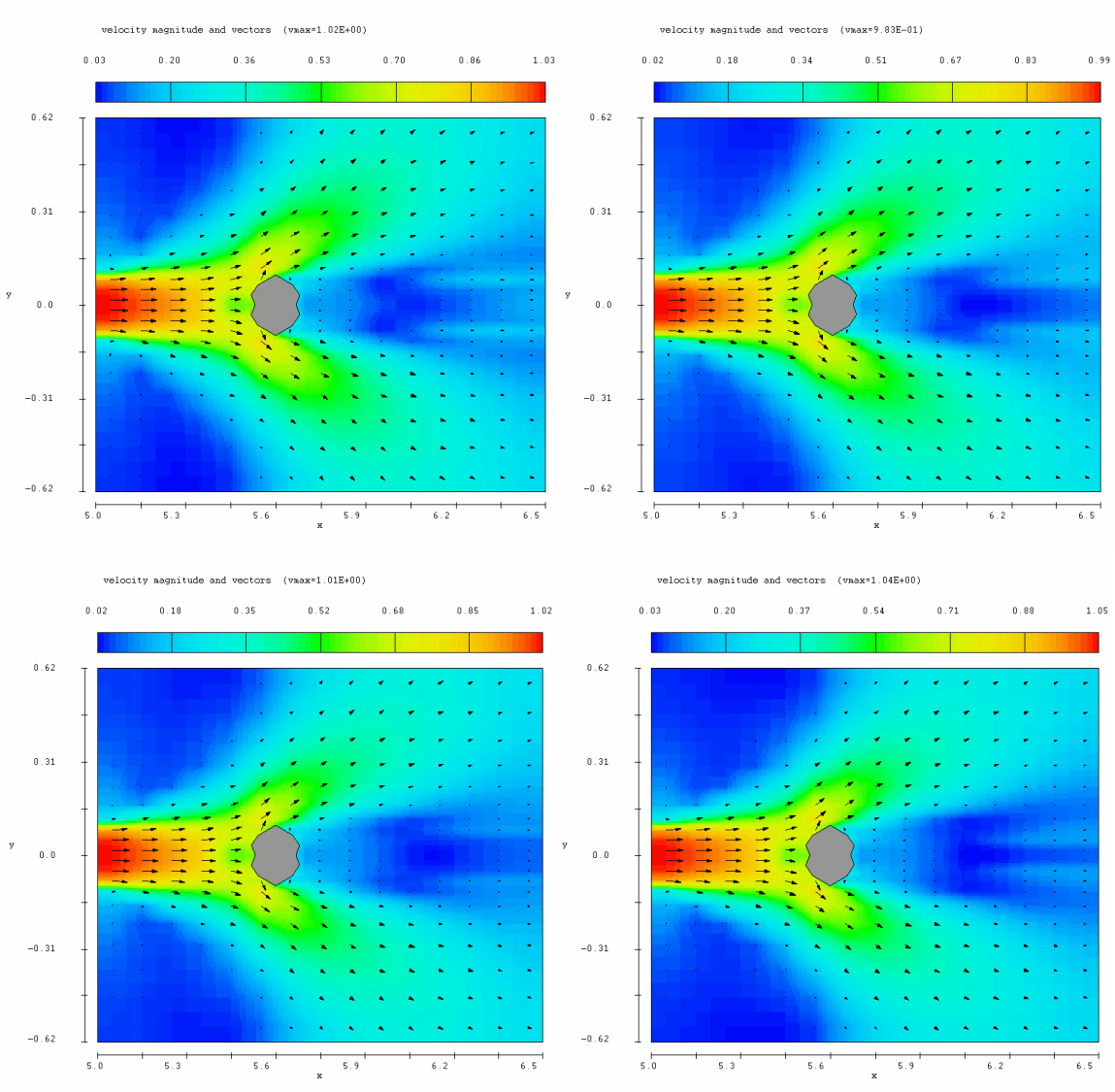
velocity magnitude and vectors (vmax=1.02E+00)
0.03 0.20 0.36 0.53 0.70 0.86 1.03
velocity magnitude and vectors (vmax=9.83E-01)
0.02 0.18 0.34 0.51 0.67 0.83 0.99
velocity magnitude and vectors (vmax=1.01E+00)
0.02 0.18 0.35 0.52 0.68 0.85 1.02
velocity magnitude and vectors (vmax=1.04E+00)
0.03 0.20 0.37 0.54 0.71 0.88 1.05
0.62 0.31 0.0 -0.31 -0.62
y
5.0 5.3 5.6 5.9 6.2 6.5
x

Fig. 34 (cont.)

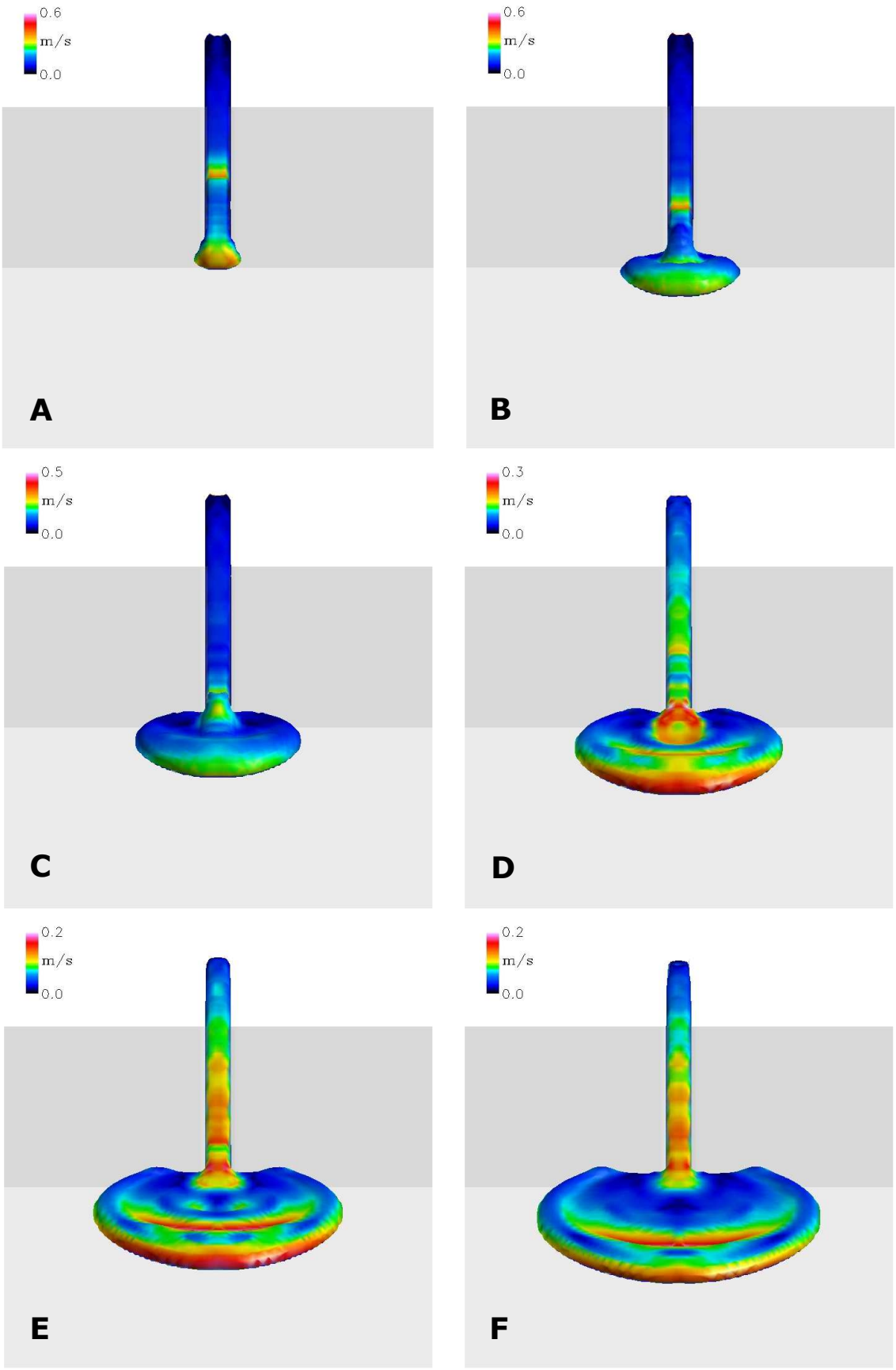

Fig. 35. Time series of a turbidity current's reaction to hydraulic jump in the slope-break conditions of channel outlet (front view showing velocity magnitude as colour spectrum; simulation Run 47 (Table 1) with the same setup as in Run 6 (Fig. 24), but using sediment scour model). The ten snapshots (A-J) correspond to flow time of 6 to 15 sec. The velocity scale is in m/s (note that the scale values change from snapshot to snapshot).

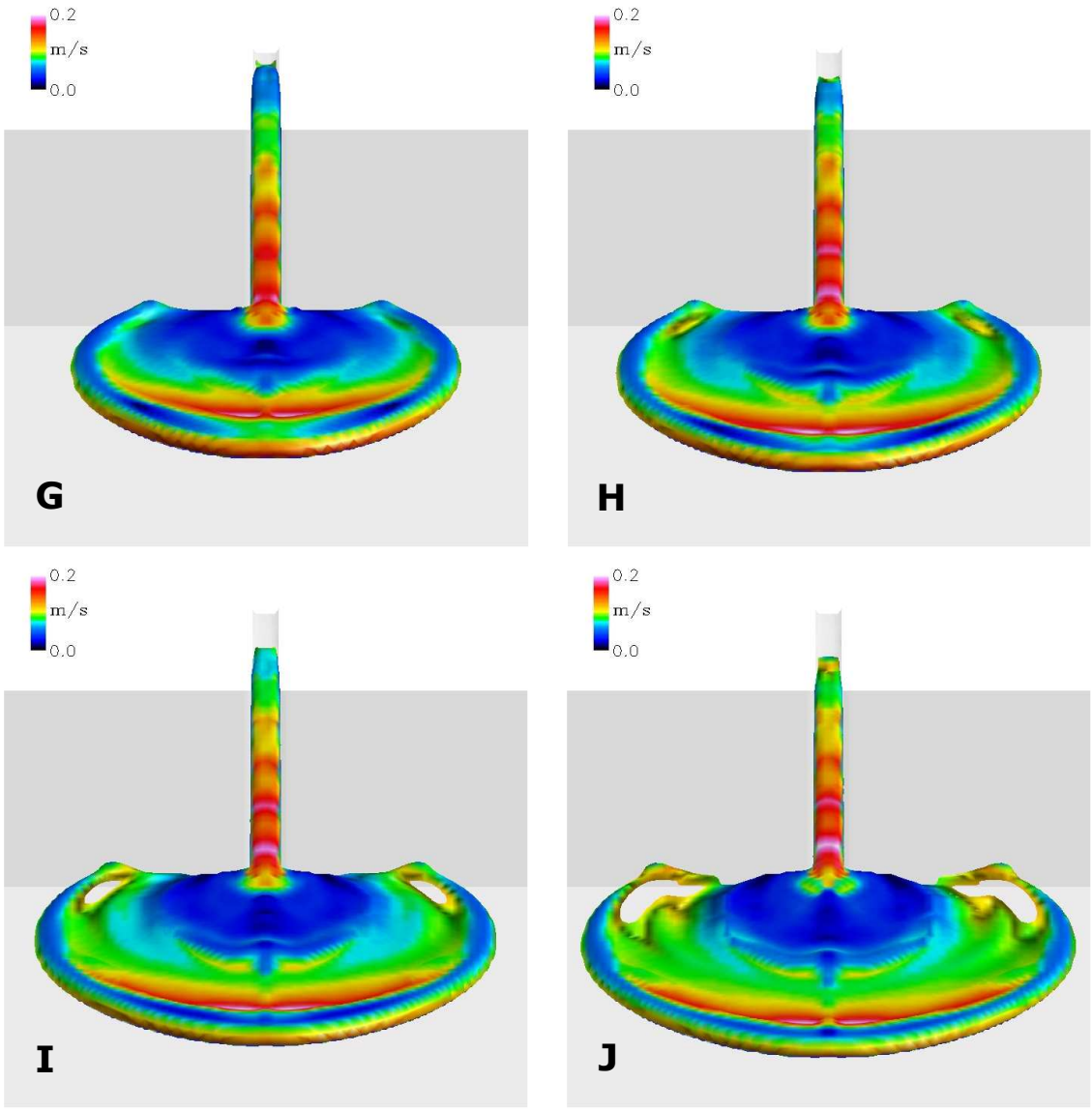

Fig. 35 (cont.)

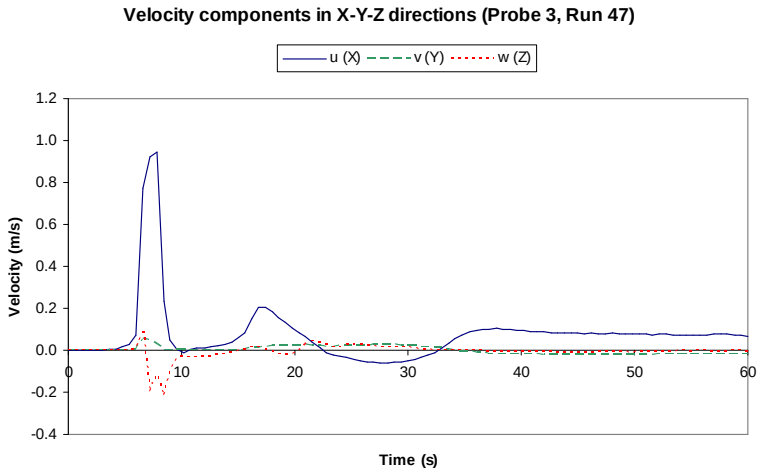

Fig. 36. Time series of a turbidity current's velocity components in the hydraulic-jump area at channel mouth (Simulation Run 47 (Table 1), probe 3 location as in Fig. 24). Note the x-velocity component of the turbidity current's tail showing a backward-moving wave of flow, the negative vertical (z-direction) velocity reflecting the current's plunge and the velocity in y-direction reflecting lateral flow expansion.

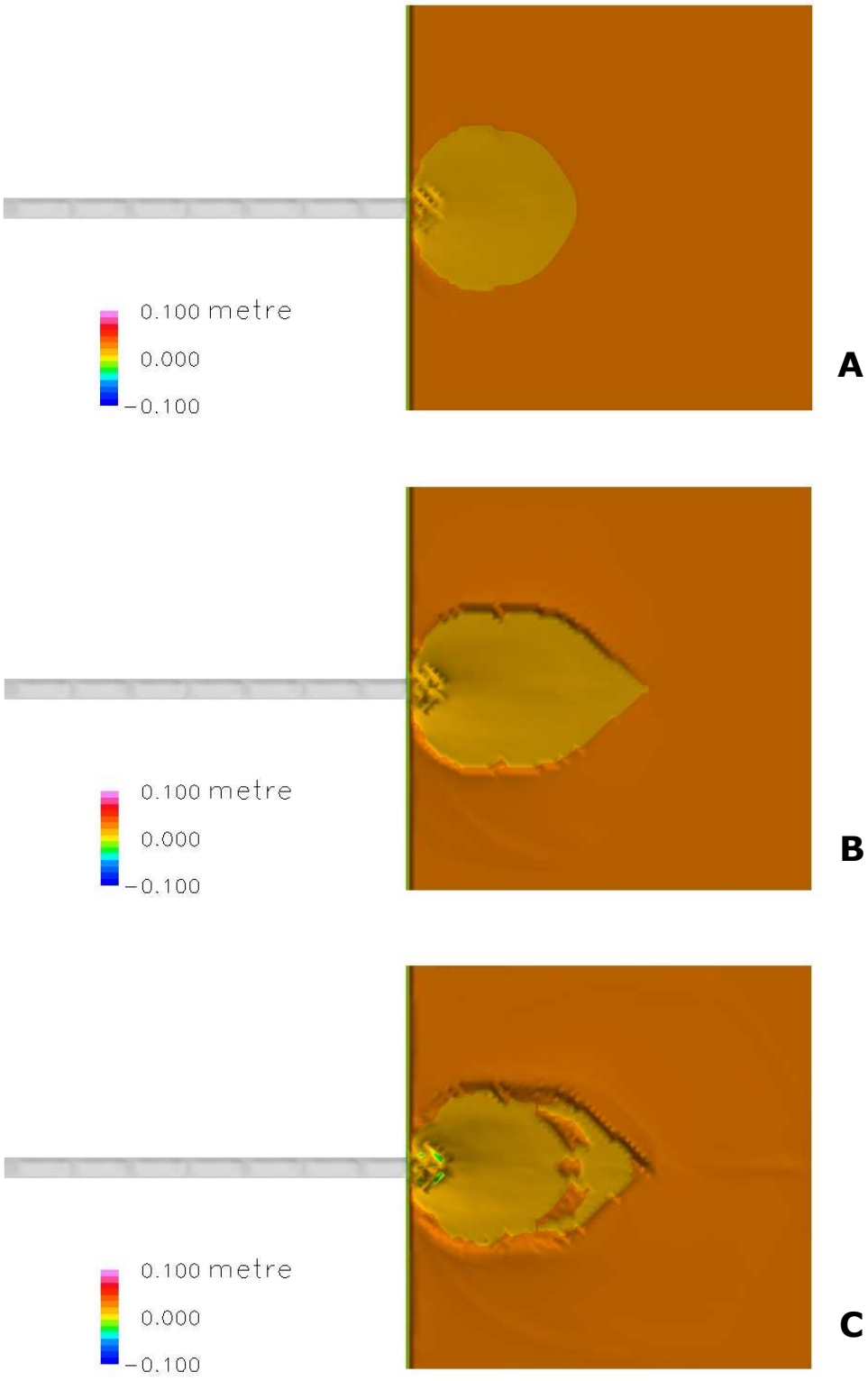

Fig. 37. Plan view of a turbidity current responding to hydraulic jump at channel outlet (simulation Run 47 (Table 1) with setup as in Run 6 (Fig. 24), but using sediment scour model). The expansion table was covered with a 10-cm layer of mono-sized fine sand, same as transported by the current. The eight snapshots (A-H) show changes in bed level (erosion and deposition) at flow time of 10, 15, 20, 25, 30, 40, 50 and 60 sec. The colour scale pertains to floor relief.

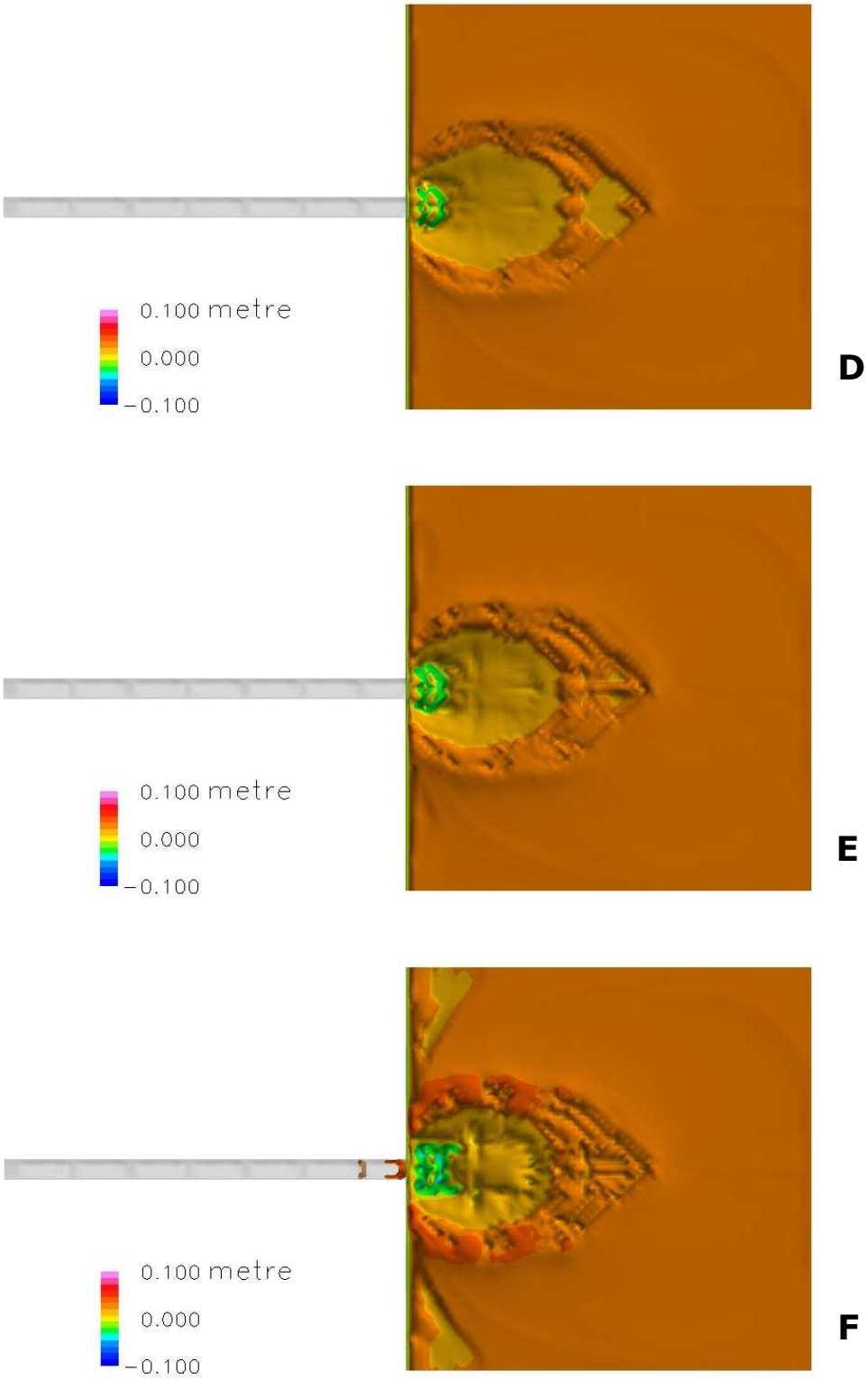
0.100 metre
0.000
−0.100
D
0.100 metre
0.000
−0.100
E
0.100 metre
0.000
−0.100
F

Fig. 37 (cont.)

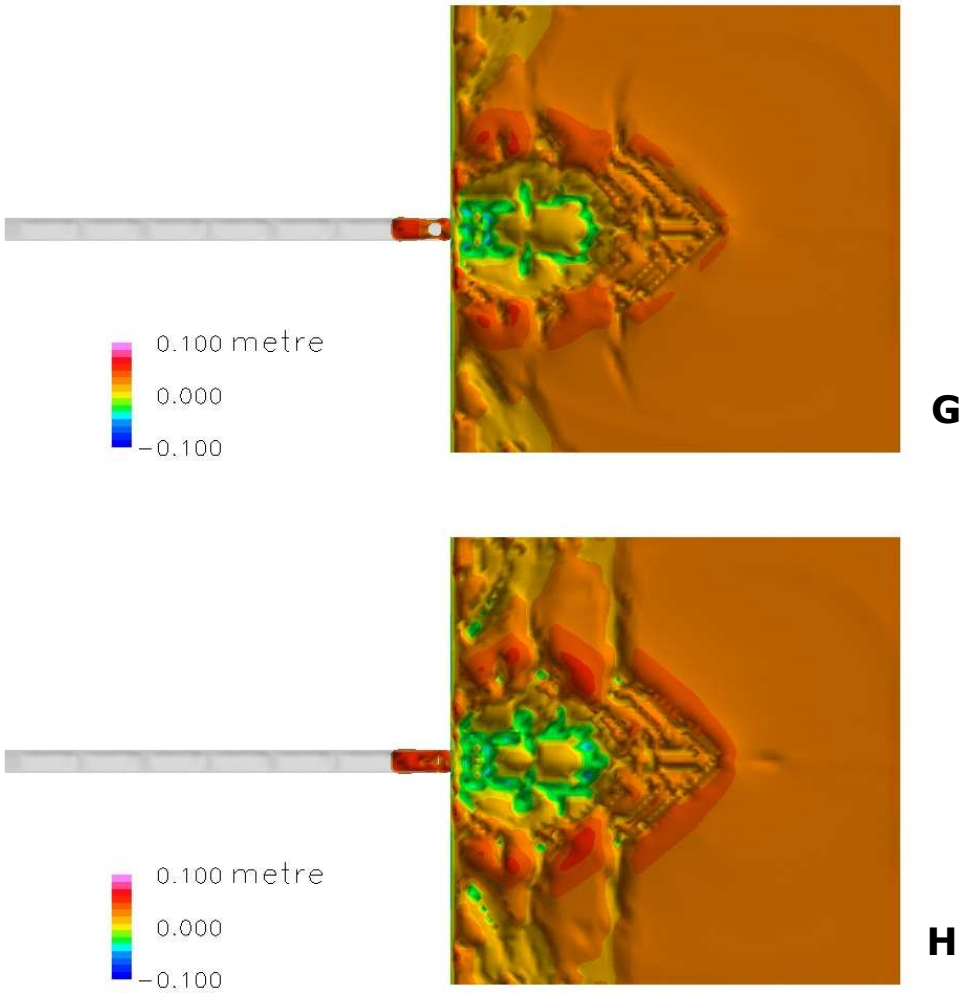

Fig. 37 (cont.)

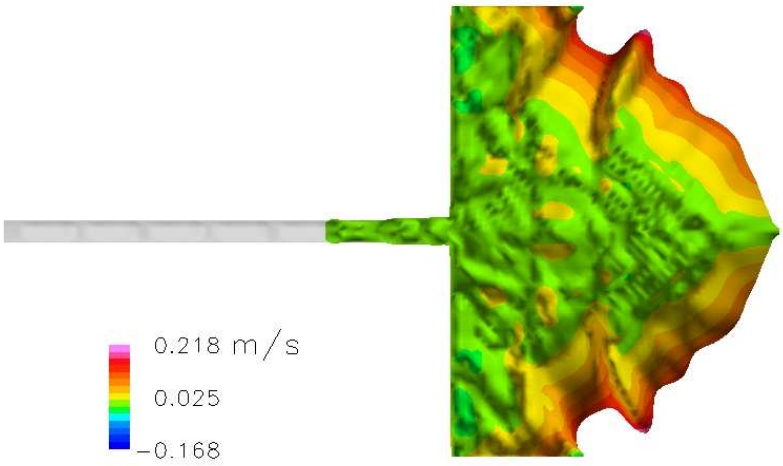

Fig. 38. The y-velocity component (after 60 sec. flow) of turbidity current's tail in hydraulic-jump area, showing pronounced pulses of a lateral drainage of flow waves reflected backwards from the current-produced scour relief (cf. floor topography in Fig. 37). Run 47 (Table 1); setup as in Fig. 24.

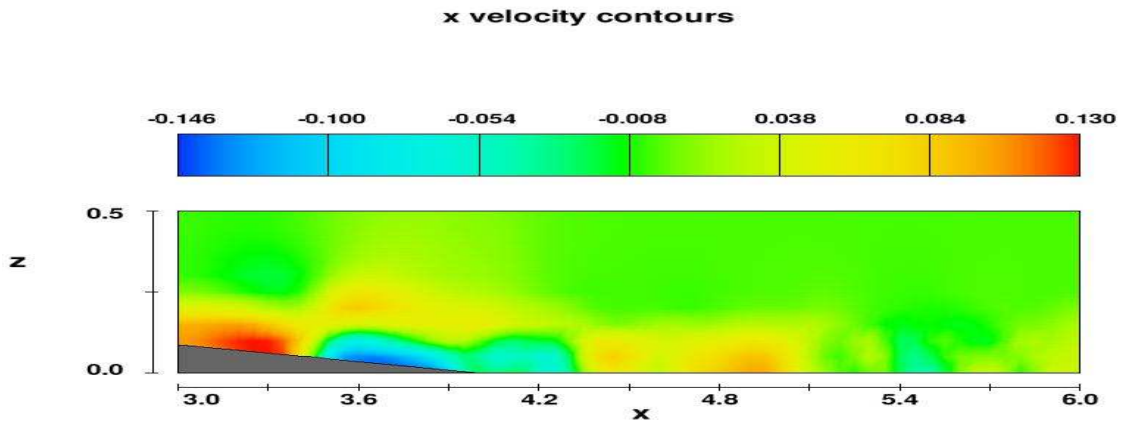

Fig. 39. The x-velocity component (after 35.5 sec. flow) of turbidity current's tail in hydraulic-jump area (side view), showing a backward-moving wave of flow (displayed in blue) reflected from the current-produced scour relief (cf. floor topography in Fig. 37). Run 47 (Table 1); setup as in Fig. 24. The scales units on x and z axes are metres and the velocity scale is in m/s.

4.2. Large-scale simulations

In this chapter, results are presented from a numerical experiment performed to assess the capability of the Flow-3D™ model to up-scale laboratory currents to natural conditions. In this numerical experiment, simulated velocity profiles have been qualitatively compared to in-situ velocity measurements of full-scale turbidity currents in a natural setting. The in-situ measurements were performed by Xu et al (2004) and focused on the velocity structure of turbidity currents. Two of the four recorded events have been simulated and their results compared with the measured data (Xu et al, 2004).

Modern events in the Monterey canyon system – From December 2002 to November 2003, the U.S. Geological Survey (USGS) and Naval Postgraduate School (NPS) deployed three oceanographic moorings along the axis of the Monterey Submarine Canyon at water depths of 820, 1020 and 1450 m (Fig. 40). Each mooring had a downward-looking acoustic Doppler current profiler (ADCP) at 69 m above the bed. Instrument packages with CTDs, transmissometers and sediment traps were located approximately 16 and 70 m above the bed, while similar packages with the addition of single point current-meters were located 170 m above the bed and either at 300 m (R1 and R2) or 400 m above the bed (R3). In-situ measurements of the velocity structure of four turbidity currents, with maximum along-canyon velocity of 190 cm/s, were recorded. Two turbidity currents coincided with storms that produced the highest swells and the biggest stream flows during the year-long deployment. The first turbidity current occurred 11.5 days after the moorings were deployed and was rather slow, with a maximum along-canyon velocity reaching 75 cm/s at R3. The second turbidity current, recorded just 3 days later, moved much faster. This event was observed by all three moorings (Fig. 41), with maximum along-canyon velocities of 190, 160 and 180 cm/s at R1, R2 and R3, respectively.

Simulation of the Monterey large-scale flows - Based on the topographic setting of the Monterey Canyon area and the measurements of the two turbidity-current events (Xu et al., 2004), the initial conditions for a series of Flow-3D™ simulations have been estimated. The measurements of velocity were sufficient to assess flow thickness, duration and initial velocity at the canyon head, but had a time spacing of 1 hour and hence were not detailed when it comes to the flow-velocity time series. The sediment scour and RNG models (see earlier section 3.3) were employed in the simulations. Furthermore, the volumetric sediment concentration and exact grain-size distribution in the flows are unknown. An initial concentration of 9 vol.%, fine-grained sand load and uniform bed roughness have been assumed for the simulations. Additional simplifying assumptions included lack of oceanic water circulation and negligible Coriolis force. The bathymetry and hydrostatic pressure were fully accounted for, and the resolution of the 3D computational grid was selected at the

highest level. Because of the lack of signal of the first event in the upper Monterey Canyon (Fig. 41, top left), this flow is inferred to have originated from the Soquel Canyon, whereas there is little doubt that the second event originated from the uppermost Monterey Canyon (Fig. 40). Trial simulations were performed to estimate an initial velocity that would yield a flow matching the velocity measured at the nearest mooring point. On this basis, the initial velocities of 1.25 and 1.50 m/s have been selected for the first and second event, respectively.

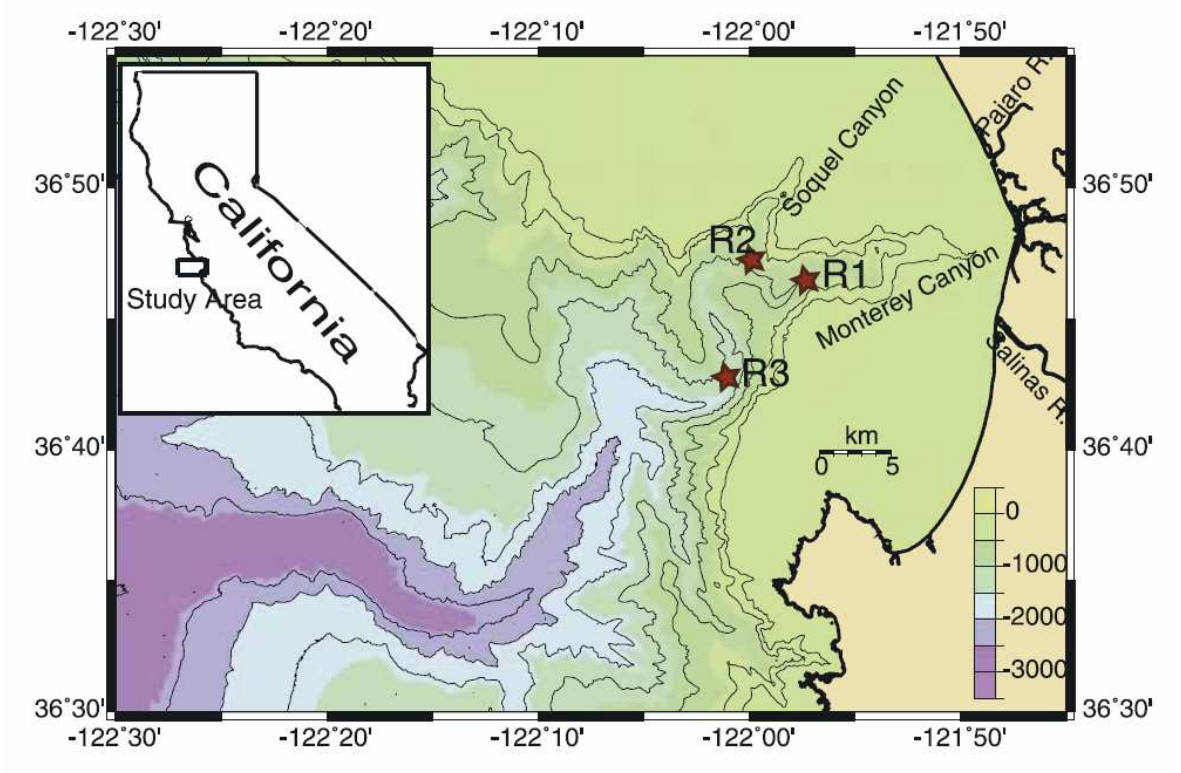

Fig. 40. A map of the Monterey and Soquel Canyons (from Xu et al, 2004). The three moorings (R1, R2, and R3) were deployed at 820, 1020 and 1450 m water depths.

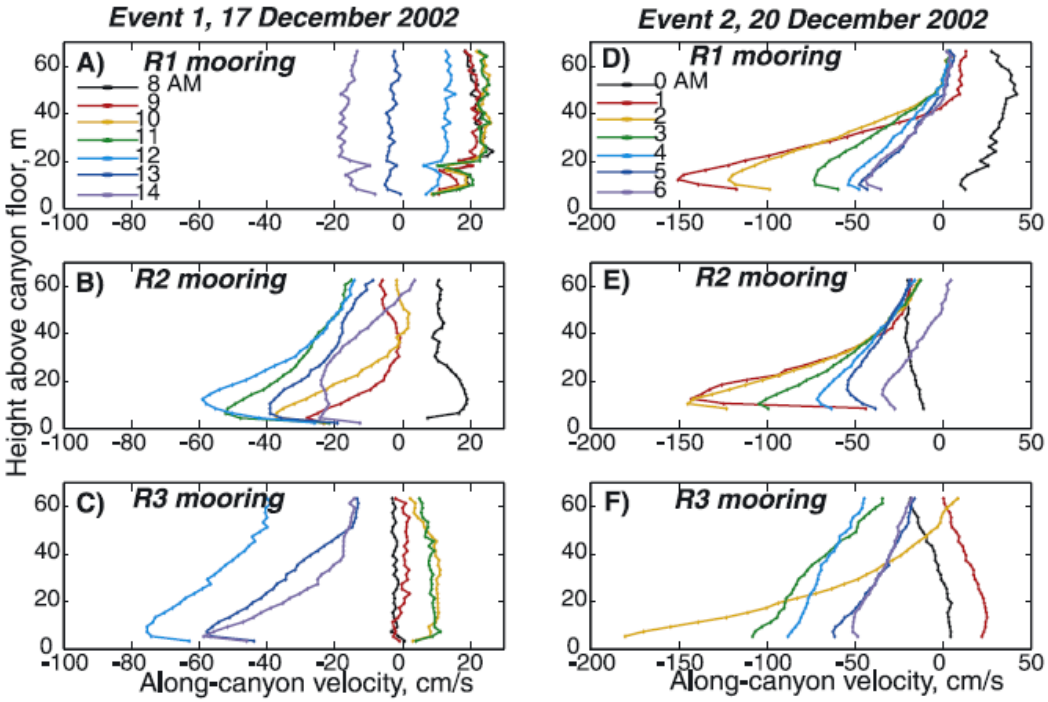

Fig. 41. Hourly vertical velocity profiles of turbidity current event 1 (left) and 2 (right). From Xu et al. (2004).

Results — The best-fit simulation runs for the first and the second event are shown as snapshot series in Figures 42 and 43, respectively. Examples of more detailed velocity time series for an estimated mid-height of each flow at the mooring locations are given in Figure 44.

The range of simulated velocities for the first flow event corresponds rather well to the measurements from the mooring station R2, though less well to the measurements from R1 (cf. Figs. 41 and 44). The flow appears to have lost capacity by dilution over a relatively short distance (Fig. 42) and displayed significant velocity fluctuations (Fig. 44), which can be attributed to the highly rugged floor topography of the Soquel Canyon. A major loss of momentum occurred when the flow plunged at high angle into the Monterey Canyon, crashing against the southern wall of its bend (Fig. 42).

The second flow event, in contrast, developed a considerably longer body and strongly accelerated between stations R1 and R2, and further towards the second sharp bent of the Monterey Canyon – before plunging against the bend's western wall (Fig. 43). The apparent decline of the flow velocity at station R3 (Fig. 44) may suggest waning, whereas the flow appears to have experienced a new waxing phase after passing this station. The range of simulated velocities corresponds rather well to the R1 measurements and nearly perfectly to the R2 measurement.

The likely reason of the discrepancies is that the volumetric sediment concentration and exact grain-size distribution in the flows remains unknown.

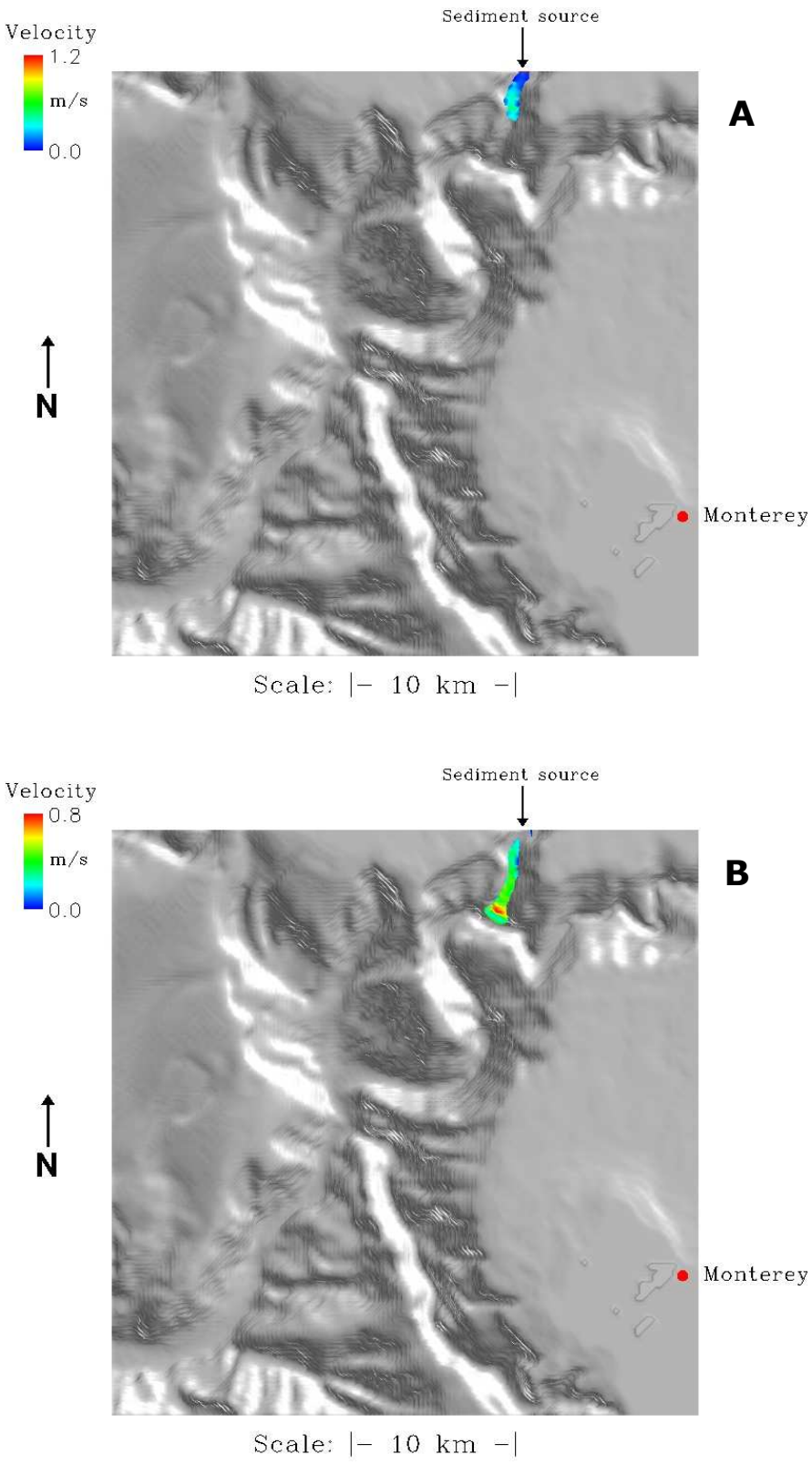

Fig. 42. Simulation of event 1, with source in the Soquel Canyon. The twelve snapshots (A-L) correspond to the flow of 1 to 12 hours. The flow is displayed as in terms of its velocity magnitude. Scale: 34x34 km.

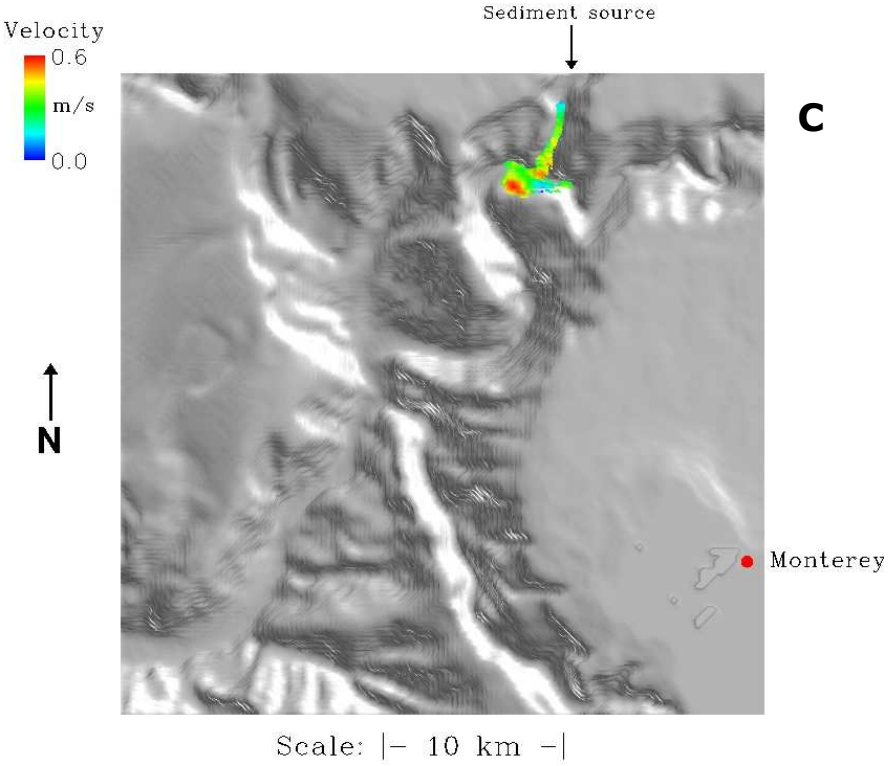
Velocity
0.6
m/s
0.0
Sediment source
C
N
Monterey
Scale: |– 10 km –|

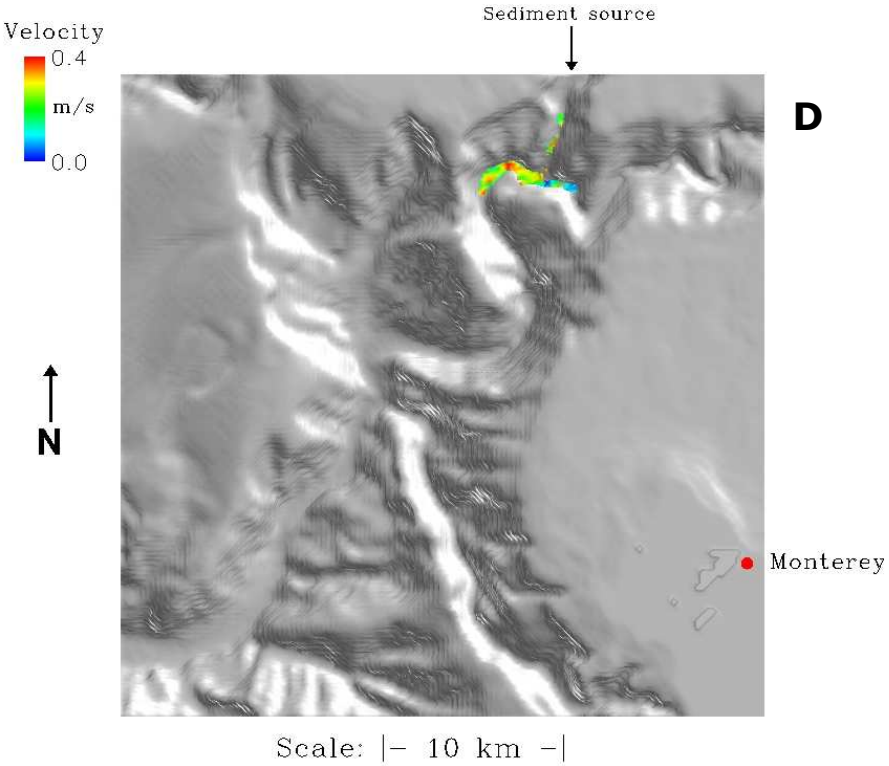
Velocity
0.4
m/s
0.0
Sediment source
D
N
Monterey
Scale: |– 10 km –|

Fig. 42 (cont.)

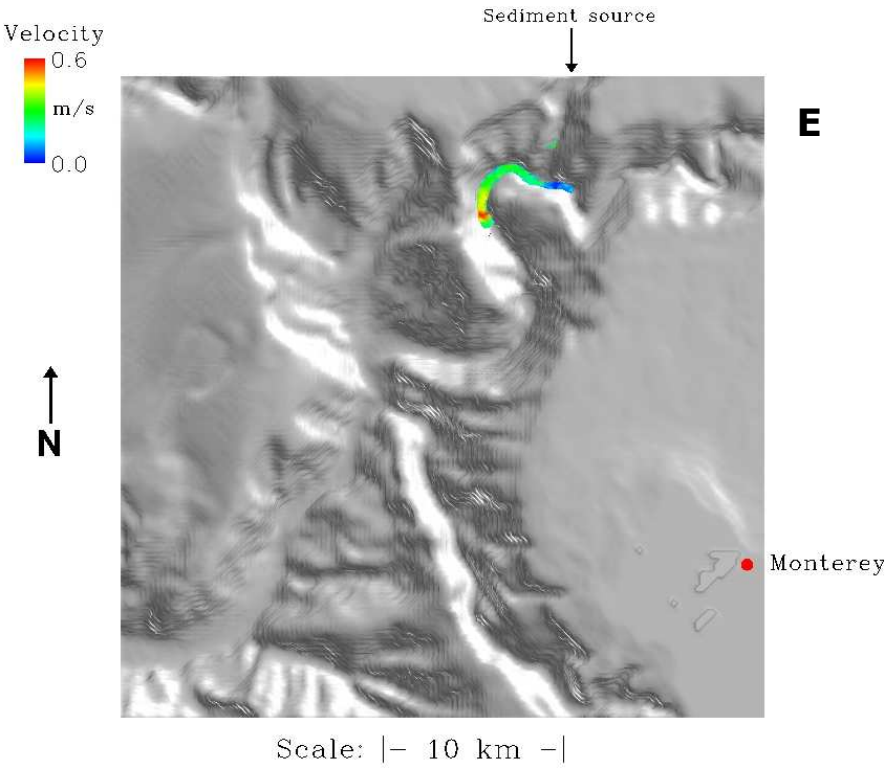
Velocity
0.6
m/s
0.0
Sediment source
E
N
Monterey
Scale: |– 10 km –|

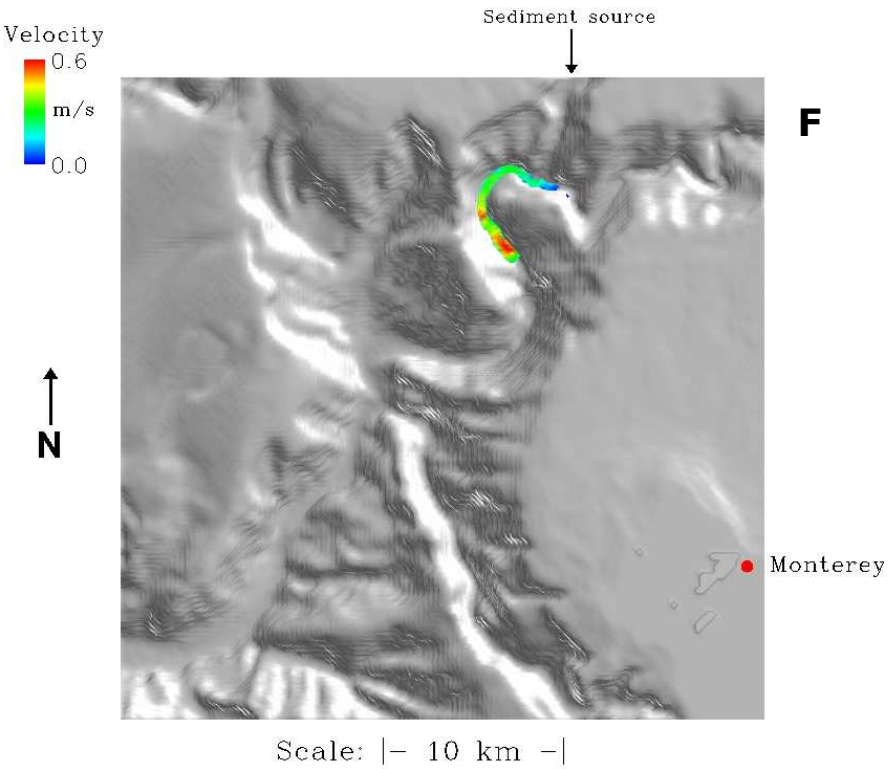
Velocity
0.6
m/s
0.0
Sediment source
F
N
Monterey
Scale: |– 10 km –|

Fig. 42 (cont.)

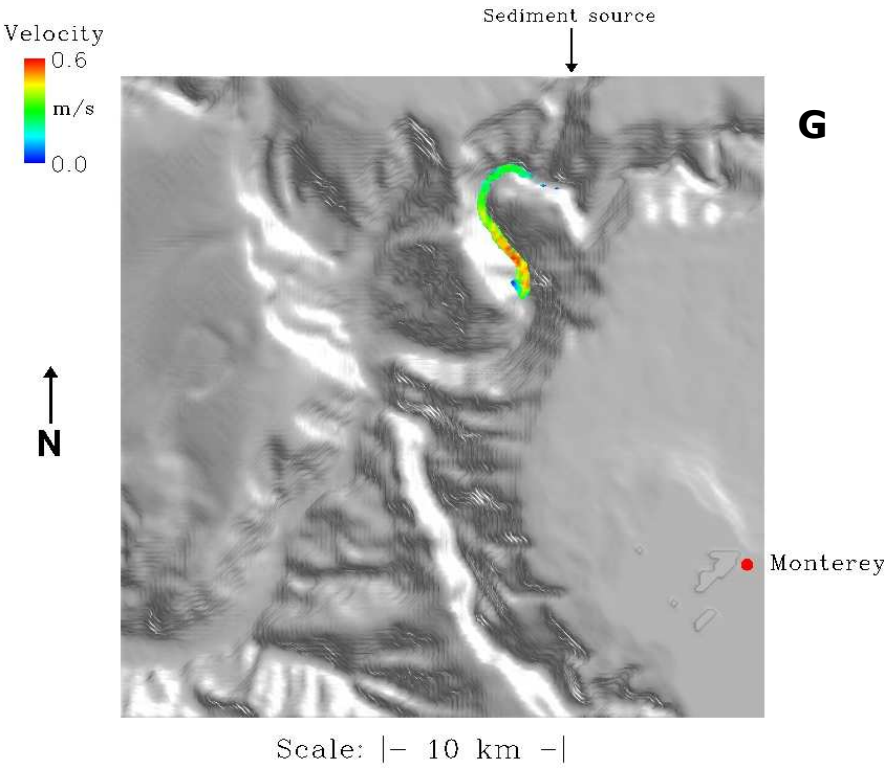
Velocity
0.6
m/s
0.0
Sediment source
G
N
Monterey
Scale: |– 10 km –|

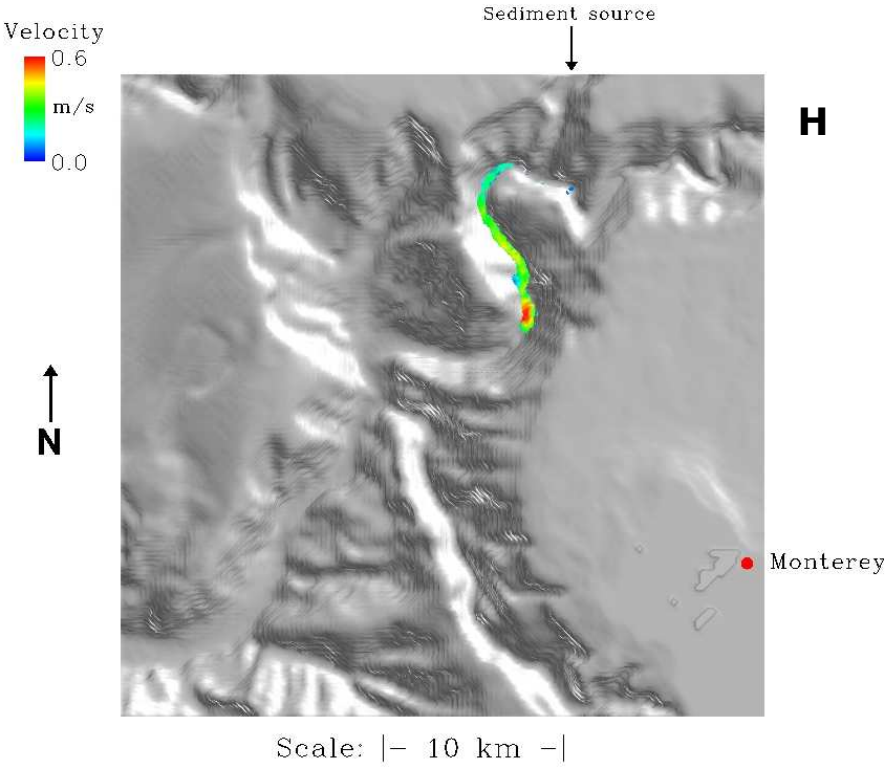
Velocity
0.6
m/s
0.0
Sediment source
H
N
Monterey
Scale: |– 10 km –|

Fig. 42 (cont.)

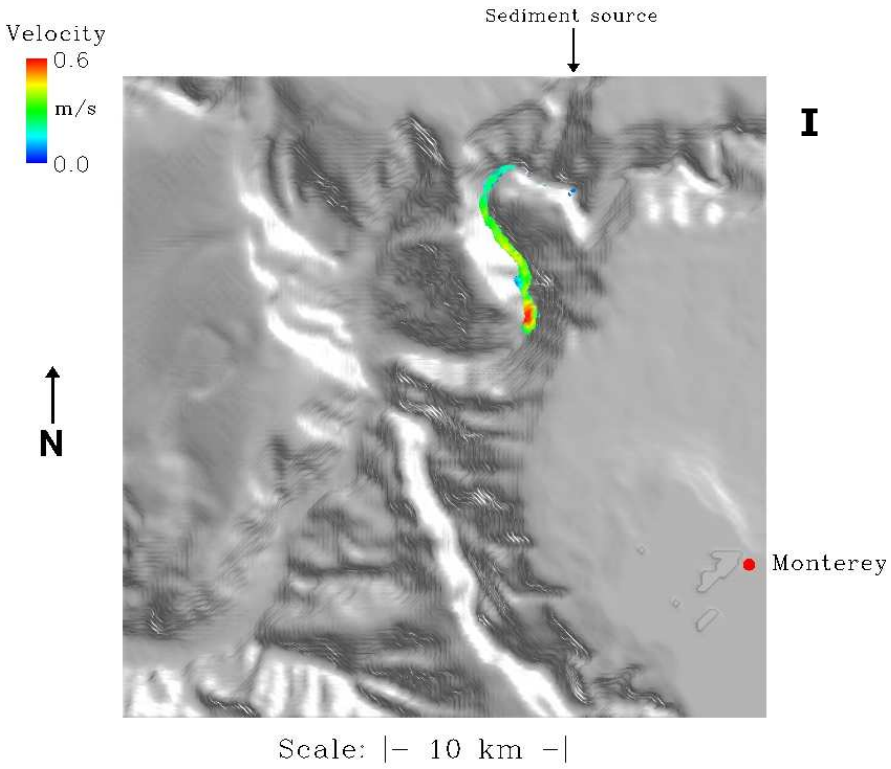
Velocity
0.6
m/s
0.0
Sediment source
I
N
Monterey
Scale: |– 10 km –|

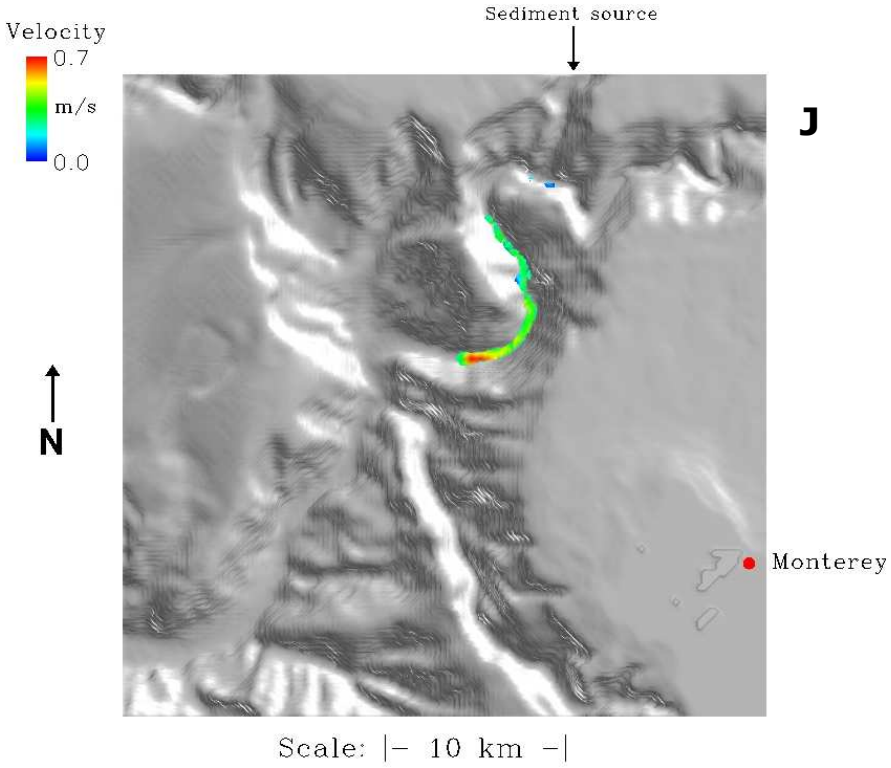
Velocity
0.7
m/s
0.0
Sediment source
J
N
Monterey
Scale: |– 10 km –|

Fig. 42 (cont.)

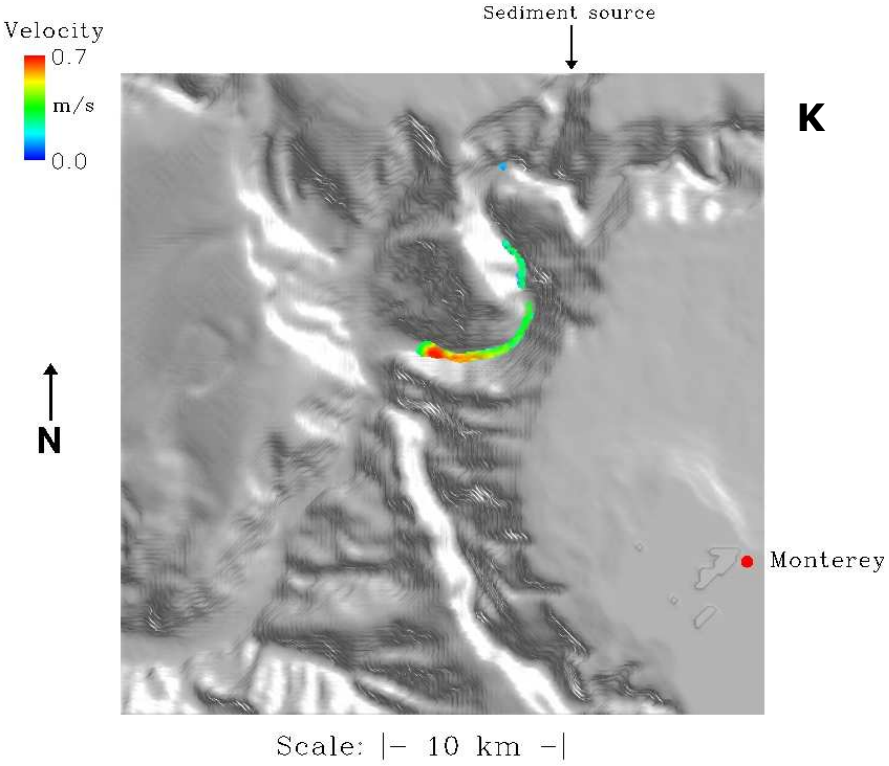
Velocity
0.7
m/s
0.0
Sediment source
K
N
Monterey
Scale: |– 10 km –|

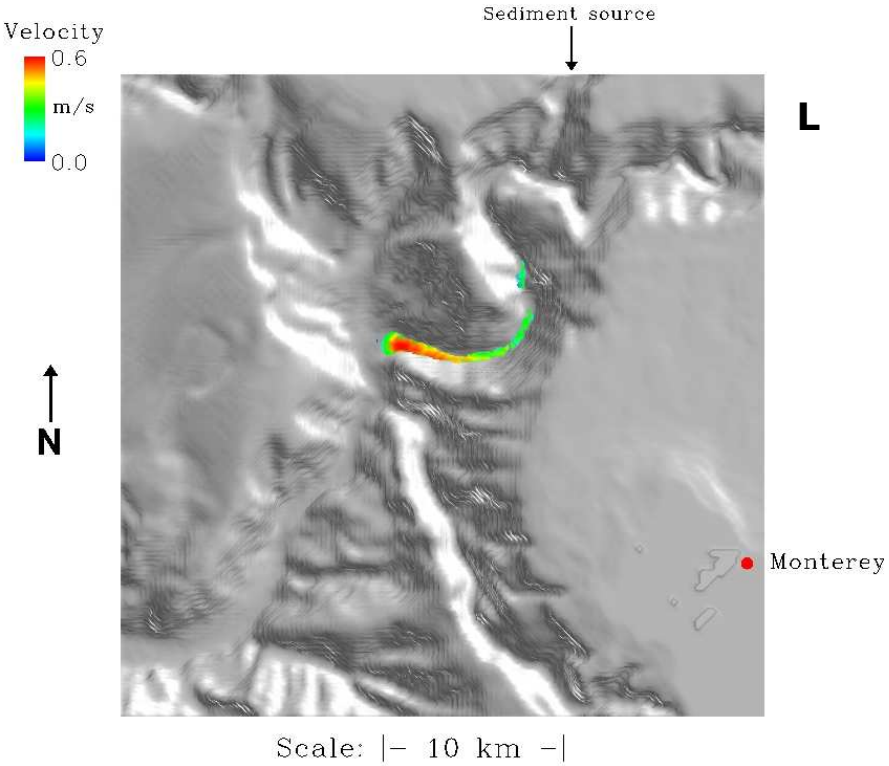
Velocity
0.6
m/s
0.0
Sediment source
L
N
Monterey
Scale: |– 10 km –|

Fig. 42 (cont.)

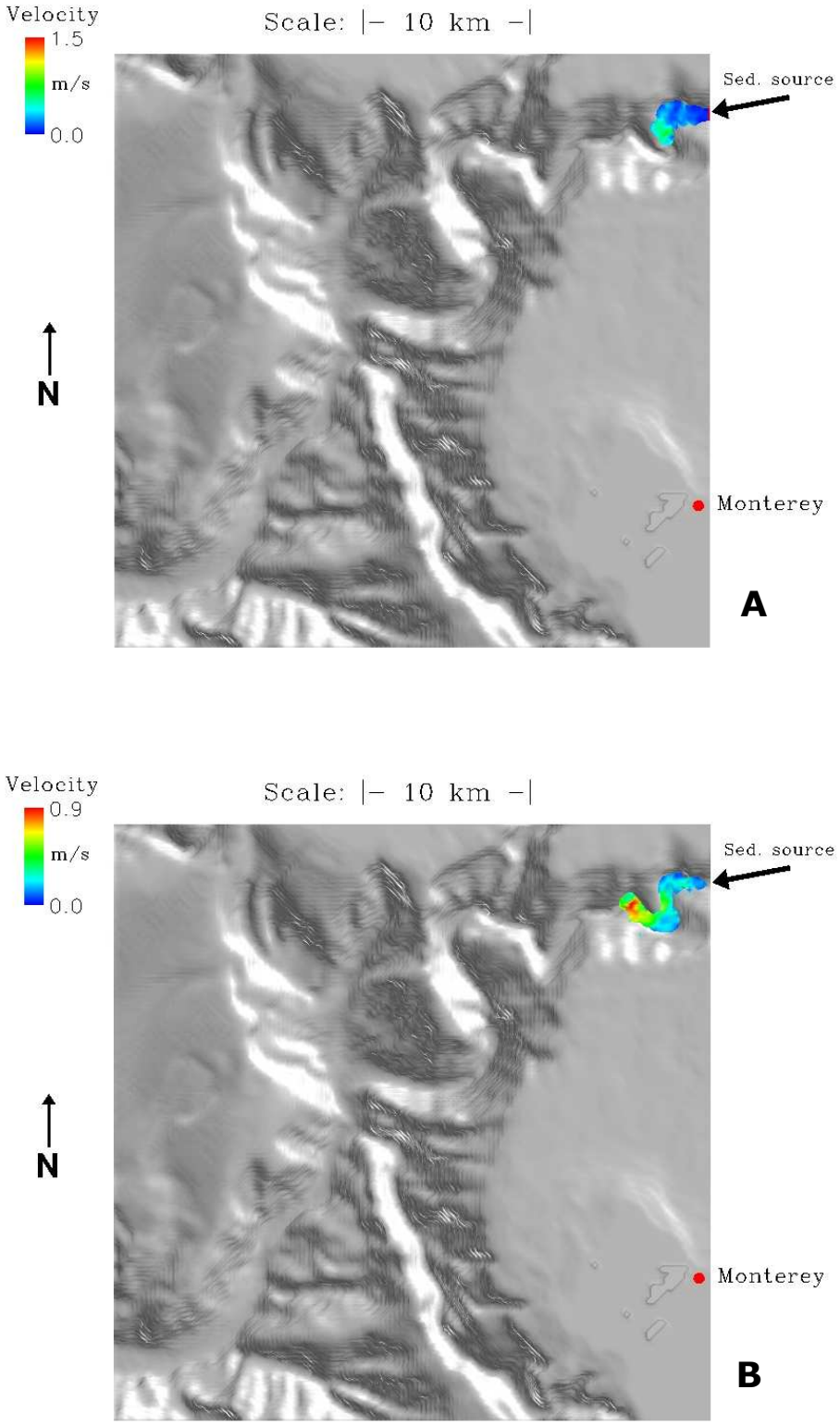

Fig. 43. Simulation of event 2, with source in the uppermost Monterey Canyon. The twelve snapshots (A-J) correspond to the flow of 1 to 12 hours. The flow is displayed as in terms of its vel. magnitude. Scale: 34x34 km.

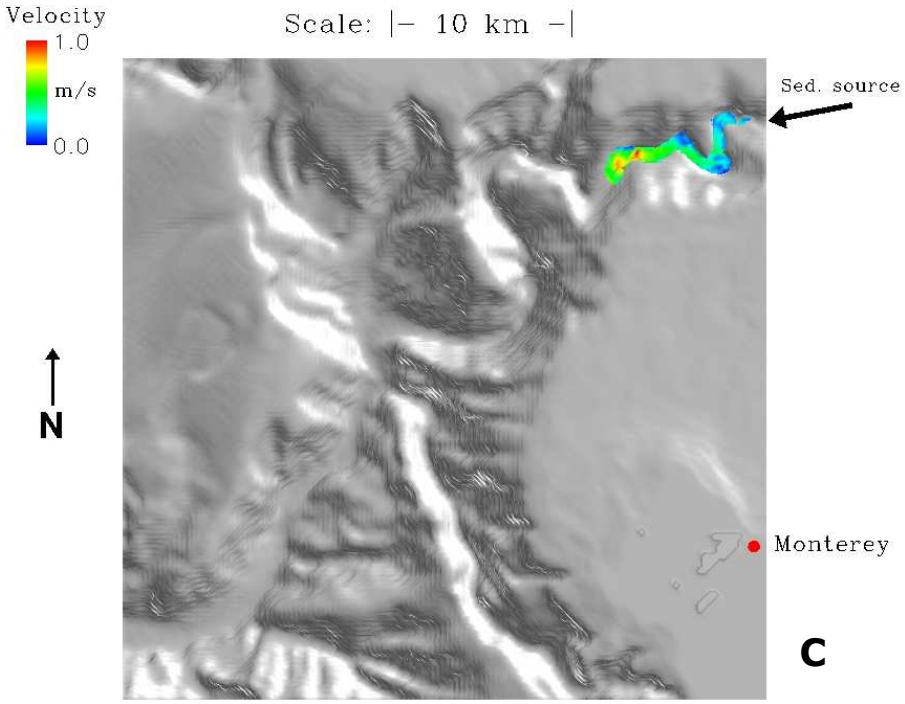
Velocity
1.0
m/s
0.0
Scale: |– 10 km –|
Sed. source
N
Monterey
C

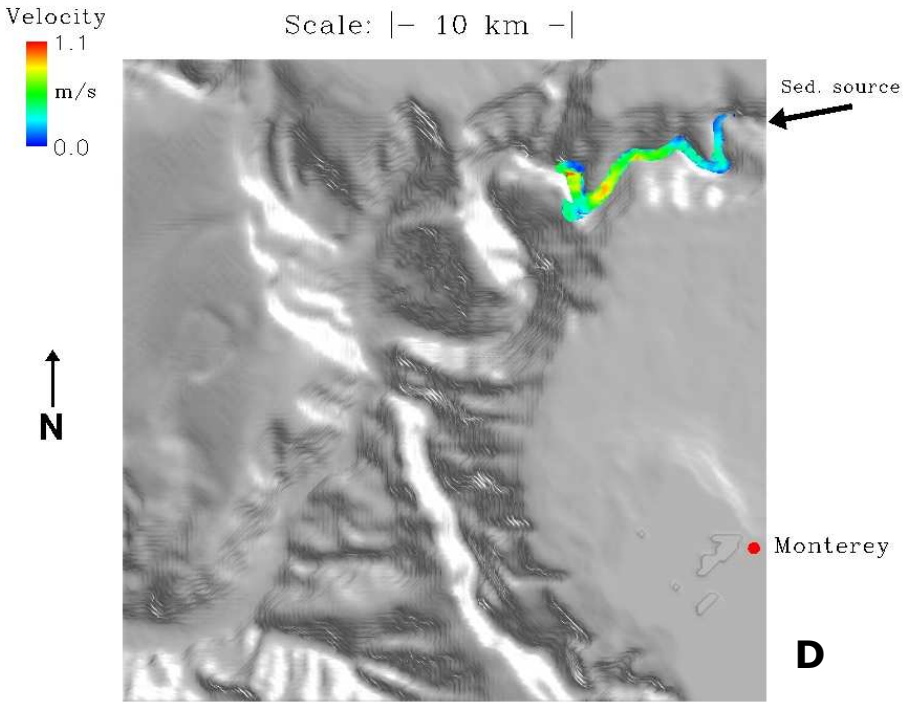
Velocity
1.1
m/s
0.0
Scale: |– 10 km –|
Sed. source
N
Monterey
D

Fig. 43 (cont.)

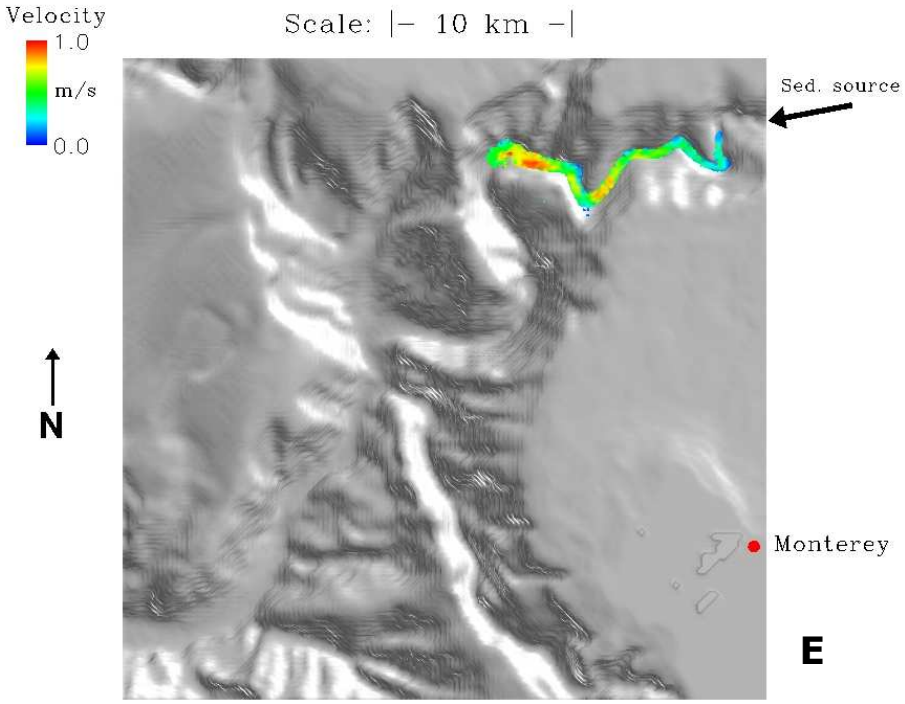
Velocity
1.0
m/s
0.0
Scale: |– 10 km –|
Sed. source
N
Monterey
E

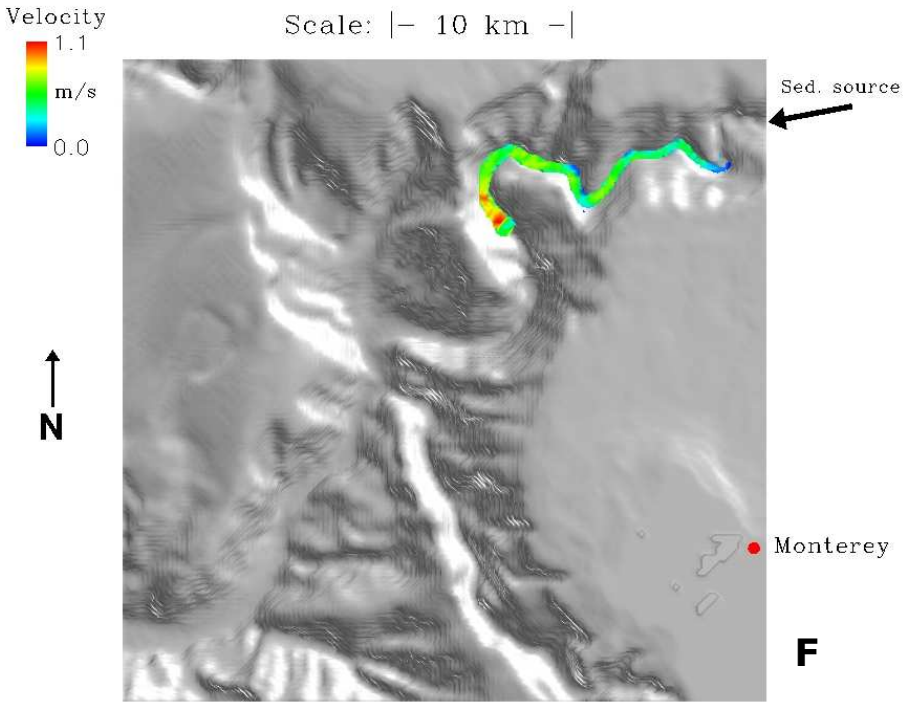
Velocity
1.1
m/s
0.0
Scale: |– 10 km –|
Sed. source
N
Monterey
F

Fig. 43 (cont.)

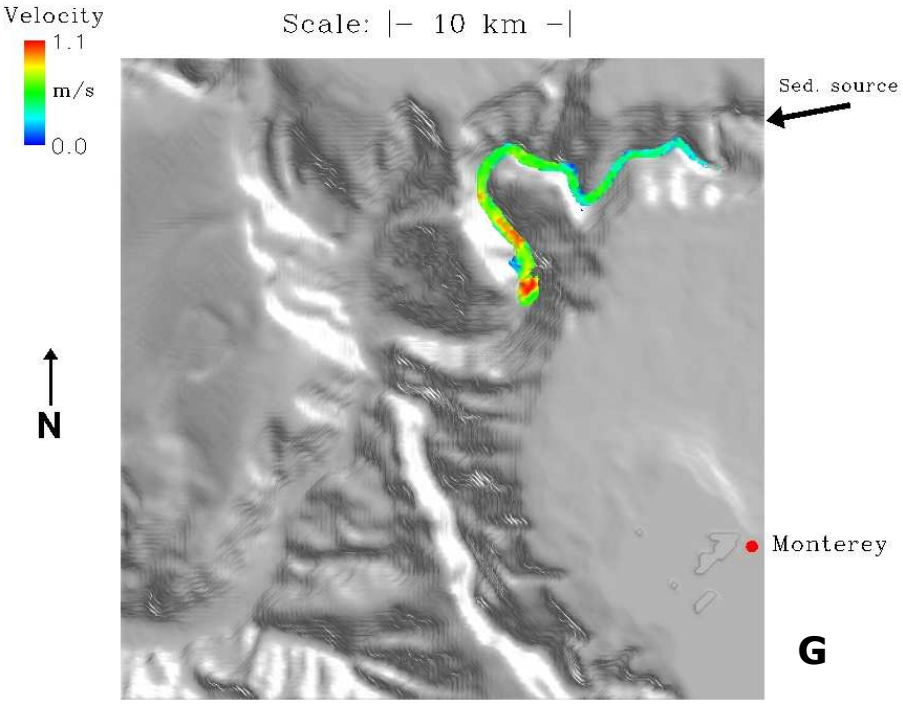
Velocity
1.1
m/s
0.0
Scale: |– 10 km –|
Sed. source
N
Monterey
G

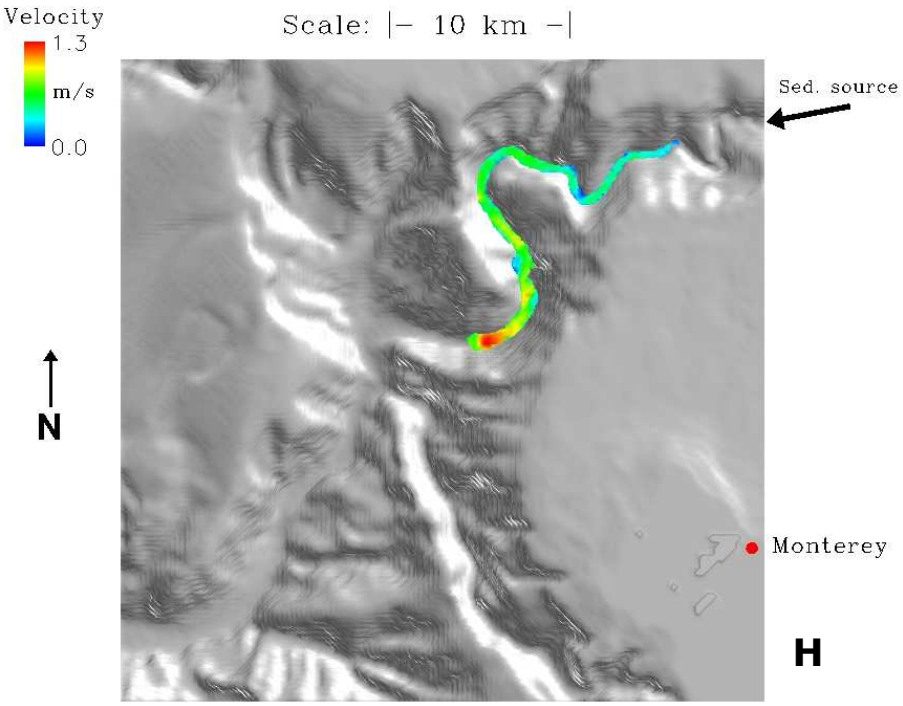
Velocity
1.3
m/s
0.0
Scale: |– 10 km –|
Sed. source
N
Monterey
H

Fig. 43 (cont.)

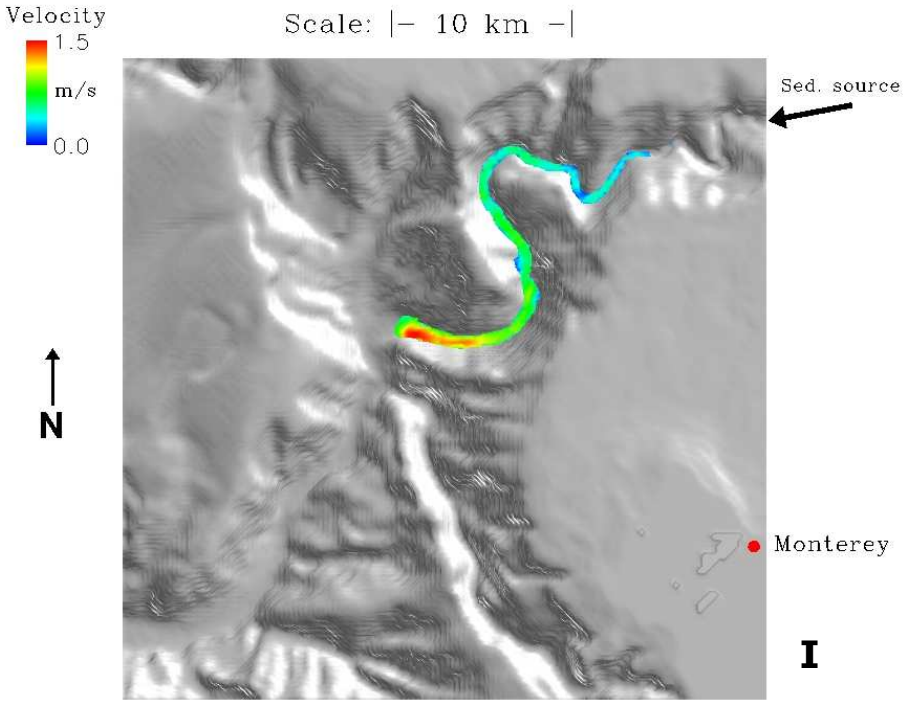
Velocity
1.5
m/s
0.0
Scale: |– 10 km –|
Sed. source
N
Monterey
I

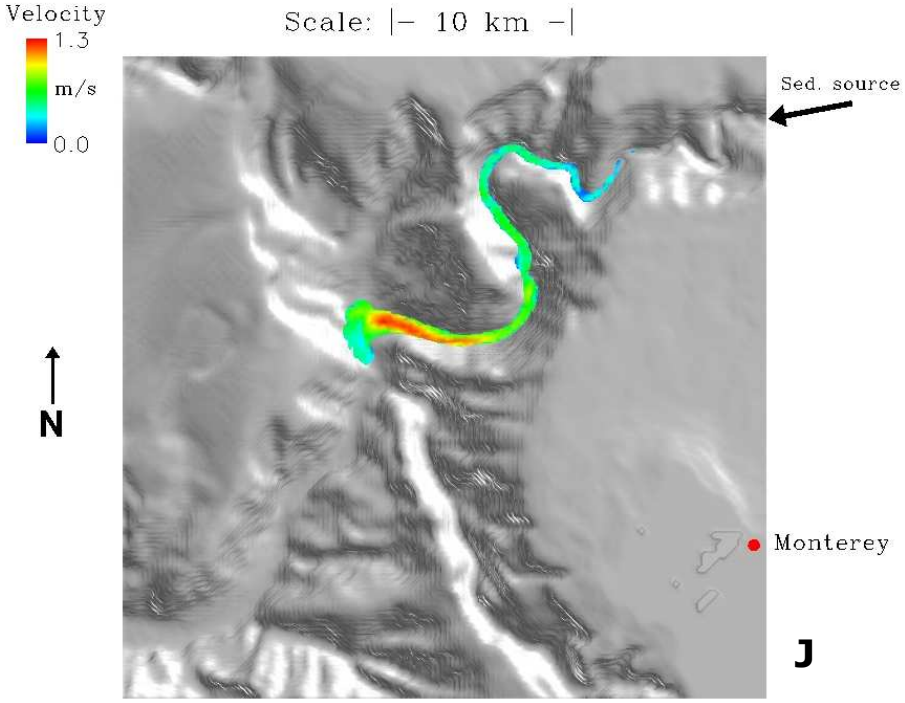
Velocity
1.3
m/s
0.0
Scale: |– 10 km –|
Sed. source
N
Monterey
J

Fig. 43 (cont.)

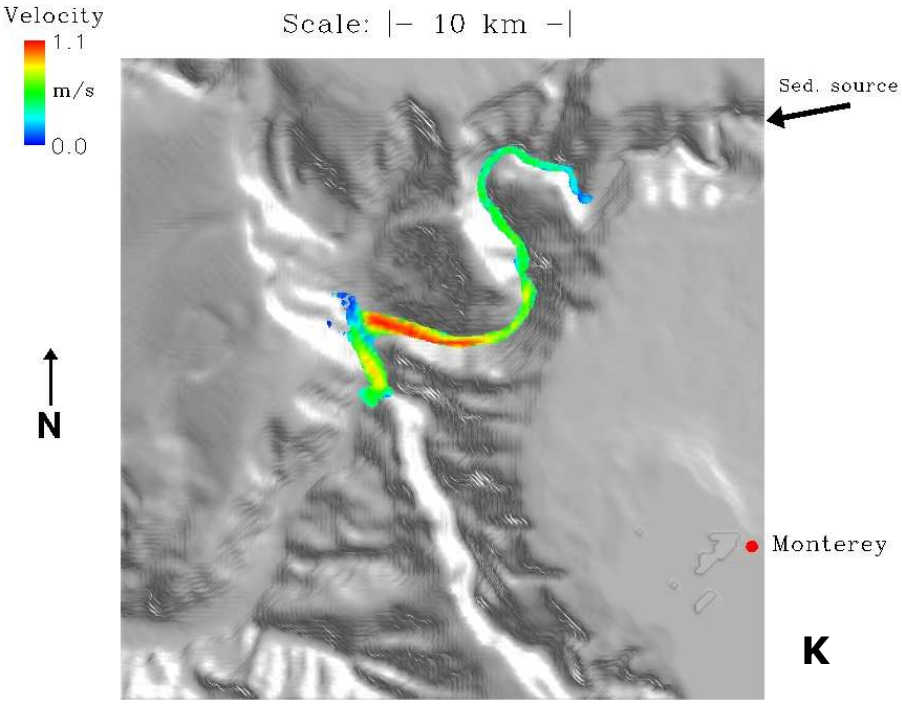
Velocity
1.1
m/s
0.0
Scale: |– 10 km –|
Sed. source
N
Monterey
K

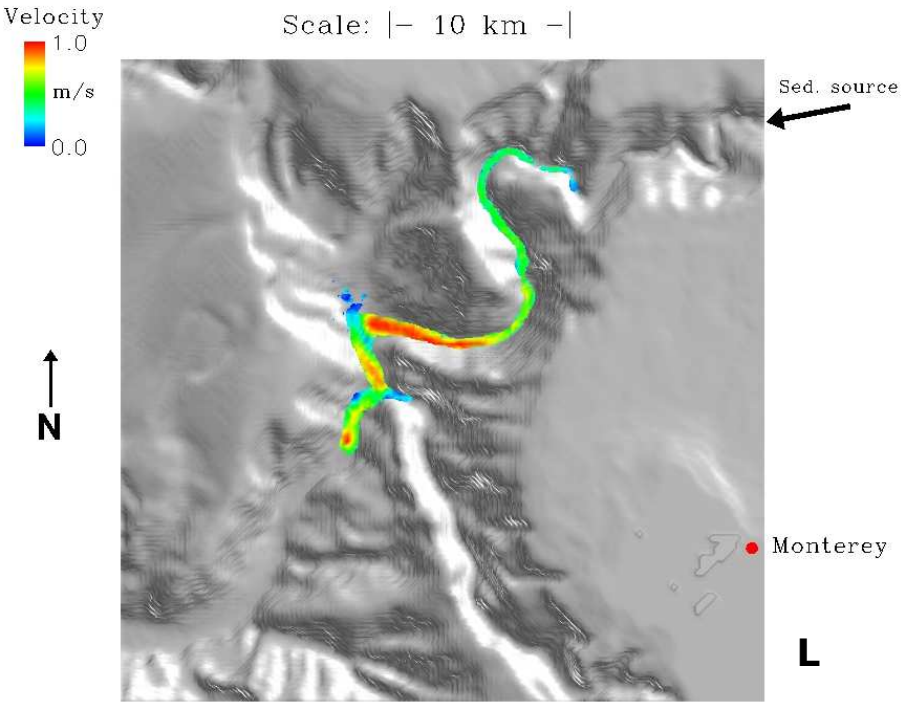
Velocity
1.0
m/s
0.0
Scale: |– 10 km –|
Sed. source
N
Monterey
L

Fig. 43 (cont.)

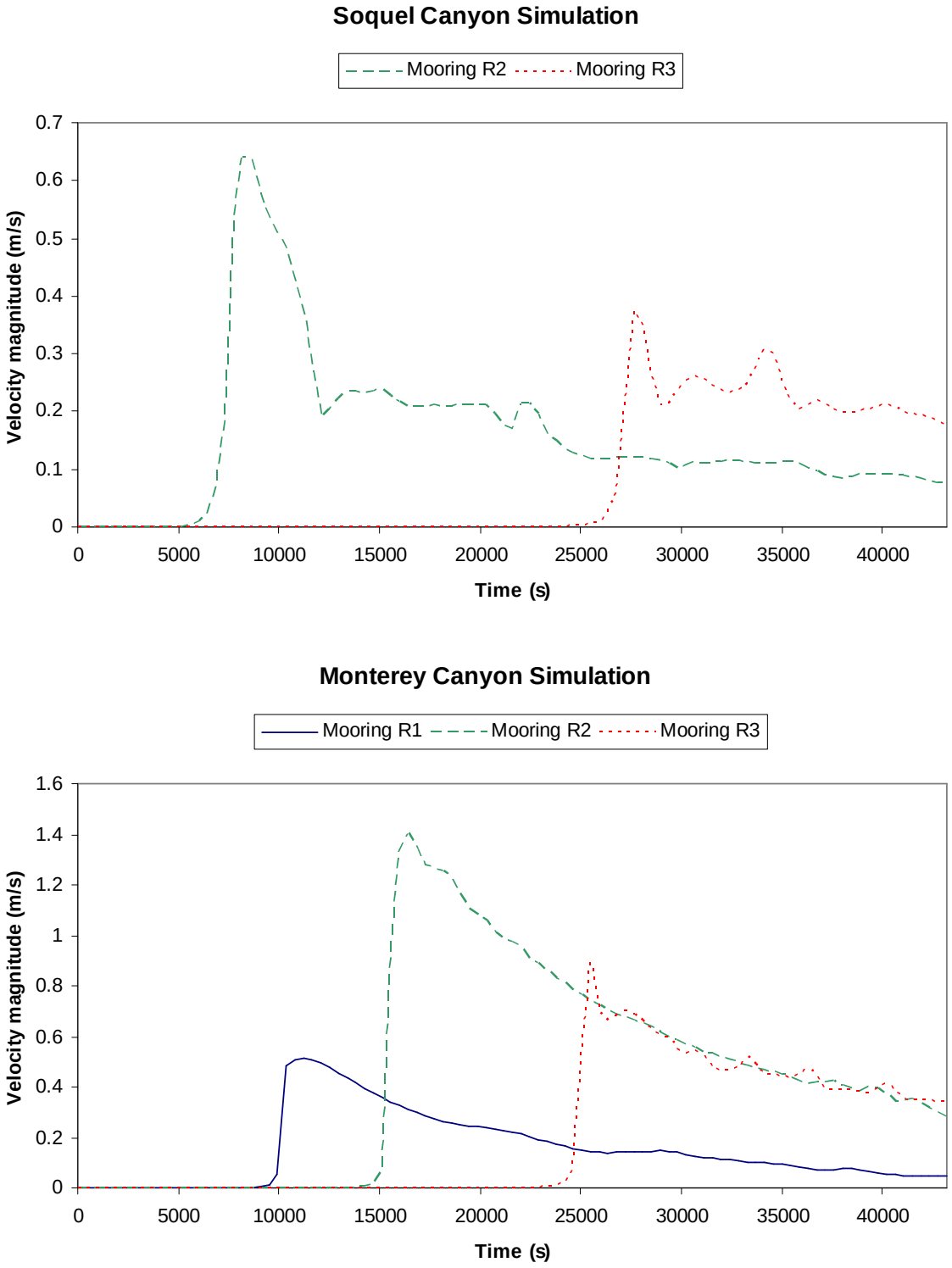

Fig. 44. Simulated multi-location velocity time series for the flow events sourced from the Soquel (top) and Monterey (bottom) canyons, in each case for a height of 30 m above the canyon floor (mooring locations as shown in Fig. 40).

5. CONCLUSIONS

- The present study has evaluated the usefulness of Flow-3D™ as a possible means of simulating the hydrodynamic behaviour of turbidity currents and hence as an attractive alternative to laboratory experiments.
- The comparison of numerical and laboratory data indicates that the CFD-based Flow-3D™ models can give realistic results and are quite suitable for this kind of simulations.
- The use of a CFD software, such as the Flow-3D™, has several great advantages:
    - It allows a much wider range of flow parameters to be determined and continuously monitored with a relatively high accuracy.
    - It permits the response and relative importance of the individual flow parameters to be assessed with respect to changes in the initial conditions.
    - It allows turbidity currents to be up-scaled to natural conditions and simulations to be performed on a 'real-life' basin scale.
    - It provides an unprecedented insight in the detailed hydrodynamic aspects of turbidity current.
- The software can readily be adapted to any experimental setup and a wide range of initial conditions:
    - Both surge-type and sustained turbidity currents can be simulated, including confined and unconfined flows of high and low density.
    - A turbidity current's erosional capacity and response to hydraulic jump, or slope-break conditions.
    - The sensitivity of turbidity current to seafloor topographic features can be evaluated for different conditions.
    - The spatial dispersal of sediment and its various grain-size fractions under different flow conditions can be predicted.
- The study indicates that our understanding of turbidites and their variation can be significantly improved by this type of experimental research.

REFERENCES

Alexander, J. and Morris, S.A. (1994) Observations on experimental non-channelized turbidites: thickness variations around obstacles*. Journal of Sedimentary Petrology*, **64**, 899-909.

Allen, J.R.L. (1971) Mixing at turbidity-current heads, and its geological implications. *Journal of Sedimentary Petrology*, **41**, 97-113.

Allen, J.R.L. (1982) *Sedimentary Structures – Their Character and Physical Basis (Volume 1 & 2).* Elsevier, Amsterdam, 1256 p.

Allen, J.R.L. (1991) The Bouma division A and the possible duration of turbidity currents. *Journal of Sedimentary Research,* **61***,* 291-295.

Altikanar, M.S., Graf, W.H. and Hopfinger, E.J. (1996) Flow structure in turbidity currents. *Journal of Hydraulic Research, IAHR,* **34**, 713-718.

Ames, W.F. (1992) *Numerical Methods for Partial Differential Equations*. 3rd Edition, Academic Press (USA), 433 p.

Atkins, P.W. (1990) *Physical Chemistry*. Oxford University Press, Oxford, 995 p.

Baas, J.H., van Kesteren, W. and Postma, G. (2004) Deposits of depletive, quasi-steady high-density turbidity currents: a flume analogue of bed geometry, structure and texture. *Sedimentology*, **51**, 1053-1089.

Bagnold, R.A. (1954) Experiments on a gravity-free dispersion of large solid spheres in a Newtonian fluid under shear. *Proceedings of the Royal Society of London*, **A225**, 49-63.

Bagnold, R.A. (1962) Auto-suspension of transported sediment: turbidity currents. *Proceedings of the Royal Society of London*, **A265**, 315-319.

Barnes, H.A., Hutton, J.F. and Walters, K. (1989) *An Introduction to Rheology*. Elsevier, Amsterdam, 199 p.

Bates, C.C. (1953) Rational theory of delta formation. *American Association of Petroleum Geologists Bulletin*, **37**, 2119-2162.

Best, J., Kirkbride, A. and Peakall, J. (2001) Mean flow and turbulence structure of sediment-laden gravity currents: new insights using ultrasonic Doppler velocity profiling. In: McCaffrey, W.D., Kneller, B.C. and Peakall, J. (Eds), *Particulate Gravity Currents. International Association of Sedimentologists, Special Publication*, **31***,* 159-172.

Beverage, J.P. and Culbertson, J.H. (1964) Hyperconcentrations of suspended sediment. *Proceedings of the American Society of Civil Engineers, Journal of Hydraulic Division*, **90**, 117-128.

Blystad, P., Brekke, H., Færseth, R.H., Larsen, B.T., Skogseid, J. and Tørudbakken, B. (1995) Structural elements of the Norwegian continental shelf, Part II: The Norwegian Sea Region. *Norwegian Petroleum Directorate Bulletin*, **8**, 45 p.

Bouma, A.H. (1962) *Sedimentology of Some Flysch Deposits: A Graphic Approach to Facies Interpretation.* Elsevier, Amsterdam, 168 p.

Bouma, A.H., DeVries, M.B. and Stone, C.G. (1997) Reinterpretation of depositional processes in a classic flysch sequence (Pennsylvanian Jackfork Group), Ouachita Mountains, Arkansas and Oklahoma: Discussion. *American Association of Petroleum Geologists Bulletin*, **81**, 470-472.

Bouma, A.H., Normark, W.R. and Barnes, N.E. (Eds.) (1985) *Submarine Fans and Related Turbidite Systems.* Springer-Verlag, New York, 351 p.

Britter, R.W. and Linden, P.F. (1980) The motion of the front of a gravity current down an incline. *Journal of Fluid Mechanics*, **91**, 531-543.

Britter, R.W. and Simpson, J.E. (1978) Experiments on the dynamics of a gravity-current head. *Journal of Fluid Mechanics*, **88**, 223-240.

Buckee, C., Kneller, B.C., and Peakall, J. (2001) Turbulence structure in steady, solute-driven gravity currents. In: McCaffrey, W.D., Kneller, B.C. and Peakall, J. (Eds), *Particulate Gravity Currents. International Association of Sedimentologists Special Publication,* **31***,* p. 173-188.

Burgess, P.M. and Hovius, N. (1998) Rates of delta progradation during highstands: consequences for timing of deposition in deep-marine systems. *Journal of the Geological Society of London*, **155**, 217-222.

Campbell, C.S. (1989a) The stress tensor for simple shear flows of a granular material. *Journal of Fluid Mechanics,* **203**, 449-473.

Campbell, C.S. (1989b) Self-lubrication of long runout landslides. *Journal of Geology*, **97**, 653-665.

Campbell, C.S. (1990) Rapid granular flows. *Annual Reviews in Fluid Mechanics,* **22**, 57-92.

Carter, R.M. (1975) A discussion and classification of subaqueous mass-transport with particular application to grain flow, slurry flow and fluxoturbidites. *Earth-Science Reviews*, **11**, 145-177.

Chu, F.H., Pilkey, W.D. and Pilkey, O.H. (1979) An analytical study of turbidity-current steady flow. *Marine Geology*, **33**, 205-220.

Coleman, J.L., Jr. (1997) Reinterpretation of depositional processes in a classic flysch sequence (Pennsylvanian Jackfork Group), Ouachita Mountains, Arkansas and Oklahoma: Discussion. *American Association of Petroleum Geologists Bulletin*, **81**, 466-469.

Craig, R.F. (1987) *Soil Mechanics*. 4th Edition, Van Nostrand Reinhold, U.K., 410 p.

Crowell, J.C. (1957) Origin of pebbly mudstones. *Geological Society of America Bulletin*, **68**, 993-1009.

D'Agostino, A.E. and Jordan, D.W. (1997) Reinterpretation of depositional processes in a classic flysch sequence (Pennsylvanian Jackfork Group), Ouachita Mountains, Arkansas and Oklahoma: Discussion. *American Association of Petroleum Geologists Bulletin*, **81**, 473-475.

Doreen, J.M., Jr. (1951) Rubble bedding and graded bedding in Talara Formation of northwestern Peru. *American Association of Petroleum Geologists Bulletin*, **35**, 1829-1849.

Dott, R.H., Jr. (1963) Dynamics of subaqueous gravity depositional processes. *American Association of Petroleum Geologists Bulletin*, **47**, 104-128.

Duncan, W.J. (1953) *Physical Similarity and Dimensional Analysis.* Edward Arnold & Co., London, 156 p.

Drake, T.G. (1990) Structural features in granular flows. *Journal of Geophysical Research*, **B95**, 8681-8696.

Dzułyński, S. and Sanders, J.E. (1962) Current marks on firm mud bottoms. *Connecticut Academy of Arts and Sciences Transactions*, **42**, 57-96.

Einstein, H.A. (1950) The bed-load function for sediment transportation in open-channel flows. *U.S. Department of Agriculture, Soil Conservation Service Technical Bulletin*, **1026**, 71 p.

Ellison, T.H. and Turner, J.S. (1959) Turbulent entrainment in stratified flows. *Journal of Fluid Mechanics*, **6**, 423-448.

Fisher, R.V. (1971) Features of coarse-grained, high-concentration fluids and their deposits. *Journal of Sedimentary Petrology*, **41**, 916-927.

Fisher, R.V. (1983) Flow transformations in sediment gravity flows. *Geology*, **11,** 273-274.

Fisher, R.V. (1986) Systems of transport and deposition within pyroclastic surges: evidence from Mount St. Helens, Washington. *EOS Transactions of the American Geophysical Union, **67***, 1246.

French, R.H. (1985) *Open-Channel Hydraulics*. McGraw-Hill, New York, 704 p.

Friedman, G.M. and Sanders, J.E. (1997) Dispelling the myth of seafloor tranquillity. *Geotimes*, **42**, 24-27.

Gani, M. R. (2004) From turbid to lucid: a straightforward approach to sediment-gravity flows and their deposits. *The Sedimentary Record*, **2**, 4-8.

Garcia, M.H. (1990) Depositing and eroding sediment-driven flows: turbidity currents. Unpubl. Ph.D. Thesis, St. Anthony Falls Hydraulic Laboratory, University of Minnesota (USA), 179 p.

Garcia, M.H. (1993) Hydraulic jumps in sediment-driven bottom currents. *Journal of Hydraulic Engineering*, *ASCE*, **119**, 1094-1117.

Garcia, M.H. (1994) Depositional turbidity currents laden with poorly sorted sediment. *American Society of Civil Engineers*, *Journal of Hydraulic Engineering*, **120**, 1240-1263.

Gardner, J.V. and Kidd, R.B. (1983) Sedimentary processes on the Iberian continental margin viewed by long-range side-scan sonar, Part 1: Gulf of Cadiz. *Oceanologica Acta*, **6**, 245-254.

Gee, M.J.R., Masson, D.G., Watts, A.B. and Allen, P.A. (1999) The Saharan debris flow: an insight into the mechanics of long-runout submarine debris flows. *Sedimentology*, **46**, 317-335.

Guo, J. (2002) Hunter Rouse and Shields diagram. In: *Proceedings from the 13th IAHR-APD Congress*, Singapore, No. 2, p. 1096-1098.

Hallworth, M.A. and Huppert, H.E. (1998) Abrupt transitions in high-concentration, particle-driven gravity currents. *Physics of Fluids*, **10**, 1083-1087.

Hampton, M.A. (1972) The role of subaqueous debris flows in generating turbidity currents. *Journal of Sedimentary Petrology*, **42**, 775-793.

Hampton, M.A. (1975) Competence in fine-grained debris flows. *Journal of Sedimentary Petrology*, **45**, 834-844.

Harlow, F.H. and Nakayama, P.I. (1967) Turbulence transport equations. *Physics of Fluids*, **10**, 2323-2332.

Heezen, B.C. and Ewing, M. (1952) Turbidity currents and submarine slumps and the 1929 Grand Banks earthquake. *American Journal of Science*, **250**, 849-873.

Heimsund, S., Hansen, E.W.M. and Nemec, W. (2002) Computational 3D fluid-dynamics model for sediment transport, erosion and deposition by turbidity currents. In: Knoper, M. and Cairncross, B. (Ed.) *Abstracts, International Association of Sedimentologists 16th International Sedimentological Congress*, Rand Afrikaans Univ., Johannesburg, p. 151-152.

Heimsund, S., Hansen, E.W.M. and Nemec, W. (2003a) Computational 3-D fluid-dynamics model for sediment transport, erosion and deposition by turbidity currents. In: Nakrem, H.A. (Ed.), *Abstracts and Proceedings of the Geological Society of Norway (NGF)*, Den 18. Vinterkonferansen, Oslo, No. 1, p. 39.

Heimsund, S., Hansen, E.W.M. and Nemec, W. (2003b) Numerical CFD simulation of turbidity currents and comparison with laboratory data. In: Hodgetts, D., Hodgson, D. and Smith, R. (Ed.), *Slope Modelling Workshop Abstracts, Experimental, Reservoir and Forward Modelling of Turbidity Currents and Deep-Water Sedimentary Systems*, Liverpool Univ., p. 13.

Heimsund, S., Möller, N., Guargena, C. and Thompson, L. (2004) The control of seafloor topography on turbidite sand dispersal in the Ormen Lange field: a large-scale application of Flow-3D™ simulations. In: Martinsen, O.J. (Ed.), *Abstracts and Proceedings of the Geological Society of Norway (NGF)*, Deep Water Sedimentary Systems of Arctic and North Atlantic Margins, Stavanger, No. 3, p. 25.

Heimsund, S., Möller, N., Guargena, C. and Thompson, L. (2005a) Field-scale modeling of turbidity currents by FLOW-3D™ simulations. In: *Workshop Abstracts, Modeling of Turbidity Currents and Related Gravity Currents*, Univ. of California, Santa Barbara, 2 p.

Heimsund, S. (2005b) FLOW-3D™ simulation of the Ormen Lange field, Mid-Norway Continental Shelf. Unpubl. Report to A/S Norske Shell, Complex Flow Design AS, Trondheim, 24 p.

Heimsund, S., Möller, N. and Guargena, C. (2006) FLOW-3D™ simulation of the Ormen Lange field, mid-Norway. In: Hoyanagi, K., Takano, O. and Kano, K. (Ed.), *Abstracts, International Association of Sedimentologists 17th International Sedimentological Congress*, Fukuoka, Vol. B, p. 107.

Hiscott, R.N. (1994a) Loss of capacity, not competence, as the fundamental process governing deposition from turbidity currents. *Journal of Sedimentary Research*, **A64**, 209-214.

Hiscott, R.N. (1994b) Traction-carpet stratification in turbidites – fact or fiction? *Journal of Sedimentary Research,* **A64**, 204-208.

Hiscott, R.N. (1995) Traction-carpet stratification in turbidites – fact or fiction? Reply. *Journal of Sedimentary Research*, **A65**, 704-705.

Hiscott, R.N. and James, N.P. (1985) Carbonate debris flows, Cow Head Group, western Newfoundland. *Journal of Sedimentary Petrology*, **55**, 735-745.

Hiscott, R.N., Pickering, K.T., Bouma, A.H., Hand, B.M., Kneller, B.C., G. Postma and Soh., W. (1997) Basin-floor fans in the North Sea: sequence stratigraphic models vs. sedimentary facies: Discussion. *American Association of Petroleum Geologists Bulletin*, **81**, 662-665.

Hopfinger, E.J. and Tochon-Danguy, J.C. (1977) A model study of powder-snow avalanches. *Journal of Glaciology*, **19**, 343-356.

Hsu, K.J. (1959) Flute- and groove-casts in pre-Alpine flysch, Switzerland. *American Journal of Glaciology*, **19**, 343-356.

Hughes-Clarke, J.E., Shor, A.N., Piper, D.J.W. and Mayer, L.A. (1990) Large-scale current-induced erosion and deposition in the path of the 1929 Grand Banks turbidity current. *Sedimentology*, **37**, 613-620.

Iverson, R. M. (1997) Physics of debris flows. *Reviews in Geophysics*, **35**, 245-296.

Janbu, N.E., Nemec, W., Kırman, E. and Őzaksoy, V. (2007). Facies anatomy of a channelized sand-rich turbiditic system: the Eocene Kusuri Formation in the Sinop Basin, north-central Turkey. In: Nichols, G., Paola, C. and Williams, E.A. (Eds.), *Sedimentary Environments, Processes and Basins — A Tribute to Peter Friend*. *International Association of Sedimentologists Special Publication* (in press).

Johnson, A.M. (1970) *Physical Processes in Geology.* Freeman, Cooper and Company, San Francisco, 557 p.

Johnson, A.M. and Rodine, J.R. (1984) Debris flow. In: Brunsden, D. and Prior, D.B. (Eds.), *Slope Instability.* John Wiley and Sons, Chichester, p. 257-361.

Johnson, D. (1938) The origin of submarine canyons. *Journal of Geomorphology*, **1**, 111-340.

Johnson, K.S., Paull, C.K., Barry, J.P. and Chavez, F.P. (2001). A decadal record of underflows from a coastal river into the deep sea. *Geology*, **29**, 1019-1022.

Keedwell, M.J. (1984) Rheology and Soil Mechanics. Elsevier Applied Science Publishers, London, 323 p.

Kelts, K. and Hsu, J. (1980) Resedimented facies of 1875 Horgen slumps in Lake Zurich and process model of longitudinal transport of turbidity currents. *Eclogae Geologicae Helveticae*, **73,** 271-281.

Knapp, R.T. (1938) Energy balance in streams carrying suspended load. *Transactions of the Amercan Geophysical. Union*, **1**, 501-505.

Kneller, B.C. (1995) Beyond the turbidite paradigm: physical models for deposition of turbidites and their implications for reservoir prediction. In: Hartley, A.J. and Prosser, D.J. (Eds.), *Characterization of Deep Marine Clastic Systems. Geological Society of London Special Publication*, **94**, p. 31-49.

Kneller, B.C., Bennet, S.J. and McCaffrey, W.D. (1997) Velocity and turbulence structure of gravity currents and internal solitary waves: potential sediment transport and the formation of wave ripples in deep water. *Sedimentary Geology*, **112**, 235-250.

Kneller, B.C., Bennet, S.J. and McCaffrey, W.D. (1999) Velocity, turbulence and fluid stresses in experimental gravity currents. *Journal of Geophysical Research*, **A104**, 5281-5291.

Kneller, B.C. and Buckee, C. (2000) The structure and fluid mechanics of turbidity currents: a review of some recent studies and their geological implications. *Sedimentology*, **47**, 62-94.

Kneller, B.C. and Branney, M.J. (1995) Sustained high-density turbidity currents and the deposition of thick massive sands. *Sedimentology*, **42**, 607-616.

Komar, P.D. (1971) Hydraulic jumps in turbidity currents. *Geological Society of America Bulletin*, **82**, 1477-1481.

Komar, P.D. (1977) Computer simulation of turbidity-current flow and the study of deep-sea channels. *The Sea*, **6**, 603-621.

Kuenen, P.H. (1937) Experiments in connection with Daly's hypothesis on the formation of submarine canyons. *Leidse Geologische Mededelingen*, **8**, 327-335.

Kuenen, P.H. (1950) Turbidity currents of high density. *Proceedings of the 18th International Geological Congress (1948)*, **8**, p. 44-52.

Kuenen, P.H. (1957) Sole markings of graded greywacke beds. *Journal of Geology*, **65**, 231-258.

Kuenen, P.H. and Migliorini, C.I. (1950) Turbidity currents as a cause of graded bedding. *Journal of Geology*, **58**, 91-127.

Lambert, A. and Giovanoli, F. (1988) Records of riverborne turbidity currents and indications of slope failures in the Rhone delta of Lake Geneva. *Limnology and Oceaonography*, **33**, 458-468.

Larson, R.G. (1999) *The Structure and Rheology of Complex Fluids*. Oxford University Press, Oxford, 663 p.

Laval, A., Cremer, M., Beghin, P. and Ravenne, C. (1988) Density surges: two-dimensional experiments. *Sedimentology*, **35**, 73-84.

Lawson, D.E. (1982) Mobilization, movement and deposition of active subaerial sediment flows, Matanuska Glacier, Alaska. *Journal of Geology*, **90**, 279-300.

Leigh, N.S. and Harley, A. (1992) Mega debris-flow deposits from the oligo-micence Pindos foreland basin, western mainland Greece: implication for transport mechanisms in ancient deep-marine basins. *Sedimentology*, **39**, 1003-1012.

Lowe, D.R. (1979) Sediment-gravity flows: their classification, and some problems of applications to natural flows and deposits. In: Doyle, L.J. and Pilkey, O.H. (Eds.), *Geology of Continental Slopes. Society of Economic Paleontologists and Mineralogists Special Publication*, **27**, p. 75-82.

Lowe, D.R. (1982) Sediment-gravity flows, II: Depostional models with special reference to the deposits of high-density turbidity currents. *Journal of Sedimentary Petrology*, **52**, 279-297.

Lowe, D.R. (1988) Suspended-load fallout rate as an independent variable in the analysis of current structures. *Sedimentology,* **35**, 765-776.

Lowe, D.R.. (1997) Reinterpretation of depositional processes in a classic flysch sequence (Pennsylvanian Jackfork Group), Ouachita Mountains, Arkansas and Oklahoma: Discussion. *American Association of Petroleum Geologists Bulletin*, **81**, 460-465.

Lowe, D.R. and Guy, M. (2000) Slurry-flow deposits in the Britannia Formation (Lower Cretaceous), North Sea: a new perspective on the turbidity current and debris flow problem. *Sedimentology,* **47**, 31-70.

Lowe, D.R., Guy, M. and Palfrey, A. (2003) Facies of slurry-flow deposits, Britannia Formation (Lower Cretaceous), North Sea: implications for flow evolution and deposit geometry. *Sedimentology,* **50**, 45-80.

Mastbergen, D.R. and Van den Berg, D.H. (2003) Breaching in fine sands and the generation of sustained turbidity currents in submarine canyons. *Sedimentology*, **50**, 625-637.

McCaffrey, W.D., Kneller, B.C. and Peakall, J. (Eds) (2001) *Particulate Gravity Currents. International Association of Sedimentologists Special Publication,* **31***,* 302 p.

McTigue, D.F. (1982) A nonlinear constitutive model for granular materials: applications to gravity flows. *Journal of Applied Mechanics,* **49**, 291-296.

Middleton, G.V. (1966a) Experiments on density and turbidity currents, I: Motion of the head. *Canadian Journal of Earth Sciences*, **3**, 523-546.

Middleton, G.V. (1966b) Experiments on density and turbidity currents, II: Uniform flow of density currents. *Canadian Journal of Earth Sciences*, **3**, 627-637.

Middleton, G.V. (1967) Experiments on density and turbidity currents, III: Deposition of sediment. *Canadian Journal of Earth Sciences*, **4**, 475-505.

Middleton, G.V. (1993) Sediment deposition from turbidity currents. *Annual Review of Earth and Planetary Sciences*, **21**, 89-114.

Middleton, G.V. and Hampton, M.A. (1973) Sediment-gravity flows: mechanics of flow and deposition. In: Middleton, G.V. and Bouma, A.H. (Eds.), *Turbidites and Deep-Water Sedimentation.* Pacific Section of the Society of Economic Paleontologists and Mineralogists. Short Course Lecture Notes, Los Angeles, p. 1-38.

Middleton, G.V. and Southard, J.B. (1984) *Mechanics of Sediment Movement.* Society of Economic Paleontologists and Mineralogists, Short Course No. 3 Lecture Notes, 401 p.

Milne, J. (1897) Suboceanic changes. *Geographical Journal*, **10**, 129-146 & 259-289.

Morris, S.A. and Alexander, J. (2003) Changes in flow direction at a point caused by obstacles during passage of a density current. *Journal of Sedimentary Research*, **73**, 621-629.

Mulder, T. and Alexander, J. (2001) The physical character of subaqueous sedimentary density flows and their deposits. *Sedimentology*, **48**, 269-299.

Mulder, T., Migeon, S., Savoye, B. and Faugeres, J.C. (2001) Inversely-graded turbidite sequences in the deep Mediterranean: a record of deposits from flood-generated turbidity currents? *Geo Marine Letters*, **21**, 86-93.

Mulder, T. and Syvitski, J.P.M. (1995) Turbidity currents generated at river mouths during exceptional discharges to the world oceans. *Journal of Geology*, **103**, 285-299.

Mulder, T., Syvitski, J.P.M., Migeon, S., Faugeres, J.C. and Savoye, B. (2003) Marine hyperpycnal flows: initiation, behaviour and related deposits. A review. *Marine and Petroleum Geology*, **20**, 861-882.

Mulder, T., Syvitski, J.P.M. and Skene, K. (1998) Modelling of erosion and deposition by sediment-gravity flows generated at river mouths. *Journal of Sedimentary Research*, **68**, 124-137.

Mulder, T. and Syvitski, J.P.M. (1996) Climatic and morphologic relationships of rivers: implications of sea-level fluctuations on river loads. *Journal of Geology*, **104**, 509-523.

Mutti, E. (1985) Turbidite systems and their relations to depositional sequences. In: Zuffa, G.G. (Ed.), *Provenance of Arenites.* D. Reidel Publishing Company, Dordrecht, p. 65-93.

Mutti, E. and Normark, W.R. (1991) An integrated approach to the study of turbidite systems. In: Weimer, P. and Link, W.H. (Eds.), *Seismic Facies and Sedimentary Processes of Submarine Fans and Turbidite Systems.* Springer-Verlag, New York, p. 75-106.

Mutti, E. and Ricci-Lucchi, F. (1972) Turbidites of the northern Apennines: introduction to facies analysis. *International Geology Review*, **20**, 125-166.

Mutti, E., Tinterri, R., Benevelli, G. Angella, S., di Biase, D. and Cavanna, G. (2003) Deltaic, mixed, and turbidite sedimentation of ancient forland basins. *Marine and Petroleum Geology*, **20**, 733-755.

Nakajima, T. (2006) Hyperpycnites deposited 700 km away from river mouths in the central Japan Sea. *Journal of Sedimentary Research*, **76**, 60-73.

Nemec, W. (1990) Aspects of sediment movement on steep delta slopes. In: Colella, A. and Prior, D.B. (Eds.), *Coarse-Grained Deltas*. *International Association of Sedimentologists Special Publication,* **10**, 29-73.

Nemec, W. (1995) The dynamics of deltaic suspension plumes. In: Oti, M.N., Postma, G. (Eds.), *The Geology of Deltas*. A.A. Balkema, Rotterdam, p. 31-93.

Nemec, W. (1997) *Deep-water massive sandstones*. Lecture Abstract, Norwegian Geological Society (NGF) Meeting, 14th October 1997, Stavanger, 3 p.

Nemec, W., Kazancı, N. and Mitchell, J.G. (1998) Pleistocene explosions and pyroclastic currents in west-central Anatolia. *Boreas,* **27**, 311-332.

Nemec, W. and Postma G. (1991) Inverse grading in gravel beds. In: *Abstracts, International Association of Sedimentologists 12th Regional Meeting*. Univ. of Bergen, Bergen, p. 38.

Nemec, W. and Steel, R.J. (1984) Alluvial and coastal conglomerates: their significant features and some comments on gravelly mass-flow deposits. In: Koster, E.H. and Steel, R.J. (Eds.), *Sedimentology of Gravels and Conglomerates*. *Canadian Society of Petroleum Geology Memoir,* **10**, p. 1-30.

Normark, W.R. (1970) Growth patterns of deep-sea fans. *American Association of Petroleum Geologists Bulletin*, **54**, 2170-2195.

Normark, W.R., Moore, J.G. and Torresan, M.E. (1993) Giant volcano-related landslides and the development of the Hawaiian Islands. In: Schwab, W.C., Lee, H.J. and Twichel, D.C. (Eds.), *Submarine Landslides: Selected Studies in the US Exclusive Economic Zone*. *U.S. Geological Survey Bulletin*, *2002*, 184-196.

Paola, C. (2000) Quantitative models of sedimentary basin filling. *Sedimentology*, **47**, 121-178.

Parker, G. (1982) Conditions for the ignition of catastrophically erosive turbidity currents. *Marine Geology*, **46**, 307-327.

Parker, G., Garcia, M.H., Fukushima, Y. and Yu, W. (1987) Experiments on turbidity currents over an erodible bed. *Journal of Hydraulic Research, IAHR*, **25**, 123-147.

Parsons, J.D. (1998) *Mixing Mechanisms in Density Intrusions.* Unpubl. Ph.D. Thesis, University of Illinois, Urbana-Campaign, 324 p.

Payton, C.E. (Ed.) (1977) Seismic Stratigraphy – Applications to Hydrocarbon Exploration. *American Association of Petroleum Geologists Memoir*, **26**, 516 p.

Peakall, J., Ashworth, P. and Best, J. (1996) Physical modeling in fluvial geomorphology: principles, applications, and unresolved issues. In: Rhoads, B.L. and Thorn, C.E. (Eds.), *The Scientific Nature of Geomorphology*. John Wiley and Sons, Chichester, p. 221-253.

Peakall, J., McCaffrey, W. D. and Kneller, B. C. (2000) A process model for the evolution, morphology, and architecture of sinuous submarine channels. Journal of *Sedimentary Research*, **70**, 434-448.

Pickering, K.T., Hiscott, R.N. and Hein, F.J. (1989) Deep-marine environments: clastic sedimentation and tectonics. Unwin Hyman, London, 416 p.

Pierson, T.C. (1981) Dominant particle support mechanisms in debris flows at Mt. Thomas, New Zealand, and implications for flow mobility. *Sedimentology*, **28**, 49-60.

Posamentier, H.W., Erskine, R. and Mitchum R., Jr. (1991) Models of submarine fan deposits within a sequence-stratigraphic framework. In: Weimer, P. and Link, W.H. (Eds.), *Seismic Facies and Sedimentary Processes of Submarine Fans and Turbidite Systems*. Spinger-Verlag, New York, p. 127-137.

Postma, G. (1986) Classification for sediment-gravity-flow deposits based on flow conditions during sedimentation. *Geology*, **14**, 291-294.

Postma, G., Nemec, W. and Kleinspehn, K.L. (1988) Large floating clasts in turbidites: a mechanism for their emplacement. *Sedimentary Geology*, **58**, 47-61.

Prandtl L. (1952) *The Essentials of Fluid Dynamics*. Blackie & Son, London, 452 p.

Prior, D.B., Suhayda, J.N., Lu, N.Z., Bornhold, B.D., Keller, G.H., Wiseman, W.J., Wright, L.D. and Yang, Z.S. (1989) Storm-wave reactivation of a submarine landslide. *Nature*, **341**, 47-50.

Rimoldi, B., Alexander, J. and Morris, S.A. (1996) Experimental density currents entering density-stratified water: analogues for turbidites in Mediterranean hypersaline basins. *Sedimentology*, **43**, 527-540.

Savage, S.B. and Hutter, K. (1989) The motion of a finite mass of granular material down a rough incline. *Journal of Fluid Mechanics*, **199**, 177-215.

Savage, S.B. and Lun, C.K.K. (1988) Particle size segregation in inclined chute flow of dry cohesionless granular solids. *Journal of Fluid Mechanics*, **189**, 311-335.

Shanmugam, G. (1996) High-density turbidity currents: are they sandy debris flows? *Journal of Sedimentary Research*, **66**, 2-10.

Shanmugam, G. (2000) 50 years of the turbidite paradigm (1950s-1990s): deep-water processes and facies models – a critical perspective. *Marine and Petroleum Geology*, **17**, 285-342.

Shanmugam, G. (2002) Ten turbidite myths. Earth-Science Reviews, **58**, 311-341.

Shanmugam, G., Bloch, R.B., Damuth, J.E. and Hodgkinson, R.J. (1997) Basin-floor fans in the North Sea: sequence stratigraphic models vs. sedimentary facies: Reply. *American Association of Petroleum Geologists Bulletin*, **81**, 666-672.

Shanmugam, G., Bloch, R.B., Mitchell, S.M., Beamish, G.W.J., Hodgkinson, R.J., Damuth, J.E., Straume, T., Syvertsen, S.E. and Shields, K.E. (1995) Basin-floor fans in the North Sea: sequence stratigraphic models vs. sedimentary facies. *American Association of Petroleum Geologists Bulletin*, **79**, 477-512.

Shanmugam, G. and Moiola, R.J. (1995) Reinterpretation of depositional processes in a classic flysch sequence (Pennsylvanian Jackfork Group), Ouachita Mountains, Arkansas and Oklahoma. *American Association of Petroleum Geologists Bulletin*, **79**, 672-695.

Shanmugam, G. and Moiola, R.J. (1997) Reinterpretation of depositional processes in a classic flysch sequence (Pennsylvanian Jackfork Group), Ouachita Mountains, Arkansas and Oklahoma: Reply. *American Association of Petroleum Geologists Bulletin*, **81**, 476-491.

Shanmugam, G., Moiola, R.J. and Damuth, J.E. (1985) Eustatic control of submarine fan development. In: Bouma, A.H., Normark, W.R. and Barnes, N.E. (Eds.), *Submarine Fans and Related Turbidite Systems*. Springer-Verlag, New York, p. 23-28.

Sharp, R.P. and Nobles, L.H. (1953) Mudflow of 1940 at Wrightwood, Southern California. *Bulletin of the Geological Society of America*, **64**, 547-560.

Sheldon, P.G. (1928) Some sedimentation conditions in middle-portage rocks. *American Journal of Science*, **15**, 243-252.

Shepard, F.P., Marshall, N.F., McLoughlin, P.A. and Sullivan, G.G. (1979) *Currents in Submarine Canyons and Other Seavalleys.* American Association of Petroleum Geologists, Ann Arbor (Michigan), 174 p.

Siegenthaler, C., Fringer, W., Kelts, K. and Wang, S. (1987) Earthquake and seiche deposits in Lake Lucerne, Switzerland. *Eclogae Geologicae Helveticae*, **80**, 241-260.

Simm, R.W., Weaver, P.P.E., Kidd, R.B. and Jones, E.J.W. (1991) Late quarternary mass movements on the lower continental rise and abyssal plain off western Sahara. *Sedimentology*, **38**, 27-40.

Simpson, J.E. (1987) *Gravity Currents in the Environment and in the Laboratory*. Ellis Horwood Ltd., Chichester, 244 p.

Simpson, J.E. and Britter, R.E. (1979) The dynamics of the head of a gravity current advancing over a horizontal surface. *Journal of Fluid Mechanics*, **94**, 477-495.

Skene, K.I., Mulder, T. and Syvitski, J.P.M. (1997) INFLO1: A model predicting the behaviour of turbidity currents generated at river mouths. *Computer and Geosciences*, **23**, 975-991.

Slatt, R.M., Weimer, P. and Stone, C.G. (1997) Reinterpretation of depositional processes in a classic flysch sequence (Pennsylvanian Jackfork Group), Ouachita Mountains, Arkansas and Oklahoma: Discussion. *American Association of Petroleum Geologists Bulletin*, **81**, 449-459.

Sloff, C.J. (1997) *Sedimentation in Reservoirs*. Unpubl. Ph.D. thesis, The Delft University of Technology, 270 p.

Sohn, T.K. (1995) Traction-carpet stratification in turbidites – fact or fiction? Discussion. *Journal of Sedimentary Research*, **A65**, 703-704.

Sohn, T.K. (1997) On traction-carpet sedimentation. *Journal of Sedimentary Research*, **67**, 502-509.

Sohn, T.K. (1999) Rapid development of gravelly high-density turbidity currents in marine Gilbert-type fan deltas. Lorento Basin, Baja California Sur, Mexico. Discussion. *Sedimentology*, **46**, 757-761.

Southard, J.B. (1971) Representation of bed configurations in depth-velocity-size diagrams. *Journal of Sedimentary Petrology*, **41**, 903-915.

Southard, J.B. and Boguchwal, L.A. (1973) Flume experiments on the transition from ripples to lower flat bed with increasing sand size. *Journal of Sedimentary Petrology*, **43**, 1114-1121.

Stanley, D.J. (1963) Vertical petrographic variability in Annot Sandstone turbidites. *Journal of Sedimentary Petrology*, **33**, 783-788.

Stow, D.A.V. and Shanmugam, G. (1980) Sequence of structures in fine-grained turbidites: comparison of recent deep-sea and ancient flysch sediments. *Sedimentary Geology*, **25**, 23-46.

Sullwold, H.H., Jr. (1961) Turbidites in oil exploration. In: Peterson, J.A. and Osmond, J.C. (Eds.), *Geometry of Sandstone Bodies*. American Association of Petroleum Geologists, Tulsa (Oklahoma), p. 63-81.

Tucker, M.E. (2001) *Sedimentary Petrology – An Introduction to the Origin of Sedimentary Rocks*. Blackwell Science, Oxford, 262 p.

Takahashi, T. (1991) *Debris Flow*. A.A. Balkema, Rotterdam, 165 p.

Tokaty, G.A. (1971) *A History and Philosophy of Fluid Mechanics*. G.T. Foulis, Henly-on-Thames (UK), 272 p.

Van Rijn, L.C. (1987) *Mathematical Modeling of Morphological Processes in the Case of Suspended Sediment Transport*. Unpubl. Ph.D. Thesis, The Delft University of Technology, 208 p.

Vrolijk, P.J. and Southard, J.B. (1997) Experiments on rapid deposition of sand from high-velocity flows. *Geoscience Canada*, **24**, 45-54.

Walker, R.G. (1978) Deep-water sandstone facies and ancient submarine fans: models for exploration for stratigraphic traps. *American Association of Petroleum Geologists Bulletin*, **62**, 932-966.

Wasson, R.J. (1979) Sedimentation history of the Mundi-Mundi alluvial fans, western New South Wales. *Sedimentary Geology*, **22**, 21-51.

Wesseling, P. (2001) *Principles of Computational Fluid Dynamics*. Springer-Verlag, Berlin, 644 p.

Winn, R.D., Jr. and Dott, R.H., Jr. (1979) Deep-water fan-channel conglomerates of Late Cretaceous age, southern Chile. *Sedimentology*, **26**, 203-228.

Wright, L.D., Yang, Z.-S., Bornhold, B.D., Keller, G.H., Prior, D.B. and Wisenam, W.J., Jr., (1986) Hyperpycnal flows and flow fronts over the Huanghe (Yellow River) delta front. *Geo-Marine Letters*, **6**, 97-105.

Xu, J.P., Noble, M.A. and Rosenfeld, L.K. (2004) In-situ measurements of velocity structure within turbidity currents. *Geophysical Research Letters*, **31**, L09311, doi:10.1029/2004GL019718.

Yakhot, V. and Orszag, S.A. (1986) Renormalization group analysis of turbulence, I. Basic theory. *Journal of Scientific Computing*, **1**, 1-51.

Yakhot, V. and Smith, L.M. (1992) The renormalization group, the e-expansion and derivation of turbulence models. *Journal of Scientific Computing*, **7**, 35-61.

Zeng, J., Lowe, D.R., Prior, D.B., Wiseman, W.J., Jr. and Bornhold, B.D. (1991) Flow properties of turbidity currents in Bute Inlet, British Columbia. *Sedimentology*, **38**, 975-996.

APPENDIX

REPORT

Report to A/S Norske Shell

FLOW-3D™ simulation of the Ormen Lange field, Mid-Norway Continental Shelf

by

Snorre Heimsund

on behalf of
Complex Flow Design A/S
P.O. Box 1248
7462 Trondheim
Norway

December 2005

CONTENTS

List of figures

1 Executive Summary

Complex Flow Design A/S was commissioned by A/S Norske Shell to provide numerical simulations of the influence of basin-floor topography on the spatial pattern of sediment dispersal in the Ormen Lange field, mid-Norway Shelf. This study is based on a pilot project carried out for Hydro, Norske Shell's partner in the field, in 2003 and aimed to analyse with Flow-3D™ simulations the response of turbidity currents to a number of possible seafloor topographic configurations. The variants of palaeotopography to be used are based on 3D seismic models of the basal surface of the Egga reservoir unit derived from a restoration (overburden backstripping) and decompaction study performed by the Midland Valley Exploration Ltd (MVE 2004).

The focus of the present study is thus on the sensitivity of turbidity currents to particular topographic configurations and on the resulting patterns of sediment dispersal on the seafloor. In addition, an assessment of the numerical modelling framework for similar future studies is to be made.

The initial boundary conditions for the simulations (including seafloor topography, location of turbidity-current source and initial flow characteristics) have been selected on the basis of the afore-mentioned MVE's (2004) study and other available literature. Since the actual flow conditions at the time of deposition are unknown, a range of assumptions for the initial flow conditions had to be made and assessed on a trial-and-error basis. On the basis of the available well-core samples, the turbidity currents are inferred to have been high-density, surge-type, homogenous flows with an average sediment grain size of fine sand grade.

The results of the study show that turbidity currents are highly sensitive to subtle variation in basin-floor topography. The Egga reservoir unit was probably supplied with sediment from an entry point in the southeast. The sediment transport directions are thought to be mainly to the north, due to a subtle topographic confinement to the east and west. As the primary topographic relief was gradually smoothed out by sediment accumulation, the whole area of interest became increasingly as a bypass zone for sediment.

2 Introduction

The Complex Flow Design A/S was requested by A/S Norske Shell, on behalf of the Ormen Lange partnership, to undertake a numerical forward-modelling study of the Egga reservoir unit in order to improve the understanding of the pattern of sediment supply/transport and dispersal in the area of Ormen Lange field (Fig. 1). It is a continuation of a pilot project carried out for Hydro and the Ormen Lange partnership in 2003 and aimed at analysing the response of turbidity currents to a number of possible basin-floor topographic configurations.

The basin-floor topography used is based on models of the basal surface of the Egga Reservoir Unit derived from a back-stripping and decompaction study carried out by the Midland Valley Exploration Ltd (MVE 2004). The topography above the Ormen Lange field is extremely rough (Fig. 2), affected by the Recent Storegga Slide, one of the largest mass movements known (Bugge et al. 1988). Multiple realizations of a 3-D model were sequentially decompacted and backstripped and the effects of folding and sliding were removed. The decompaction was carried out using lithology maps for two heterolithic intervals to control the impact on decompaction of spatially varying lithology.

The Egga Reservoir Unit (Figure 3) comprises deep-marine turbidite deposits of Upper Cretaceous (Maastrichtian) to Lower Tertiary (Danian) age (Gjelberg et al. 2001). These rocks are ascribed to the Jorsalfare Formation and Egga Member of the Våle Formation respectively (Smith & Möller 2003). The turbidites are considered to have been sourced from the southeast and deposited within a north-south elongated, structurally controlled sub-basin conforming to the position of the present structural high (Walker 2001, Gjelberg et al. 2002, Möller et al. 2004).

The computational fluid dynamics software FLOW-3D™ has been adopted for this study to simulate the influence of basin-floor topography on the spatial pattern of sediment dispersal by turbidity currents in the Ormen Lange field. Turbidity currents may respond to the topography in different ways, with an erosional or non-erosional sediment bypass in some areas, local spilling over basin-floor highs, ponding in local depressions, flow deflection and/or flow reversal on an opposing slope. Therefore, it is crucial to monitor the 3-D flow behavior in order to understand the resulting spatial patterns of sediment dispersal on the basin-floor. As the depositional system evolves, its topography will inevitably change and so

will also the spatial behavior of the successive flows. This feedback phenomenon can be studied and its effects on sediment dispersal can be recognized by an incremental, step-by-step simulation of successive flows. In this way, the zones of erosion and sand-on-sand deposition, the non-erosional zones of sand sandwiching by mud and the sand-starved zones of turbidite pinch-out can be recognized and mapped.

This report summarizes the determination of the modeling framework, and the results of the FLOW-3D™ simulations of the Ormen Lange field.

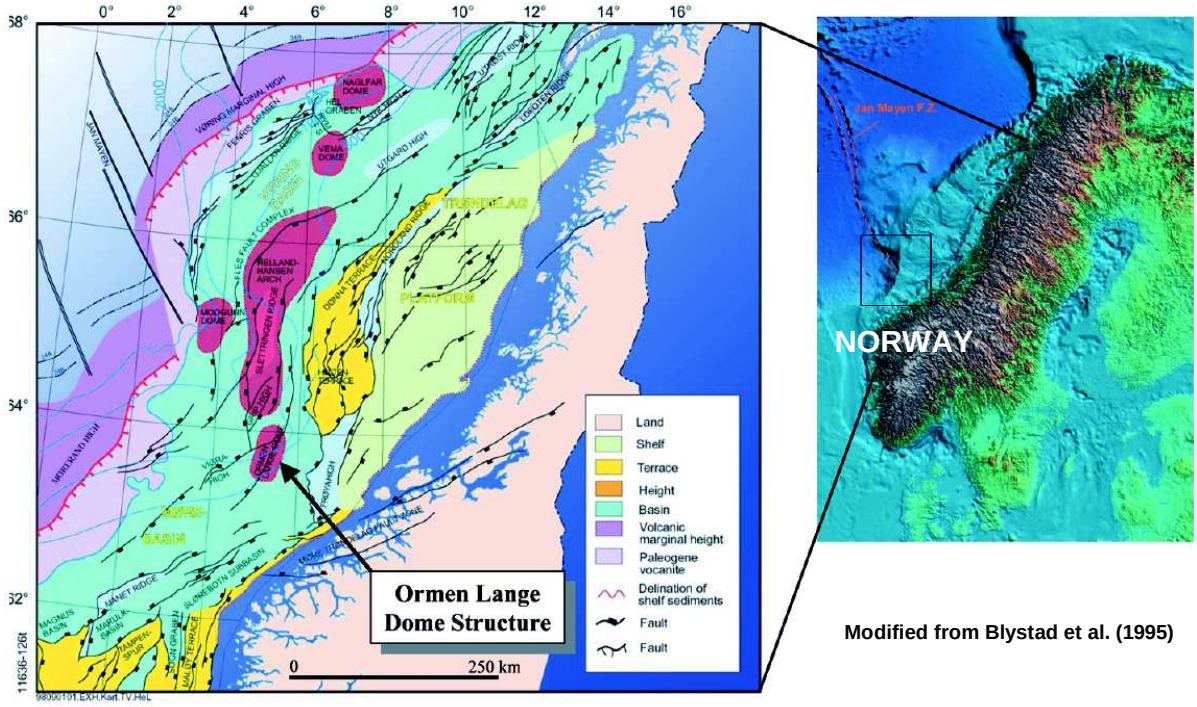

Figure 1. Location of the Ormen Lange field (Blystad et al. 1995).

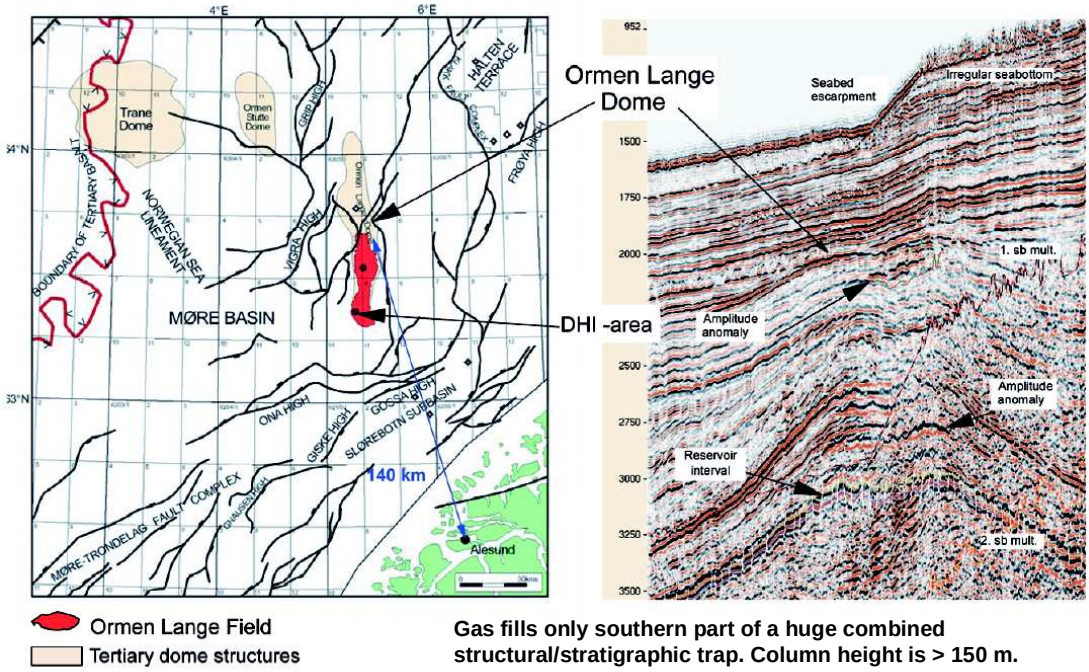

Figure 2. Structural map and seismic cross-section (Möller et al. 2004).

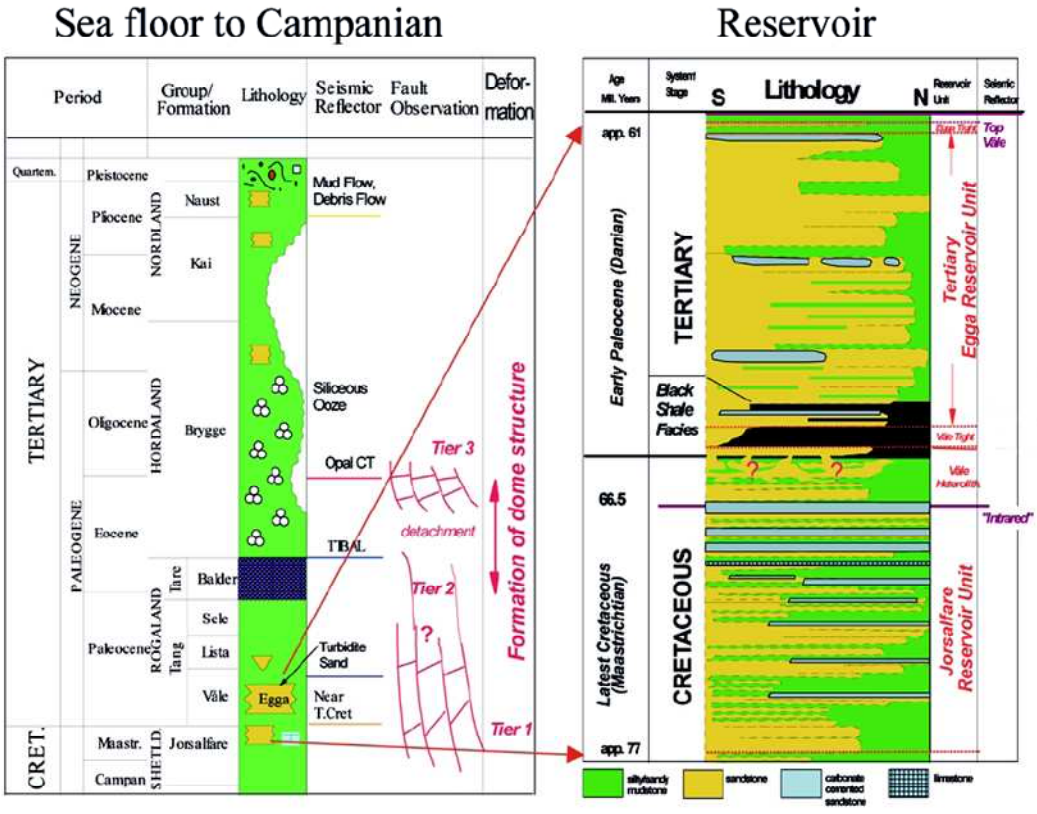

Figure 3 Stratigraphy (Möller et al. 2004).

3 Methodology

3.1 Computational Fluid Dynamics

A relatively new deterministic numerical method in this field of sedimentological research, known as Computational Fluid Dynamics (CFD), has been adopted for this study. CFD is commonly accepted as referring to the broad topic encompassing the numerical solution, by computational methods, of the governing equations which describe fluid flow, the set of the Navier-Stokes equations, continuity and any additional conservation equations (Wesseling, P. 2001).

As a developing science, CFD has received extensive attention throughout the international community since the advent of the digital computer in the 1960s. The attraction of the subject is twofold. Firstly, the desire to be able to model physical fluid phenomena that cannot be easily simulated or measured with a physical experiment and secondly, the desire to be able to investigate physical fluid systems more cost effectively and more rapidly than with experimental procedures. There has been considerable growth in the development and application of CFD to all aspects of fluid dynamics.

In design and development, CFD programs are now considered to be standard numerical tools, widely utilized within the industry (Figure 4). CFD has thus grown from a mathematical curiosity to become an essential tool in almost every branch of fluid dynamics and there are numerous CFD software packages available today.

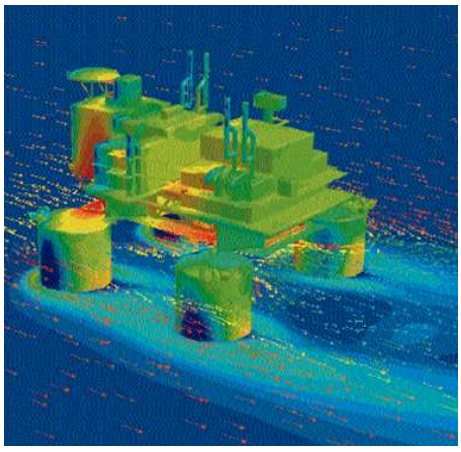

Figure 4 CFD simulation of wind shear on a rig.

3.2 FLOW-3D™

The commercial CFD package FLOW-3D™ was selected because the physical models required for this study were already incorporated in this software.

In FLOW-3D™ there currently exists a sediment scour model to predict the erosion and deposition of sediment. This model works by trying to emulate both the entrainment of sediment at the packed bed interface and the deposition of sediment from the fluid by gravity. When coupled with the fluid dynamics computed by the equations of mass and momentum conservation, the model is able to approximate the actual deposition and entrainment of sand, silt and other non-cohesive sediment.

The enhancement done for this study builds upon this original model in a number of ways:

- Addition of non-linear drifting of the suspended phase. This allows more accurate simulation of the deposition of larger and/or faster drifting sediment
- Addition of multiple species of sediment. Instead of allowing only a single sediment size, multiple species are allowed. Currently, the number is limited to 49, though it has not yet been tested with that many species sizes.
- Addition of a bed load transport model. This will approximate the rolling motion that larger sediment experiences as it rolls over the surface of the packed bed rather than becoming entrained in the bulk flow.

Non-linear drifting:
We calculate the driving force of drift first; this is the buoyancy and is in the same direction of the pressure gradient for sediment that is heavier than the suspending fluid (which must be lighter than the sediment for the model to work):

$$\mathbf{u}_\mathbf{r}^\mathbf{0} = \frac{1}{\bar{\rho}} \nabla P \left(\frac{\rho_s - \rho_f}{\rho_f} \right) \bar{f}_s \left(1 - \bar{f}_s \right). \tag{1}$$

Here ρ_f and ρ_s are the densities of the fluid and sediment, respectively, P is the local pressure, $\bar{\rho}$ is the mean density of the fluid/sediment mixture, f_s is the solid fraction and $\mathbf{u}_\mathbf{r}^\mathbf{0}$ is the relative velocity between the sediment and the fluid. This is identical to what has always been done.

The drag coefficient K is computed as

$$K = \frac{3}{8}\frac{\bar{f}_s}{d_s}\left(C_D \left\| \mathbf{u}_\mathbf{r}^\mathbf{0} \right\| + 12\frac{\mu}{\rho_f d_s} \right) \tag{2}$$

where d_s is the species sediment diameter, C_D is the species coefficient of drag and μ is the fluid viscosity. Also, we know that the drift velocity is

$$\mathbf{u}_\mathbf{drift} = \frac{\mathbf{u}_\mathbf{r}^\mathbf{0}}{K}. \tag{3}$$

Equations 2 and 3 are solved together with the quadratic formula for the coordinates of the drift velocity. The Richardson-Zaki correlation (Richardson & Zaki 1954) is used to predict the effect of the interaction of the sediment in suspension. The particle Reynolds number is computed as

$$\mathrm{Re}_p = 2\frac{\left\| \mathbf{u}_\mathbf{drift} \right\| \rho_f d_s}{\mu}. \tag{4}$$

The Richardson-Zaki exponent is computed based on the range of Reynolds number:
For Re<1:

$$R_Z = \frac{4.35}{\mathrm{Re}_p^{0.03}}. \tag{5}$$

For 1<Re<500:

$$R_Z = \frac{4.45}{\mathrm{Re}_p^{0.1}}. \tag{6}$$

For Re>500:

$$R_Z = 2.39. \tag{7}$$

The drift velocity is then adjusted according to

$$\mathbf{u}'_\mathbf{drift} = \mathbf{u}_\mathbf{drift}\left(1 - \bar{f}_s\right)^{R_z^p R_z}. \tag{8}$$

This drift velocity is used to affect the motion of the sediment separate from its advection with the fluid. This is quite straightforward in regions away from walls or the packed bed interface and is exactly what is done in FLOW-3D™'s standard drift-flux model and basically applies an additional velocity to the advection part of the transport equation for the suspended sediment. However, adjacent to blockages, care must be taken to convert suspended sediment into packed sediment. This is done by first considering the additional advection of the suspended sediment into the cell by Equation 8. Then the accumulated sediment, in addition to the suspended sediment already present in the cell, is "packed" at a rate based on the drift

velocity computed in Equation 8. This procedure is followed in each of the Cartesian directions throughout the domain wherever drifting occurs.

The entrainment model has remained unchanged; here we compute the lift velocity of the sediment adjacent to the packed bed interface as

$$\mathbf{u}_{lift} = \alpha \mathbf{n}_s \sqrt{\frac{\tau - \tau_{crit}}{\bar{\rho}}} \tag{9}$$

where α is the "lifting parameter" (scralp) parameter – which can be specified independently for each sediment species. τ_{crit} is the critical shear stress, computed from

$$\tau^0_{crit} = \Theta_{crit} g(\rho_f - \rho_s) d \tag{10}$$

where Θ_{crit} is the critical Shields parameter (scrcrt) – also specified independently for each sediment species, g is the magnitude of the gravity vector. τ_{crit} is then modified based on the following:

$$\tau_{crit} = \tau^0_{crit} \sqrt{1 - \frac{\sin^2 \varphi}{\sin^2 \zeta}}. \tag{11}$$

where ζ is the angle of repose (scrang), specified by the user, and φ is the computed interface angle (relative to the gravity vector).

Once $\mathbf{u}_{lift}$ is computed, the additional advection is computed as it was for the drifting, however, here it is the packed sediment that is both advected and simultaneously converted into suspended sediment.

For bed-load transport, the model currently used (and easily customizable in the routine scrersn.F) is from Nielsen (Chanson 2004):

$$\frac{q_s}{\sqrt{(\rho_s - \rho_f) g d^3}} = \left(\frac{12\tau}{(\rho_s - \rho_f) g d} - 0.05 \right) \sqrt{\frac{\tau}{(\rho_s - \rho_f) g d}}. \tag{11}$$

Here q_s is the volumetric sediment discharge per unit width. This value is then used to effect motion of the sediment:

$$\mathbf{u}_{\mathbf{bed-load}} = \frac{\bar{\mathbf{u}}}{\|\bar{\mathbf{u}}\|} \frac{q_s}{A}. \tag{11}$$

Here $\bar{\mathbf{u}}$ represents the mean velocity of the fluid adjacent to the packed interface, and the resulting motion is again considered an additional advection to the transport equation for the packed sediment.

3.3 Visualization

In this study separate work was also devoted to the 3-D visualization of the FLOW-3D™ results. The sedimentation processes and the evolution of the whole depositional system were visualized using the commercial CFD post-processor software package FIELDVIEW (Figure 5).

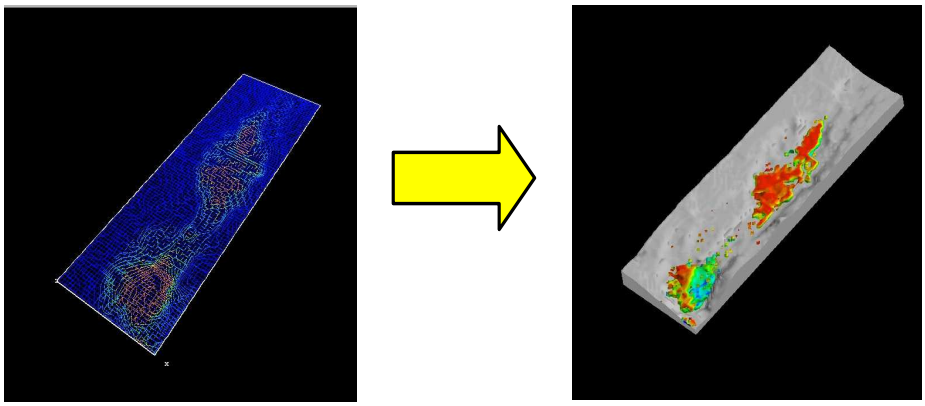

Figure 5. Fieldview visualization of FLOW-3D™ data.

4 Data Import

The basin-floor topographic surfaces used in this study are based on the 3 models (Figure 6) of the base Egga Reservoir Unit surface from a decompaction and back-stripping study performed by Midland Valley Exploration Ltd. (Stanton & Thompson 2002) which include:

- Medium (Base) Case
- High (Maximum) Case
- Low (Minimum) Case

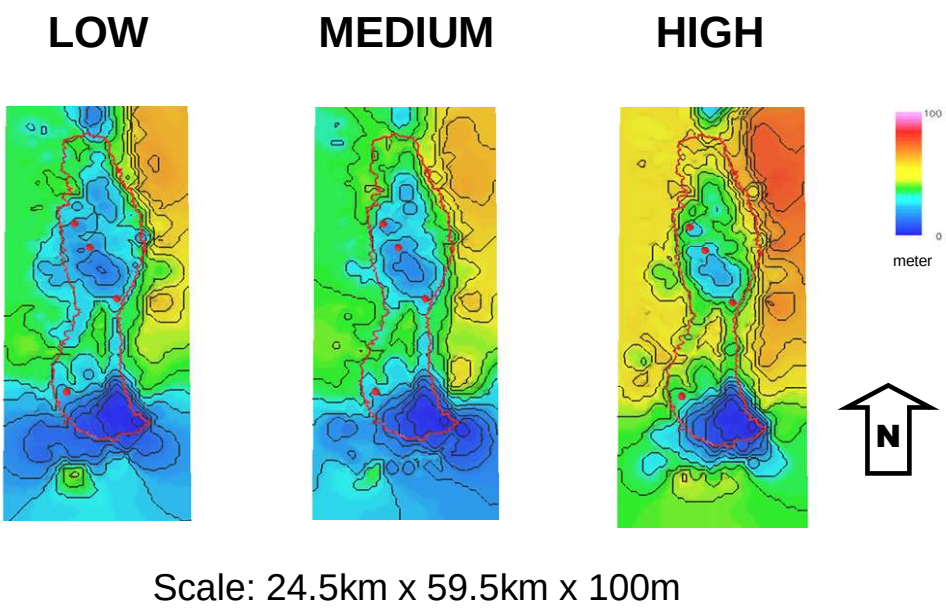

Figure 6. Base Egga topographic configurations.

These topographic surfaces were provided by Midland Valley Exploration Ltd. in the zmap file format, both in smoothed and in non-smoothed versions. A topographic surface based on the Egga Reservoir Unit isochore map and a new base Egga provided by Midland Valley Exploration Ltd. (MVE 2004) was also provided by A/S Norske Shell.

The smoothed surfaces were loaded into IRAP RMS where they were extrapolated and a regularly spaced grid was created using the mask method and then exported to ASCII Internal point format. Since the ASCII Internal point data were in UTM coordinates form they had to be converted to relative Cartesian coordinates before they could be used further. In-house

code was used to apply a regional tilt of 0.05 degrees towards the east and to up-sample the point data from 6000 to 10000 points. The extrapolated parts of the surfaces were tilted 0.5 degrees to towards the centre to avoid outflow at the boundaries. Multiple versions of these surfaces were used to capture the degree of uncertainty in the data.

Finally, the surfaces were imported into FLOW-3D™ using the software's built-in topographic data reader.

5 Simulation Setup

Based on the resolution of the exported surfaces a 3-D computational grid is selected in FLOW-3D™ with 500 meter spacing between cells horizontally and 3 meter spacing between cells vertically. The surfaces were then roughened with 0.03 mm coarse silt based on the available well-core data (Gjelberg et al. 2002 and Walker & Möller 2002).

The water depth at time of deposition is estimated to be 750 meter below sea level (Stanton & Thompson 2002), and above the topographic relief for each case. This water depth produces a hydrostatic pressure of 76 atm (7.70E+06 Pascal) at the highest point of the Base Egga surface. The acceleration of gravity is 9.81 m/s^2 at 750 meter below sea level. The ocean current in the Ormen Lange area is on average 0.5 m/s in a northward direction at 750 meter water depth (Eliassen et al. 2000).

To allow FLOW-3D™ to account for the Coriolis Effect the latitude (in degrees) in the middle of the area must be given. The UTM coordinates in the middle of the area was found to be 7039750.5 Northing and 617250.125 Easting. Since there was no mention of either zone, datum or reference system (projection) in the Midland Valley Exploration report (Stanton & Thompson 2002), it is assumed that the zone is 31, datum is NAD83 and that the reference system is west. Based on this the latitude at the centre of the area is calculated to be 63° 28' 0.34408" North or 63.46676224 in degrees.

The temperature of the sea water is on average 2.5 degrees Celsius at 750 meter water depth (Eliassen et al. 2000). The density of sea water is 1043.0 kg/m^3 at 2.5 degrees Celcius and the dynamic viscosity of sea water is 0.0012 $N \cdot s/m^2$ at 15.6 degrees Celcius (Unesco 1981). At 15 degrees Celsius the density of quartz is 2648.0 kg/m^3 (Lide 2000).

Based on the available well-core data (Gjelberg et al. 2002 and Walker & Möller 2002) the following grain-size distribution was used for the turbidity current simulations:

Minimum grain-size:	0.015 mm medium silt
Maximum grain-size:	0.5 mm coarse sand
Grain-size classes:	2 (equally spaced)
Average grain-size:	0.2 mm fine sand

There is no actual knowledge about the initial flow conditions, but based on literature (Normark 1989, Zeng et al. 1991 and Zeng & Lowe 1997) the following initial flow properties were used for the turbidity current simulations:

Sediment concentration: 10 volume % (0.5-35 volume % in the literature)
Flow velocity: 15 m/s (0.5-28 m/s in the literature)
Flow height: 20 m (5-270 m in the literature)
Flow volume: 75000 m^3/s (14000-123000 m^3/s in the literature)
Flow duration: 7200 seconds (240-7200 seconds in the literature)

There is no actual knowledge about the sediment source area and flow direction either, but based on trial-and-error the following properties were selected for the turbidity current simulations:

Sediment source: One location to the SE for each case (in UTM coordinates):

- Medium (Base) Case: 7019500.5 Northing, 622500.125 Easting
- High (Maximum) Case: 7022000.0 Northing, 629500.125 Easting
- Low (Minimum) Case: 7020000.5 Northing, 629500.0 Easting

Flow direction: 315 degrees NW

6 Results

We wish to emphasize that FLOW-3D™ simulations, while process-based and fully deterministic can be expected to yield results that are only as realistic as the "initial conditions" assumed for the topography and the turbidity currents themselves. The extent to which a modeling result matches the reality can be assessed simply by comparing selected "virtual" profiles with the actual well-core profiles of the turbiditic succession in facies terms. This would be an objective evaluation, although it might practically mean a time-consuming, trial-and-error way of assessment. But once the modeling result has been deemed to be a "good fit", it can readily be confronted with the existing reservoir model and production data; and the existing model can thus either be confirmed or modified and improved on this basis.

6.1 Hydro pilot study

The focus of the Norsk Hydro pilot project was on the influence of basin-floor topography on the spatial pattern of sand dispersal by turbidity currents.

The results of this pilot study have shown that the turbidity currents are highly sensitive to subtle variation in basin-floor configurations, and have also indicated that the Ormen Lange sub-basins were probably supplied with sediment from a single main source in the southeast, via the southern sub-basin characterized by "plunge pool" topography (Figures 7-8). The sediment transport directions were thus mainly to the north, due to subtle topographic confinement to the west and east. The simulations indicate that an initial coeval sedimentation of turbiditic sand in the southern and middle sub-basins may have occurred in these conditions, with the "saddle" area between the sub-basins acting as a bypass zone dominated by erosion and sediment resuspension. As the primary topographic relief of the southern and middle sub-basin was gradually smoothed out by sediment accumulation, this area began to act increasingly as a bypass zone – with sand transfer by turbidity currents farther to the north, possibly all the way to the northern sub-basin.

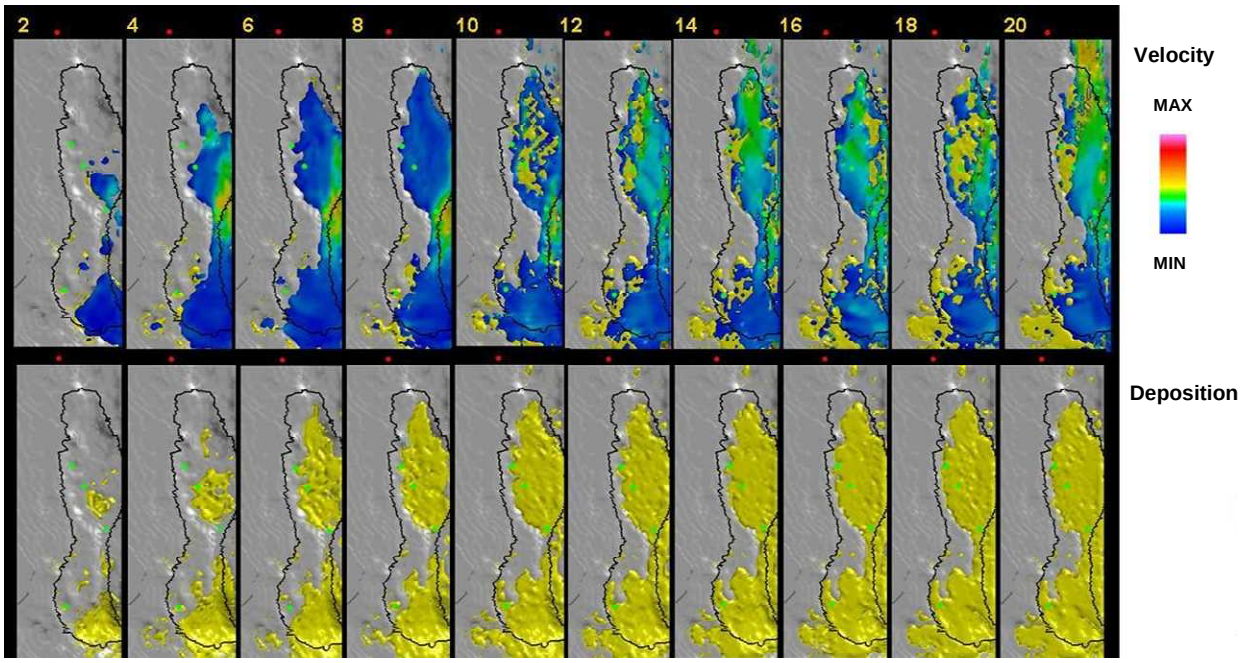

Figure 7. Top view of the basin infill evolution.

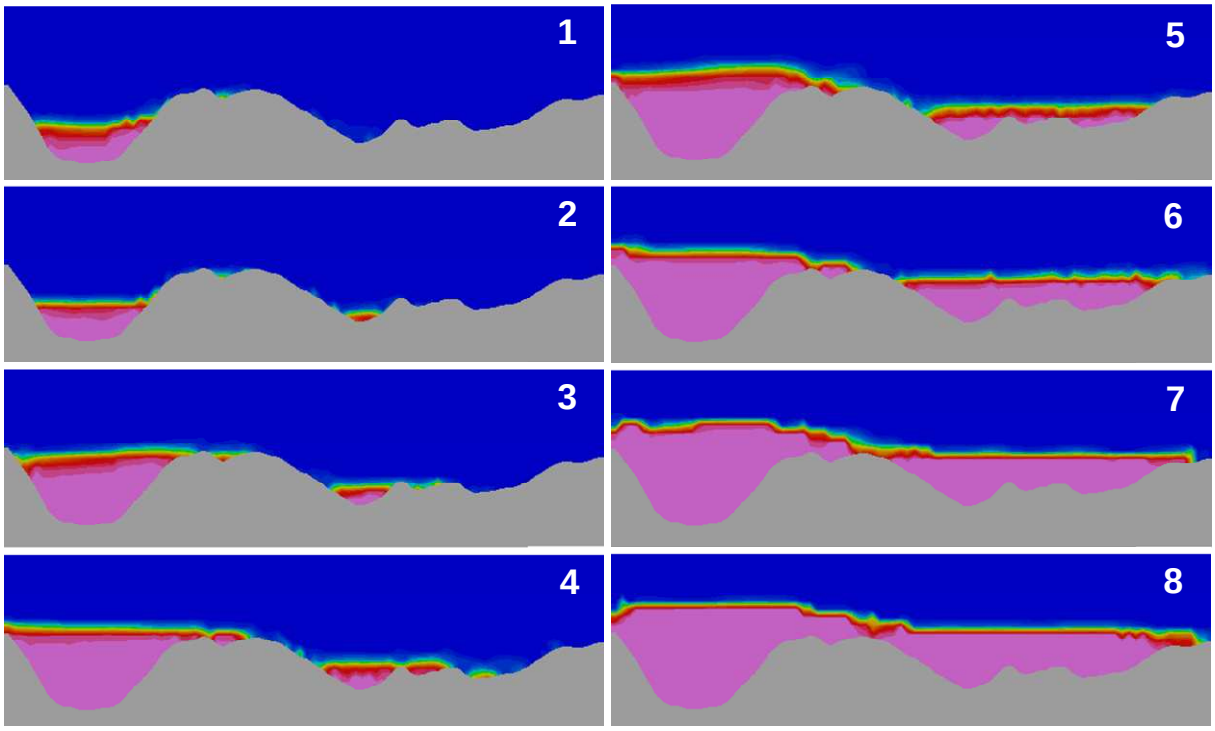

S Vertically exaggerated 50 times N

Figure 8. Cross-sections of the basin infill evolution.

Although the primary aims of that study were met and an improved understanding of turbidite sand sedimentation in the Ormen Lange field was achieved, the main limiting factor for the accuracy of the results was the lack of reliable data on the sediment source area.

6.2 Main study

This project continued with further analysis of the sensitivity of turbidity currents to a wider range of basin-floor topographic configurations and with a more detailed study of the influence of substrate topography on the spatial pattern of sediment dispersal. FLOW-3D™ software was adopted to simulate transport, erosion and deposition of a wider range of sediments – including a model that incorporates transport, erosion, re-suspension and deposition of two classes of sediments. The main focus for this study was to try to replicate the basin-fill history at the Ormen Lange field within the boundary conditions and framework established in the pilot study.

The initial part of the project focused on reviewing the simulation setup and re-evaluating the assumptions from the pilot study. All simulation input parameters were re-checked and new attempts to identify the entry point were made (Figure 9).

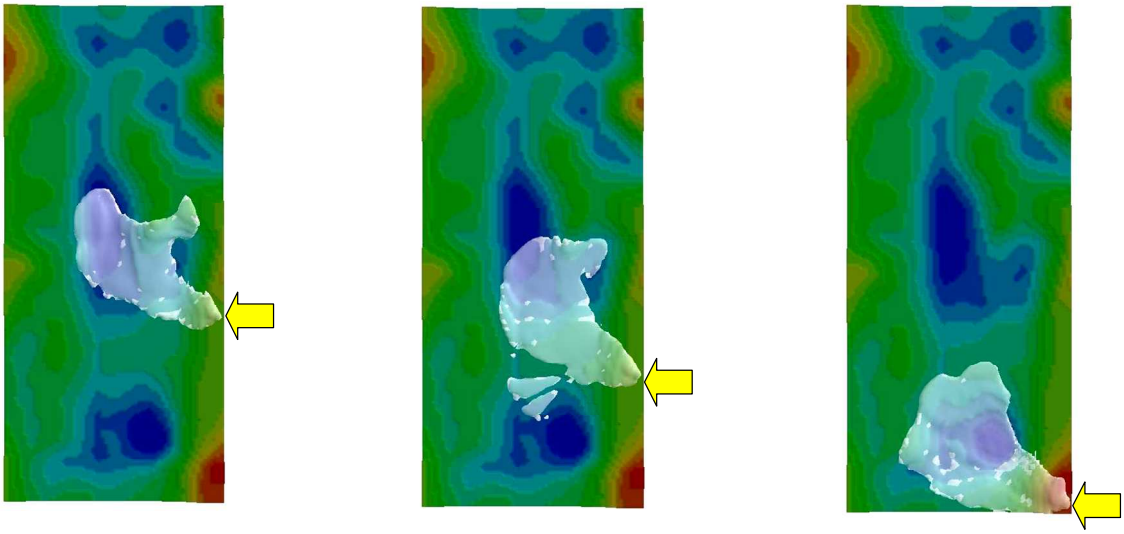

Figure 9. Different entry point locations.

Multiple simulation runs were then performed (Table 1). The simulations from the Hydro pilot were re-run with the new simulation setup. The new base Egga surface provided by Midland Valley Exploration Ltd. (MVE 2004) was then incorporated in the simulations and changed by re-enabling the regional tilt to varying extent (Runs 1-5). Even with heavy modifications to the new surface the quality could not be improved compared to the pilot study so it was abandoned in favor of the topographic surface based on the Egga Reservoir Unit isochore map provided by A/S Norske Shell (Runs 6-9).

Table 1

Run	Initial topography	Changes
1	Top Våle Tight (MVE)	Unmodified, entry point from Hydro pilot
2 Fig, 9C	”	East/North tilt, South/East entry point
3 Fig, 9B	”	”, East entry point
4 Fig, 9A	”	”, North/East entry point
5	”	Heavily modified, no realistic visualization.
6	Egga Reservoir Isochore (Shell)	Unmodified, South/East entry point
7	”	North tilt, single sediment size
8 Fig. 10	”	”, South sub-basin initially filled-in
9 Fig. 11	”	”, Two sediment grain-sizes

For the simulations using the new surface from Shell, similar sensitivity analysis of variation in regional tilt and entry point locations were performed. First a simulation with the old sediment model was attempted and then a two-step simulation using the new 2-size sediment model (Runs 8-9). The first step involved stopping the simulation after the southern depo-centre was partially filled-in with sediments (Run 8), and then the simulation resumed with a slightly vertically shifted entry point (Run 9).

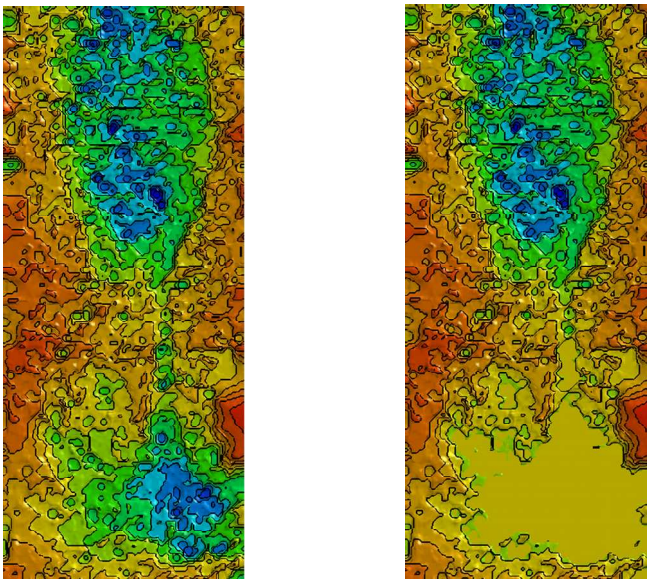

Figure 10. The filling of the southern sub-basin.

The results from this study show slightly more reservoir fill to the west compared to the pilot study. The volume of sediment deposited in the northern depo-centres has also increased when using the new 2-size sediment model that causes less erosion and thus more sediment to bypass (Figure 11).

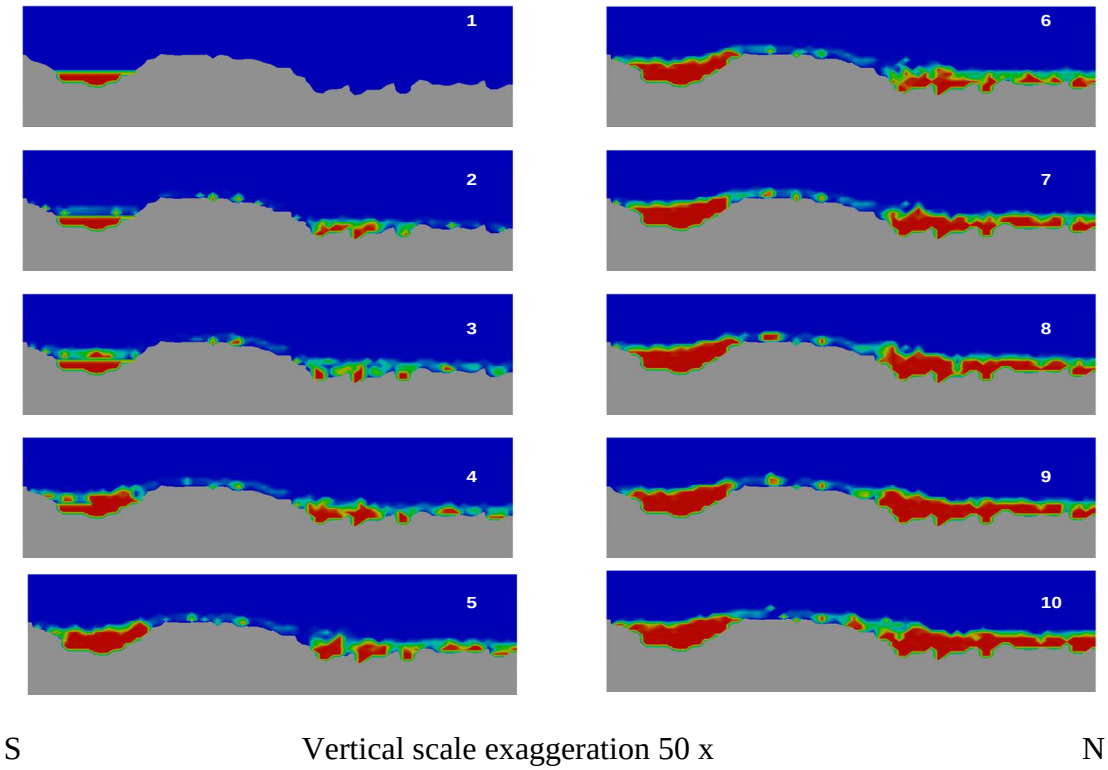

Figure 11. Cross-sections of the basin infill evolution.

7 Conclusions

The main conclusions from this study are:

- Turbidity currents are highly sensitive to subtle variation in basin-floor topography.
- The Ormen Lange depo-centers were probably supplied with sediment mainly from sources in the southeast.
- The sediment transport directions are still considered to be mainly to the north, due to subtle topographic confinement to the east and west.
- Coeval sedimentation occurs in the depo-centres with the areas in between possibly acting as a bypass zone, dominated by erosion and sediment re-suspension.
- As the primary topographic relief was gradually smoothed out by sediment accumulation, the whole area began to act increasingly as a bypass zone.
- A working model has been established that can simulate the basin infill evolution for a field such as Ormen Lange within the constrains of the current uncertainty.
- The main limiting factor for the accuracy of these simulations is the poor quality of the basin-floor topographic data especially in the assumed feeder-channel area.

8 Further Work

Further work that would enhance the understanding of the Ormen Lange field could include:

- Obtain reconstructed basin-floor topographic data covering a larger area, especially in the inferred southeastern source area, and possibly also better data on the study area's palaeo-latitudes, bathymetry, salinity, temperature and currents.
- FLOW-3D™ could be adopted to simulate an even wider range of sediments, with various "real-life" grain-size distributions, to enable modeling of more complex heterogeneities.
- 3-D visualization of the stacking patterns and the evolution of the whole depositional system, generating sets of deterministic stratigraphic surfaces to be used for correlation and verification of the Ormen Lange field (Guargena et al. 2006).

9 References

Blystad, P. et al. (1995) Structural elements of the Norwegian continental shelf, Part 2. The Norwegian Sea Region. Norwegian Petroleum Directorate Bulletin 8, 45 pp.

Bugge, T. et al. (1988) The Storegga Slide. Philosophical Transactions of the Royal Society of London A, 325, 357–388.

Chanson, H. (2004) The Hydraulics of Open Channel Flow: An Introduction - Basic Principles, Sediment Motion, Hydraulic Modeling, Design of Hydraulic Structures, Second Edition. Elsevier Butterworth-Heinemann, Burlington, USA.

Eliassen, I.K. et al. (2000) The current conditions at Ormen Lange – Storegga. Unpublished report to Norsk Hydro.

Gjelberg, J. et al. (2001) The Maastrichtian and Danian depositional setting along the eastern margin of the Møre Basin (mid-Norwegian Shelf): implications for reservoir development of the Ormen Lange Field. NPF Special Publication 10, 421-440.

Gjelberg, J. et al. (2002) Depositional model for the Ormen Lange reservoir: a summary report. O&E Norsk Hydro.

Guargena, C. et al. (2006) Reservoir Characterization – An Integral Aspect of Uncertainty Management for Opportunity Realization at the Ormen Lange Giant Gas Field Development, Norwegian Sea. GCSSEPM, Houston, USA.

Lide, R.D. (2000) CRC Handbook of Chemistry and Physics, 81st Edition. CRC Press, Boca Raton, USA.

MVE (2004) Ormen Lange Field: Decompaction and Restoration with Flexural Isostasy. Unpublished report to Norske Shell.

Möller, N. et al. (2004) A geological model for Ormen Lange: Norsk Geologisk Tidskrift, v. 84, 3, 169-190.

Normark, W.R. (1989) Observed parameters for turbidity current flow in channels, Reserve fan, Lake Superior. Journal of Sedimentary Petrology, 59, 423-431.

Richardson, J.F. & Zaki, W.N. (1954) Sedimentation and Fluidization: Part I, Transactions Institute of Chemical Engineers, 32, 35 pp.

Smith, R. & Möller, N. (2003) Sedimentology and reservoir modelling of the Ormen Lange field, mid Norway. Marine and Petroleum Geology 20, 601–613.

Stanton, H. & Thompson, L. (2002) Ormen Lange restoration and decompaction. Unpublished report to Norsk Hydro.

Unesco (1981) Tenth report of the joint panel on oceanographic tables and standards. Unesco technical papers in marine science, 36, 17-19.

Walker, R.G. (2001) A basin-filling model for Ormen Lange. Unpublished report to Norsk Hydro.

Walker, R.G. & Möller, N. (2002) Reservoir geology status report. E&D Norsk Hydro.

Wesseling, P. (2001) Principles of Computational Fluid Dynamics. Springer.

Zeng, J. et al. (1991) Flow properties of turbidity currents in Bute Inlet, British Colombia. Sedimentology, 38, 975-996.

Zeng, J. & Lowe, D.R. (1997) Numerical simulation of turbidity current flow and sedimentation: I. Theory. Sedimentology, 44, 67-84.